U.S. DEPARTMENT OF COMMERCE
National Technical Information Service

AD-A026 833

Applied Superconductivity Amplifiers and Microcomposite Wire

Harvard Univ.

Prepared For
Office of Naval Research

January 1976

Office of Naval Research
Contract N00014-76-C-0032 NR-318-003
ARPA Contract DAHC 15-73-G-16
National Science Foundation Grant DMR72-03020
National Science Foundation Grant GH-34133x

APPLIED SUPERCONDUCTIVITY: AMPLIFIERS AND MICROCOMPOSITE WIRE

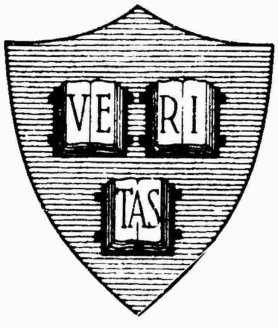

By

Arthur Davidson

January 1976

Technical Report No. 12

Division of Engineering and Applied Physics
Harvard University • Cambridge, Massachusetts

Unclassified

SECURITY CLASSIFICATION OF THIS PAGE (When Data Entered)

REPORT DOCUMENTATION PAGE		READ INSTRUCTIONS BEFORE COMPLETING FORM
1. REPORT NUMBER TR12	2. GOVT ACCESSION NO.	3. RECIPIENT'S CATALOG NUMBER
4. TITLE (and Subtitle) APPLIED SUPERCONDUCTIVITY: AMPLIFIERS AND MICROCOMPOSITE WIRE		5. TYPE OF REPORT & PERIOD COVERED Interim Report 6. PERFORMING ORG. REPORT NUMBER
7. AUTHOR(s) Arthur Davidson		8. CONTRACT OR GRANT NUMBER(s) N00014-76-C-0032, DAHC 15-73-G-16, DMR72-03020 GH-34133x
9. PERFORMING ORGANIZATION NAME AND ADDRESS Division of Engineering and Applied Physics Harvard University Cambridge, Massachusetts 02138		10. PROGRAM ELEMENT, PROJECT, TASK AREA & WORK UNIT NUMBERS
11. CONTROLLING OFFICE NAME AND ADDRESS		12. REPORT DATE January 1976 13. NUMBER OF PAGES 246
14. MONITORING AGENCY NAME & ADDRESS (if different from Controlling Office)		15. SECURITY CLASS. (of this report) Unclassified 15a. DECLASSIFICATION/DOWNGRADING SCHEDULE

16. DISTRIBUTION STATEMENT (of this Report)

This document has been approved for public release and sale; its distribution is unlimited. Reproduction in whole or in part is permitted by the U. S. Government.

17. DISTRIBUTION STATEMENT (of the abstract entered in Block 20, if different from Report)

18. SUPPLEMENTARY NOTES

PRICES SUBJECT TO CHANGE

19. KEY WORDS (Continue on reverse side if necessary and identify by block number)

Applied superconductivity
Amplifiers
Microcomposite wire

20. ABSTRACT (Continue on reverse side if necessary and identify by block number)

This report is in two parts. Part I is concerned with superconductive devices employed as amplifiers with particular emphasis on SQUID's. We show that superconductive amplifiers are electrical duals to MOSFET amplifiers and that the same types of parameters describe both types of amplifiers. In particular we show that the noise of each type of amplifier is characterized by three quantities: a minimum noise temperature, an optimum source resistance, and a constant product of noise temperature and input circuit time constant. We call this last parameter the action factor. Our analysis

DD FORM 1 JAN 73 1473 EDITION OF 1 NOV 65 IS OBSOLETE
S/N 0102-014-6601

Unclassified

SECURITY CLASSIFICATION OF THIS PAGE (When Data Entered)

20. Abstract continued

shows that amplifiers with liquid helium noise temperatures over hundreds of kilohertz can be made from superconductive devices.

Part II is a study of superconductive microcomposite wires that have potential applications in industry. The wires are a microcomposite of Cu, NB, and Sn, made by Tsuei's process. We present data taken with both conventional and SQUID apparatus. Our samples with low concentrations of Nb (5 atomic %) all show a relatively small magnetization indicative of imperfect screening of magnetic flux, and a small remnant resistivity. Samples with 10 atomic % Nb, however, have virtually perfect screening characteristics at low temperatures and in small applied magnetic fields, and show no evidence of remnant resistance. Insight gained in studying these microcomposites has led us to an amalgamation of percolation theory and the effective medium theory for conduction in inhomogeneous media. Formulas resulting from this amalgamation fit not only our data on microcomposites, but also fit data from totally different materials.

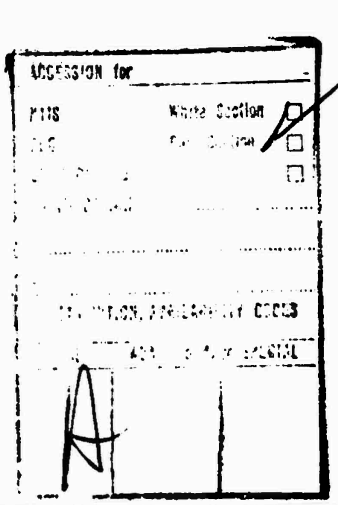

it

Office of Naval Research

Contract N00014-76-C-0032 NR-318-003

National Science Foundation Grant DMR72-03020

National Science Foundation Grant GH-34133X

ARPA Contract DAHC 15-73-G-16

APPLIED SUPERCONDUCTIVITY:

AMPLIFIERS AND MICROCOMPOSITE WIRE

By

Arthur Davidson

Technical Report No. 12

January 1976

The research reported in this document was made possible through support extended the Division of Engineering and Applied Physics, Harvard University, by the Office of Naval Research, under Contract N00014-76-C-0032 and by the Advanced Research Projects Agency under Contract DAHC 15-73-G-16 and by the National Science Foundation under Grants DMR 72-03020 and GH-34133X.

Division of Engineering and Applied Physics

Harvard University · Cambridge, Massachusetts

ABSTRACT

This report is in two parts. Part I is concerned with superconductive devices employed as amplifiers with particular emphasis on SQUID's. We show that superconductive amplifiers are electrical duals to MOSFET amplifiers and that the same types of parameters describe both types of amplifiers. In particular we show that the noise of each type of amplifier is characterized by three quantities: a minimum noise temperature, an optimum source resistance, and a constant product of noise temperature and input circuit time constant. We call this last parameter the action factor. Our analysis shows that amplifiers with liquid helium noise temperatures over hundreds of kilohertz can be made from superconductive devices.

Part II is a study of superconductive microcomposite wires that have potential applications in industry. The wires are a microcomposite of Cu, Nb, and Sn, made by Tsuei's process. We present data taken with both conventional and SQUID apparatus. Our samples with low concentrations of Nb (5 atomic %) all show a relatively small magnetization indicative of imperfect screening of magnetic flux, and a small remnant resistivity. Samples with 10 atomic % Nb, however, have virtually perfect screening characteristics at low temperatures and in small applied

magnetic fields, and show no evidence of remnant resistance. Insight gained in studying these microcomposites has led us to an amalgamation of percolation theory and the effective medium theory for conduction in inhomogeneous media. Formulas resulting from this amalgamation fit not only our data on microcomposites, but also fit data from totally different materials.

PREFACE

This report is in two distinct parts. Part I is an investigation of the characteristics of superconductive amplifiers. It was begun at the suggestion of Professor M.R. Beasley,[1] and followed the direction set earlier by him and Dr. R.S. Newbower.[2] Many of the conclusions reported here have already been published in a paper[3] written by this author with Dr. Newbower and Professor Beasley.

Part II is an account of our experiments with a new class of superconductive material: microcomposite wire. This research began as an interruption in a planned program of measurements in which a SQUID amplifier was to have measured noise properties of various superconductive devices. The properties of the microcomposites turned out to be sufficiently novel, however, that our primary interest shifted to them. Some preliminary results were published in a paper[4] by this author with Professors Beasley and M. Tinkham. This report covers the material in tne earlier paper, with additional data, interpretations, and perspective.

A Note on Units

MKS units are used throughout this report. The most used conversion in switching from cgs to MKS units is that 10^4 gauss make one tesla.

TABLE OF CONTENTS

TABLE OF CONTENTS (Continued)

TABLE OF CONTENTS (Continued)

TABLE OF CONTENTS (Continued)

LIST OF FIGURES

LIST OF FIGURES (Continued)

LIST OF FIGURES (Continued)

LIST OF FIGURES (Continued)

LIST OF TABLES

PART I

SUPERCONDUCTIVE AMPLIFIERS

CHAPTER ONE: INTRODUCTION

Superconductive devices have been used for sensitive low temperature electrical measurements for over twenty years, but their full utility as current and voltage amplifiers have never been applied. The earliest efforts used superconductors as passive devices in conventional schemes. Pippard and Pullan[5] replaced the copper coil in a conventional electro-mechanical galvanometer with a superconducting coil in 1952, and achieved sensitivities of 10^{-12} volts with an input circuit time constant of about 10 seconds. Templeton[6] in 1955 constructed a superconducting chopper to couple a low temperature experiment to a room temperature vacuum tube amplifier. He obtained sensitivities of 2×10^{-11} volts with a 0.1 second time constant. Both of these techniques were restricted to low frequency (a few hertz at most) applications. The first active superconductive device was the cryotron, so named by Buck[7] in 1956. This device, which depended on "classical" superconductivity, was originally conceived as a potential logic and memory device for application in large scale computers, but was shown by Newhouse and Edwards[8] to be applicable to linear amplification as well. The cryotron was unquestionably a wideband device

capable in principle of low noise operation, but it was beset by a host of practical problems and was never widely applied.

The only superconductive devices to be widely applied as sensitive amplifiers have been those that have relied upon the Josephson effect, deduced theoretically by B.D. Josephson[9] in 1962, and confirmed experimentally by Anderson and Rowell[10] in 1963. The first device used as a sensitive electrical detector was invented by Clarke[11] in 1966, and dubbed the SLUG (for Superconductive Low inductance Undulating Galvanometer). Since then, other devices, generically termed SQUID's[12,13] (Superconducting QUantum Interference Devices) have superceded the SLUG. These devices have been used to detect voltages as small as 10^{-16} volts in a one hertz bandwidth, but they have been applied only at low frequencies. This is a strange condition indeed, since the fundamental processes in any Josephson device occur over time intervals between nano- and picoseconds,[14] so that SQUID's or SLUG's or any of their variations should be a applicable to very high frequencies as linear amplifiers. It is ironic that the cryotron, which depends on a relatively slow phase transition for its operation, was always thought of as a high frequency device, while the Josephson devices, which are extremely fast, have been thought of and used for only very low frequencies. (An important exception

to this irony is the Josephson junction cryotron[15] which was intended to be,and is, very fast. It is at present limited to digital applications, however.)

In the following section we shall briefly examine the operation and characteristics of the various active superconducting devices, with an eye toward understanding their limitations. Then we shall analyze in considerable detail the operation of a radio-frequency biased SQUID voltmeter circuit. We choose this particular application for detailed analysis because it has been used in several experiments in this and other laboratories. Finally, we shall discuss the close analogy that exists between these devices and conventional room temperature high impedance amplifiers, and make suggestions for the further development of superconductive linear amplifiers.

CHAPTER TWO: PRESENTLY AVAILABLE SUPERCONDUCTING DEVICES

There are at present two classes of active superconducting devices suitable for small signal amplification. The first class takes advantage of only the "classical" properties of superconductors, while the second class utilizes one or another of the Josephson phenomena. Classical properties of superconductors are those that were understood before Josephson's predictions in 1962.[9] Critical currents, fields, and temperatures, and the coherence length and penetration depth in bulk and thin film superconductors are thus classical properties. A device that uses these properties is the cryotron. In the Josephson device category we shall consider the isolated Josephson junction as well as its incorporation in SLUG's and SQUID's.

2.1 Cryotrons

Cryotrons[7,8,16] operate by using the field produced by current in one superconducting path to quench superconductivity in a neighboring path. The superconductor that creates the field is called the control, while the other, whose conductance is modified by the control, is called the gate. In the original cryotron, the gate was a straight length of superconducting wire made of, say, Sn, and the control was a Pb or Nb wire wrapped tightly around

the gate. The device was operated at a temperature just beneath the critical temperature of the Sn gate (3.7 K) but well below the transition temperature of the control (9.2 K for Nb, or 7.2 K for Pb). Thus a particular magnitude of control current could drive the gate normal but leave the control superconducting. Further, if the gate had a reasonably sharp resistive transition to the normal state, a small change in the control current could cause a large change in gate current, so that both current and power gain were available. A simpler device to fabricate, and in many respects superior to the wire wound cryotron just described, is the thin film cryotron.[17] This device consists of two thin films deposited over an insulated ground plane, as shown in Fig. 1, where the two films are usually at right angles and are insulated from each other. Again, one film is the gate, made usually of Sn, and the other film (the uppermost) is the control made of Pb. Operation is exactly as described for the wire wound cryotron, but the low inductance of the control and the small size of the gate help to speed up the operation of the device.

Cryotrons, particularly the thin film versions, appeared promising on paper during their initial development, but they have never enjoyed more than limited application due to a plethora of practical problems. First it turned out that the dynamics of the phase transition on which their opera-

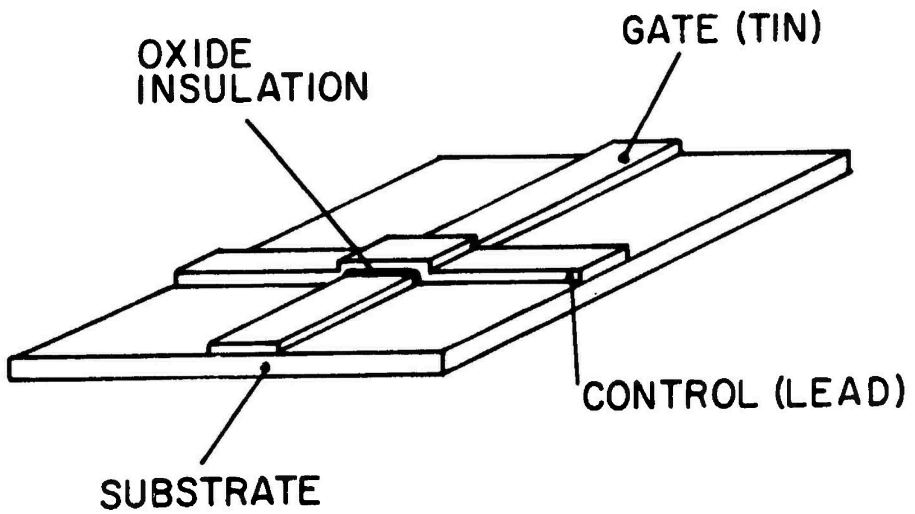

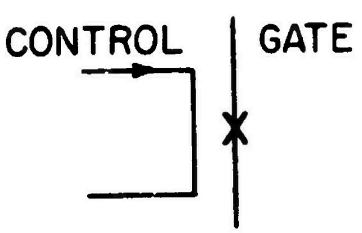

CIRCUIT SYMBOL

Fig. 1 Physical arrangement of crossed film cryotron, and circuit symbol

tion depends[18] was much slower than had been anticipated. This ruled out competitive operation in computers, the original motivation for their invention. Second, in linear operation they are plagued by flicker (1/f) noise[8] apparently due to helium boiling, which makes them nearly useless at low frequencies or dc. The source of this problem is that the gate element is nearly as sensitive to temperature fluctuations as it is to magnetic fields, when biased near its transition. Since there are measures that could be taken to reduce these temperature fluctuations, this problem is of technical, not fundamental, importance, but it is an added complication. Finally, cryotrons require large, stable current supplies for biasing, and they are difficult to couple effectively to room temperature amplifiers. The worst of these problems, however, are largely overcome by devices employing the Josephson effects.

2.2 Josephson Junctions

Many devices suitable for sensitive linear amplification have been made and investigated since Josephson's original theoretical predictions of 1962. These include devices that have used tunnel junctions, or point contact junctions, or thin film microbridge junctions.[19] The junctions, of whatever type, have been used both alone, and as part of a larger multiply-connected superconductor. They offer the

device maker both a richness of possible configurations and a richness of phenomena to harness in a practical design. The general subject of Josephson phenomena is too deep to cover properly here and the reader should refer to the bibliography for details of this vast subject. However, the basic physics underlying most of the details can be presented briefly in a simple phenomenological picture, and that will be the aim of this section. After the basic phenomena have been presented we shall examine their utility in devices.

At the operational level, Josephson junctions work much like cryotrons: a magnetic field is used to suppress superconductivity. The difference is that in Josephson junctions superconductivity is suppressed in a very small region and the suppression is not due to a thermodynamic transition. Rather, it is due to the decoupling of quantum mechanical wave functions on either side of a narrow gap. A way in which this decoupling can occur is sufficiently simple to warrant a brief discussion.[20] Begin by assuming that two parallel bulk superconductors are brought into close proximity of one another, in a configuration like that shown in Fig. 2. Let the gap between the two superconductors be either vacuum, or an insulator, or some normal metal. Let the boundaries of this gap be at $\pm a$. Since any superconductivity in the gap region will be weak, we can write down the wave functions associated with the macroscopic quantum

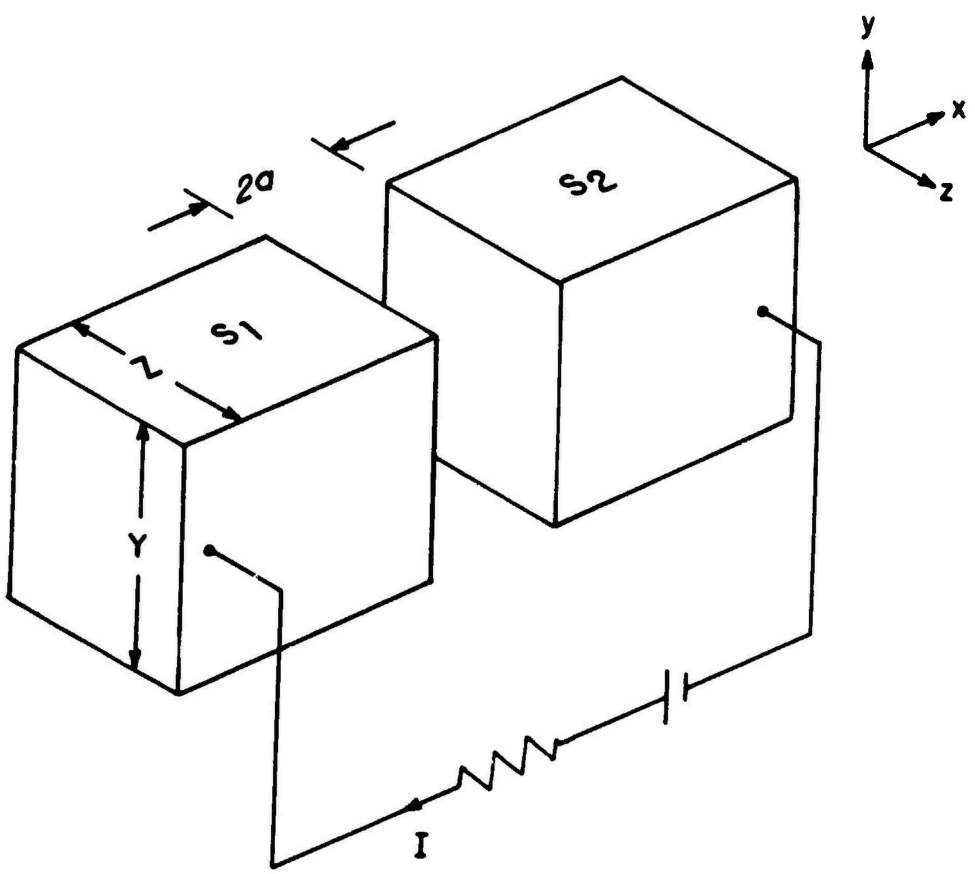

Fig. 2 Schematic Josephson junction. S_1 and S_2 are bulk superconductors separated by a barrier of width 2a.

state of each bulk superconductor independently. The problem is then equivalent to the tunneling of wave functions out of wells, and typically there will be an exponentially decaying tail from each side into the gap. Hence, in the gap or barrier, if ψ_1 is the wave function for the macroscopic quantum state on the left, and ψ_2 is the wave function on the right, we can write:

$$\psi_1 = \psi_o \exp\left[-\frac{x + a}{\xi} + i(\phi_1 + e^*Ax/\hbar)\right]$$
$$\psi_2 = \psi_o \exp\left[\frac{x - a}{\xi} + i(\phi_2 + e^*Ax/\hbar)\right] \qquad (2\text{-}1)$$

where ψ_o and ξ are real constants. ϕ_1 and ϕ_2 are the gauge-invarient phases, which differ from the explicit phases of the wave function by the vector potential term. We have assumed a vector potential A to exist directed uniformly along the x axis. Also, e* is the effective charge of a superconducting particle (that is, e* = 2e). Now due to the assumed weakness of superconductivity in the barrier, we also assume that the net wave function in the gap region is the sum $\psi = \psi_1 + \psi_2$. We now have all the information we need to calculate the supercurrent density flowing through the junction. We may use the standard quantum mechanical form for a current of particles with charge e* and mass m* (the effective mass of a superconducting particle):

$$J_s = \frac{e^*\hbar}{2m^*i}(\psi^*\vec{\nabla}\psi - \psi\vec{\nabla}\psi^*) - \frac{e^{*2}}{m^*}\psi\psi^*\vec{A} \quad \text{amp/m}^2$$
$$= \frac{e^*\hbar}{2m}|\psi_o|^2 \exp(-2a/\xi)\sin(\phi_1 - \phi_2) \; . \tag{2-2}$$

The argument of the sine in (2-2) turns out to be expressable in terms of the difference in gauge-invariant phase from -a to +a. If the explicit phase at x = -a is ϕ_- and the explicit phase at x = +a is ϕ_+ then the phase difference $\phi_1 - \phi_2$ is $\phi_- - \phi_+ + 2ae^*A/h$.

Equation (2-2) can be written more compactly with a phenomenological coefficient, J_o, and the phase difference, γ:

$$J_s = J_o \sin\gamma \tag{2-3}$$
$$\gamma = \phi_1 - \phi_2 = \phi_- - \phi_+ + 2e^*aA/\hbar$$

This result is one of the two famous Josephson equations, and we may now integrate it to obtain the total current, I_s, flowing through the junction. If the magnetic field B is uniform and in the y direction, parallel to the plane of the junction so that A points along the x direction, then we may write A = Bz. Further, if the junction has dimension Z units in the z direction, then the magnetic flux threading the junction (neglecting shielding currents flowing within

the barrier) is $\Phi = 2aZB$. In calculating this flux we have neglected the penetration depth in both bulk superconductors. If the barrier is too narrow, the fields penetrating the bulk superconductors must be taken into account. Finally, $\hbar/e^* = \Phi_o/2$ where Φ_o is the flux quantum. Then the total supercurrent flowing through the junction is

$$I_s = \int_{-Z/2}^{Z/2} \int_{-Y/2}^{Y/2} J_s dydz = I_o \sin\delta \frac{\sin(\pi\Phi/\Phi_o)}{(\pi\Phi/\Phi_o)} \qquad (2\text{-}4)$$

where $\delta = \phi_- - \phi_+$, and $I_o = J_o YZ$.

This equation means that a current of magnitude less than

$$I_o \frac{\sin(\pi\Phi/\Phi_o)}{(\pi\Phi/\Phi_o)}$$

can be carried through the junction without dissipation, provided the phase δ is allowed to adjust itself to satisfy (2-4). If a larger current is forced through, it cannot be carried as a steady state supercurrent, so that some normal current must flow, and the resulting dissipation will be manifest as a voltage across the junction. Hence by applying a current that exceeds the critical current, or by applying a magnetic field, superconduction across the junction can be quenched without quenching the superconducting state in either bulk superconductor. Further, from

(2-4), one need only apply a single flux quantum to the junction to effect a quench. For a junction with an area the order of 10^{-8} cm^2, then, it would take only about 10^{-3} tesla to reduce the critical current to zero. This is ten to one hundred times less field than is required to quench superconductivity in the cryotron. A bonus that is apparent from this analysis is that the weakened superconductivity in most types of Josephson junctions remains weak even at very low temperatures, so the critical current will be relatively independent of temperature if the bulk superconductors are well below T_c. This effect eliminates the worst problem afflicting cryotrons: the flicker noise associated with temperature fluctuations of the helium bath will not seriously affect Josephson junctions of the proper design.

There are currently two devices in use or under study that utilize a single Josephson junction in a singly connected superconducting topology. One device, which appears promising in computer applications, is an adaption of Josephson phenomena to cryotrons, and the device will be called here a Josephson junction cryotron.[15] The device is made by replacing the gate in a cryotron arrangement of thin films with a Josephson junction. This new configuration behaves qualitatively very much like the old cryotrons, except that it is not so sensitive to temperature fluctuations, it is much faster, requiring a picosecond time scale

for measuring the switching speed, and it is activated by much smaller bias currents, thus reducing the power level of the device which, in turn, allows a denser packing of the circuitry. The Josephson junction cryotron uses a tunnel junction, in which the barrier between the bulk superconductors is an insulator, and due to some normal state tunneling properties not discussed here, they exhibit a strong hysteresis that is an additional advantage in digital circuitry. It is this same hysteresis, however, that blocks a direct application to linear amplification . Other junction configurations are not hysteretic, but they have not been applied in cryotron arrangements.

The other Josephson device that has been used by itself in a singly-connected topology is a Josephson-junction noise-temperature thermometer.[21] Unlike the Josephson cryotron, this device does not use the critical current relation of (2-4), but instead takes advantage of the second fundamental Josephson equation. This equation is a general property of superconducting systems, and it relates the voltage between two superconducting regions to the quantum phase difference between them. It will not be derived here (see Feynman, reference 22, for a simple derivation) but the relation is

$$V = (\hbar/e^*)(d\gamma/dt) \qquad (2\text{-}5)$$

where V is the voltage difference, and γ is the gauge invar-

iant phase difference. Thus, if there is a potential difference V across a Josephson junction, the phase will increase (or decrease) at a rate proportional to the voltage. When such a time dependent phase is substituted into (2-5) we see that the net supercurrent must oscillate at the instantaneous angular frequency $\omega(t) = e^*V(t)/\hbar$. This oscillating supercurrent may be detected by mixing a radio frequency signal with the oscillating supercurrent in the junction itself. The external rf should have a frequency much larger than $e^*V/\hbar$. The result of mixing in the nonlinear Josephson junction will be an amplitude modulated rf signal, where the frequency of the modulation contains the voltage information. Standard radio F.M. techniques can then be used outside the dewar to demodulate the mixer product and create an amplified version of the original signal.

A possible configuration of such a Josephson device used as a thermometer is shown in Fig. 3. The Johnson noise voltage fluctuations of a resistor, R_s, are imposed on a Josephson junction biased above its critical current. Hence the total supercurrent through the junction will contain a component whose frequency is related to the instantaneous voltage across R_s. The fluctuations of this frequency are then proportional to the Johnson noise fluctuations, and by measuring the frequency with the mixing and F.M. techniques

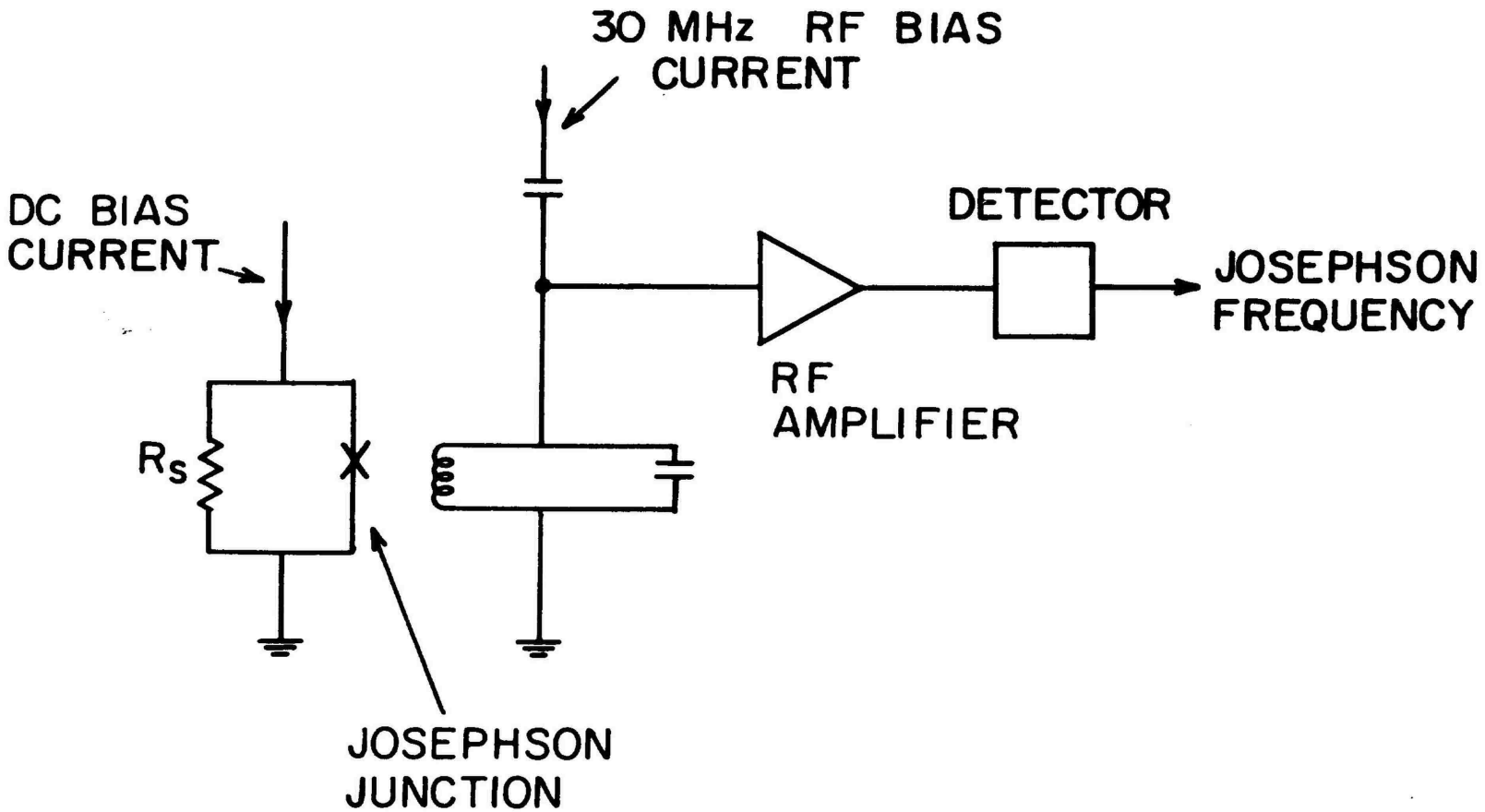

Fig. 3 Configuration of a Josephson junction noise thermometer. The detector output is an ac signal at the Josephson frequency.

mentioned above the temperature of R_s may be determined from the Johnson noise formula $\langle V^2 \rangle = 4k_B T R_s \Delta B$. Here $\langle V^2 \rangle$ is the mean square voltage fluctuation, k_B is Boltzmann's constant, T is the temperature to be determined, and ΔB is the effective bandwidth of the measurement. Circuits based on these principles[23] have been used to measure temperatures into the milli-Kelvin region with good accuracy, which gives an indication of the sensitivity possible with Josephson devices. In principle the same circuit could be used as a general purpose linear amplifier with an appropriate F.M. demodulator in the output circuit to convert the oscillating voltage back to an analog signal.

2.3 SQUID's

We have seen that a single Josephson junction is extremely sensitive to magnetic flux in its barrier, but it is not very sensitive to field. The problem is that it takes a relatively large field to make even a small quantity of flux in the small gap area of most junctions. The field sensitivity, evidently, could be increased if that area were made much larger, while maintaining Josephson coupling between the two bulk superconductors. Since the barrier must remain narrow, this would mean making a very long junction. Such a geometry would not work well because of difficulties in fabricating a large junction uniformly, and, more fundamentally,

because self screening currents within the junction would cause complications. However, there is a simple way of making a junction with effectively a very large area, and the resulting devices are called SQUID's, for Superconducting QUantum Interference Device.[12,13] Such an arrangement, shown in Fig. 4a, consists of two small area junctions incorporated into a multiply connected superconducting ring. It is much as if the center of a single large area junction had been removed, leaving the two small junctions at the extremes. In fact, the Josephson equations, (2-2) or (2-3), still apply. There are now two paths for the current to flow in, however, so there will be two terms in the expression for the total current:

$$I_s = I_o \, (\sin\gamma_1 + \sin\gamma_2) \qquad (2\text{-}6)$$

We have assumed for simplicity that the two junctions have equal critical currents, are symmetrically arranged so that as imposed current will divide symmetrically (in zero applied field), and that the flux within each junction is negligible . But in this new geometry the gauge invariant phases γ_1 and γ_2 associated with each junction are not independent. It is easy to show by integrating the vector potential around the superconducting ring that

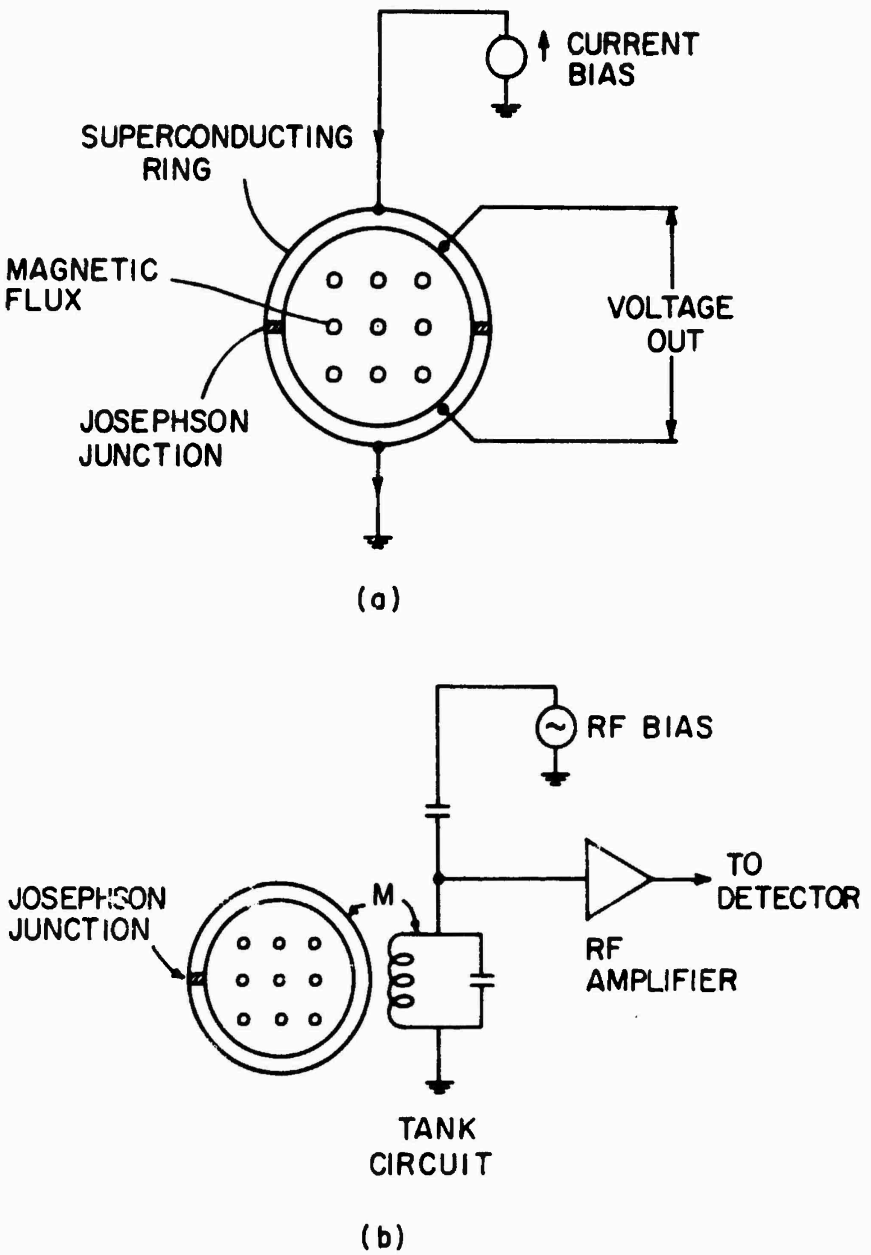

Fig. 4 a) dc SQUID configuration. b) rf SQUID configuration.

$$\gamma_1 - \gamma_2 = 2\pi\Phi/\Phi_o \qquad (2\text{-}7)$$

where Φ is now the total flux enclosed by the ring. Substituting this expression back into (2-6), we find that the critical current through the SQUID has a minimum (a zero, actually, if the two junctions are identical) whenever the total magnetic flux in the ring is an odd multiple of $\Phi_o/2$, thus making the electrical characteristics periodic in the flux quantum. Typical SQUID areas might be 10^{-2} cm^2 so that a field of only about 10^{-9} tesla is all that is required to drive the SQUID into a resistive state. The extra sensitivity to magnetic field that SQUID's thus possess over single Josephson junctions is due only to the larger area of the SQUID geometry. However, since the physically larger inductors used to couple to SQUID's can produce the required flux with very small currents, this high sensitivity to field is equivalent to a high sensitivity to current. The tiny coils required to drive single Josephson junctions require very large currents to produce the same quantum or so of magnetic flux. (In other words, the inductance of a coil of of fixed geometry scales with its linear dimensions.) Thus SQUID's are the preferred device where extreme sensitivity to fields or current is desired.

What has been described above is usually referred to as a direct current (dc) SQUID, but there is another version of

this device called a radio frequency (rf) SQUID.[13] This device consists of a single junction in a closed superconducting ring, as sketched in Fig. 4b. It behaves like the dc SQUID in that its electrical characteristics depend periodically on the flux quantum, but the measurable quantities are only accessible at radio frequencies. These rf SQUID's are currently popular because they require the fabrication of only a single junction and the high frequency circuitry actually allows some simplification in the way room temperature equipment is coupled to the SQUID. See reference 24 for a thorough discussion.

There is a third device called a SLUG that we referred to briefly in Chapter One. Its principle of operation is exactly that of the dc SQUID discussed above. Its distinctions are a unique method of fabrication and that it senses the magnetic field due to an applied current in one of its structural parts, instead of an externally applied field. See J. Clarke, reference 11 for details.

Despite the excellent sensitivity of SQUID's to magnetic fields or currents, they are not ideal circuit elements from the standpoint of designing linear amplifiers. Their periodic response to applied fields makes them extremely nonlinear so that operation without feedback is difficult at best. Complicating this intrinsic nonlinearity is the fact that the Josephson junctions that are their heart operate

at very high speeds. Extreme nonlinearity coupled with wide band response makes these devices especially susceptible to noise, so that careful shielding of the device, and whatever circuit it is coupled to, is a necessity. Furthermore, the very thing that makes SQUID's sensitive to small currents also makes them low frequency or dc devices. The large coils used to couple currents to SQUID's have a large inductance which in turn makes a long time constant in the input circuit. As we shall see in the next chapter, feedback can be used to reduce the effective time constant of the input circuit, but feedback cannot alter sensitivity: even with feedback, the original high sensitivity to current will be retained only over the original narrow bandwidth. Apparently the only way to increase the low noise bandwidth is to sacrifice some current sensitivity and make a smaller device that requires a smaller coupling coil. Hence we envision moving the two Josephson junctions of the dc SQUID closer together in an effort to obtain wider bandwidths with less current sensitivity. The limit puts us back where we started, with a single Josephson junction in a cryotron-like configuration. Hence we must choose the configuration of Josephson junctions that suits our purpose: SQUID's offer high sensitivity but slow response, while single junctions offer quick response with relatively poor sensitivity. In the following chapters are presented first a careful study of a particular

SQUID amplifier; then, using that study as a concrete example we will show how the ideas discussed briefly above apply to both superconducting and conventional amplifiers.

CHAPTER THREE: ANALYSIS OF A SQUID AMPLIFIER

SQUID magnetometers have dramatically improved the sensitivity with which voltage measurements can be made at low temperatures.[25] An available voltage sensitivity in the sub-femtovolt ($<10^{-15}$ volt) range and noise temperatures under some conditions as low as 10^{-6} K are often quoted measures of the remarkable capabilities of these devices. previous work on SQUID amplifiers[26,27] has in the main emphasized their applications as sensitive dc voltmeters. In this chapter, however, we explore their potential as low-noise amplifiers for general purpose use in the liquid helium temperature range. We discuss the construction of practical amplifiers and describe the operating characteristics (noise, bandwidths, impedance levels) of an amplifier we have built. These characteristics are also compared with those expected theoretically and with those available with the best conventional room-temperature electronics.

Conventional SQUID voltmeters have two principal shortcomings when applied as amplifiers: they have narrow bandwidths, and they exhibit their superior noise performance only for very low source impedances. These drawbacks can be overcome, however. First, the bandwidth can be extended beyond that allowed by the natural L/R time constant τ of the input circuit by using the SQUID as a null detector in a feedback circuit and taking advantage of the properties of

negative feedback to decrease the response time of the circuit. As we shall discuss in detail, using feedback properly it is possible to obtain bandwidths well in excess of $1/\tau$, although the best noise performance is still restricted to the smaller natural bandwidth. The advantages of incorporating negative feedback with SQUID voltmeters were first emphasized by McWane, Neighbor, and Newbower.[28] Subsequently, Newbower[29] and Giffard, Webb and Wheatley[27] have analyzed in greater detail the effects of feedback on the operation of SQUID's when used as null detectors. The treatment presented here derives from the work of Newbower and unlike that of Giffard et al. stresses the use of feedback to maximize bandwidth.

The second major problem encountered in attempting to use SQUID's in low-temperature amplifiers is that they exhibit their best noise characteristics only for very low source impedances. For example, micro-degree noise temperatures are available with SQUID amplifiers only for source resistances $<10^{-6}$ ohm; for SLUG's the source resistance must be less than 10^{-8} ohm. This situation arises because the SQUID is basically a current sensing device and small voltages produce large currents only for small source impedances. The deterioration of the noise characteristics of superconducting amplifiers as the source resistance increases has been discussed by Clarke, Tennant, and Woody,[30] who have successfully used

superconducting impedance matching transformers to improve the situation substantially in the case of a SLUG amplifier. Basically they use the transformer to transform the high source impedance to a lower, more favorable level. Their best effort at the time yielded noise temperatures in or below the liquid helium temperature range for source resistances less than 10^{-2} ohm.

Using impedance matching transformers with a SQUID rather than a SLUG, we have been able to obtain noise temperatures less than 4 K for source resistances up to a few ohms with relative ease. Minor improvements would be expected to yield similar or better performance for resistances up to tens of ohms. For source resistances much larger than ten ohms, however, conventional electronics becomes competitive for mose low frequency applications.

A graphic illustration of the remarkable capabilities of a properly operated SQUID amplifier is shown in Fig. 5, which shows the response of our amplifer to a 1.92 nV step input generated in a source with an internal impedance of 0.12 ohm. The noise seen on the amplifier output is due to Johnson noise from the source itself. In making the trace shown in the figure the response time of the amplifier was limited by a 100 Hz low-pass filter on its output. The response time of the amplifier itself was $\sim 10^{-4}$ second. Similar photographs of Johnson noise superimposed on a step response

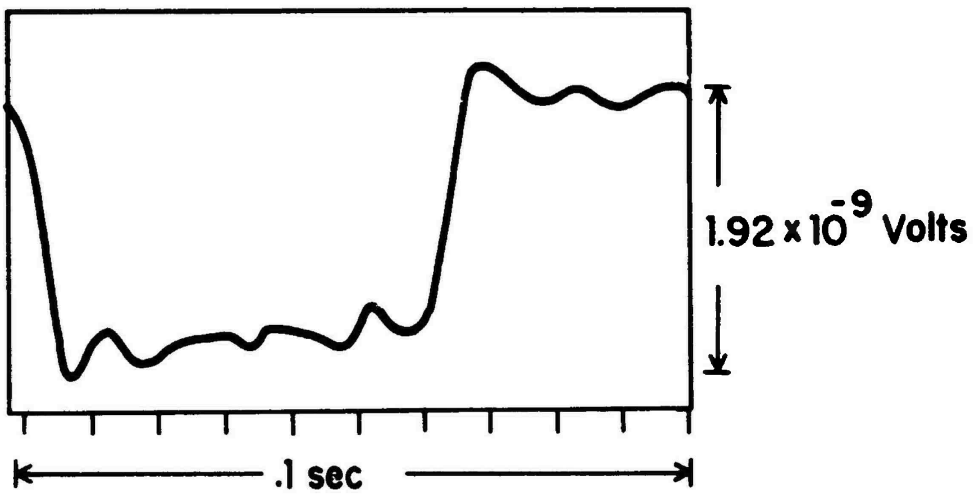

Fig. 5 Low level step response of the SQUID amplifier showing the Johnson noise of a 0.12 ohm resistor in an externally imposed 100 Hz bandwidth.

produced by SQUID voltmeters not properly matched to the source resistance or optimized for response time have required minutes to trace out.[27]

A circuit found to perform satisfactorily as an amplifier and capable of the performance indicated above is described in section 3.1 of this report. In section 3.1 we also establish the equivalent circuit of the amplifier, investigate its dynamic behavior and noise properties, and consider the performance expected when impedance matching transformers are used. In section 3.2 we describe the construction and performance of the amplifier and impedance matching transformer we have built and then compare their operating characteristics with the theoretical analysis presented in section 3.1. In section 3.3 we compare the performance of our superconducting amplifier with the best available room temperature amplifiers.

3.1 Theory of Operation

A. Basic Circuit

The basic amplifier circuit we have studied is shown schematically in Fig. 6a. In this circuit a SQUID magnetometer is used as a null detector in a self-balancing feedback arrangement. The signal voltage V_S produces an error current I_E which is sensed by the SQUID and used to generate a feedback current $I_F = V_O/R_O$ which produces a voltage

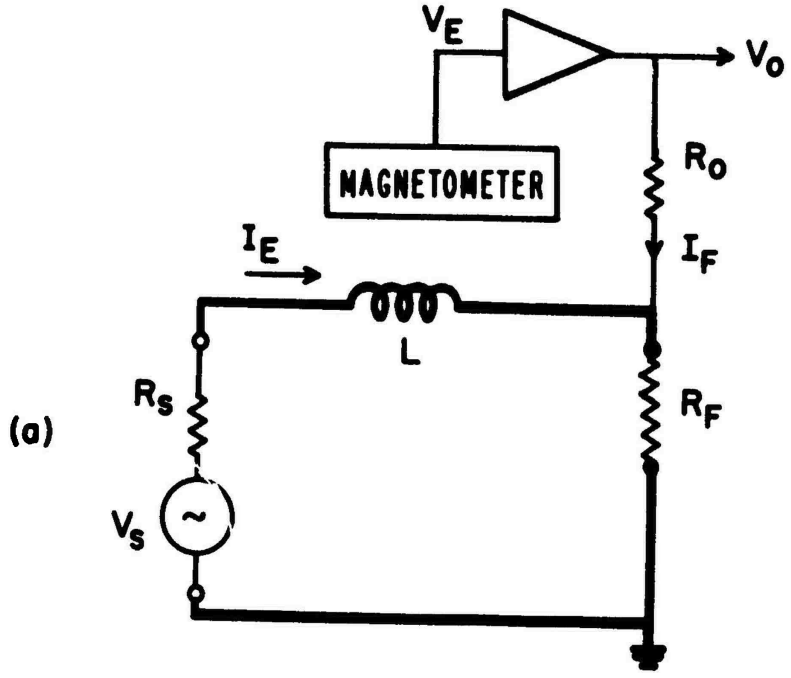

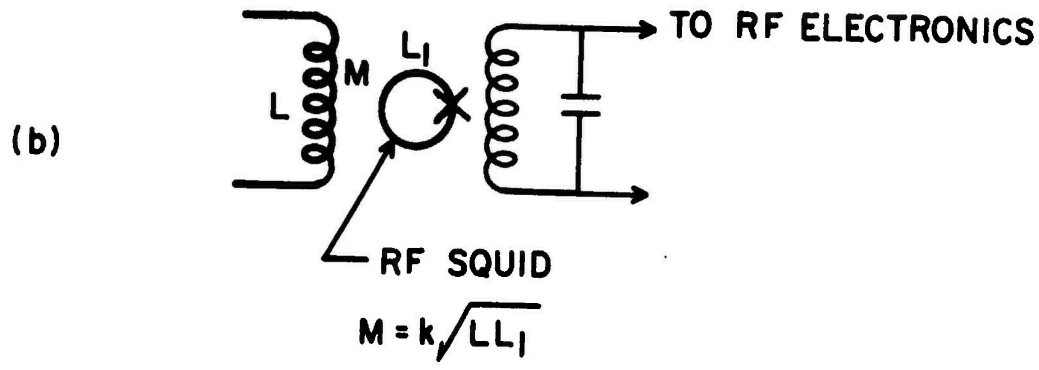

Fig. 6 a) Basic amplifier circuit. b) rf SQUID magnetometer circuit. The heavy lines indicate superconducting current paths.

across R_F that tends to reduce I_E. At balance when $I_E = 0$, $V_S = I_F R_F$ by Ohm's law, and therefore $V_O/V_S = R_O/R_F$. As is typical of negative feedback circuits, the overall gain of the amplifier is independent of the gain of the individual active elements and the input is potentiometric. In real circuits this voltage gain may range up to 10^{10}.

The magnetometer itself consists of a superconducting coil L and a SQUID which senses the current through the coil. Since the superconducting coil has zero resistance the component of the current through the null detector due to the signal is given by V_S/R_S (one usually chooses $R_F<R_S$), so that the null detector is extremely sensitive at low source resistances. The extraordinary noise performance results because the thermal noise in the source, proportional to $\sqrt{R_S}$, decreases more slowly with decreasing R_S than does the minimum detectable voltage. (The actual situation is more complicated and is discussed below.) A schematic of a superconducting amplifier incorporating a SQUID magnetometer is shown in Fig. 6b for the particular case of an rf SQUID. The details of the operation and instrumentation of the SQUID will not be discussed here since they are amply discussed in the literature. (For example, see reference 25 and the references therein.)

The basic circuit shown in Fig. 6a was first used as a superconducting dc voltmeter by McWane, Neighbor, and

Newbower[28] and has subsequently been widely adopted. As we shall see, it can also function nicely as an amplifier, with several advantages. First, when the loop gain in high, the error current is kept small and the circuit has a high-impedance potentiometric input. Second it provides a means by which a sensitive but non-linear (in fact periodic) device such as a SQUID can be used to construct a linear amplifier with large dynamic range. Finally, negative feedback reduces the response time of the circuit substantially below the natural L/R time constant of the null detector loop. This faster response is particularly important for an amplifier. As we show in detail below, in the absence of complicated compensating networks, the ultimate bandwidth of this amplifier is determined by the response time associated with the feedback resistor, R_F.

The equivalent circuit we have found to satisfactorily account for the dynamic behavior of this amplifier is shown in Fig. 7. Here L_S is the inductance of the source, L_F is the inductance of the feedback resistor, and L_L is the inductance of the null detector itself plus any stray inductance L' in the central loop not explicitly accounted for in the source or feedback resistor. Series inductances and not shunt capacitances are of primary importance in determining the frequency response of this circuit since the resistances involved are very small. The SQUID null detector has been

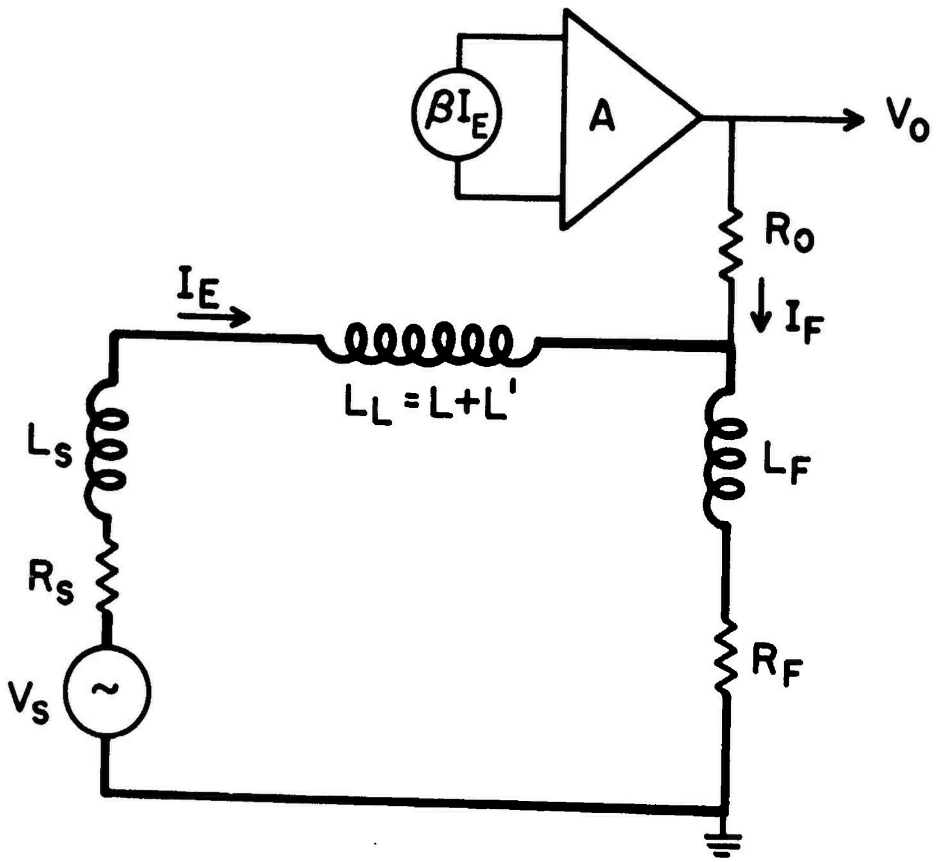

Fig. 7 SQUID amplifier circuit. The SQUID is modeled as a linear current controlled voltage source with output voltage to input current ratio β.

modeled as a current-controlled voltage source with output $V(I_E) = \beta I_E$. The amplifier in this figure stands for the entire chain of electronics (lock-ins, amplifiers, filter, etc.) which actually come between the SQUID detection circuits and the final feedback voltage.

B. Frequency Response and Bandwidth of the Amplifier

An approximate solution for the transfer function of the circuit shown in Fig. 7 is easily obtained. Summing voltages around the central loop we have

$$V_S = I_E(R_S + R_F) + \dot{I}_E(L_L + L_S + L_F) + I_F R_F + \dot{I}_F L_F \quad (3\text{-}1)$$

where because of feedback

$$I_F = \frac{A\beta I_E}{R_O} \equiv K I_E \quad . \quad (3\text{-}2)$$

Assuming V_S varies sinusoidally in time, we are led to the equation

$$V_S = I_E[R_T + i\omega L_T + (R_F + i\omega L_F)K] \quad (3\text{-}3)$$

where $R_T = R_S + R_F$, $L_T = L_L + L_S + L_F$ are the total loop resistances and inductances respectively. Finally, if $KR_F/R_T >> 1$ as is usually the case,

$$\frac{V_o}{V_S} = \frac{R_o}{R_F} \frac{1}{1 + i\omega(\tau_F + \tau_T R_T/KR_F)} \qquad (3\text{-}4)$$

where $\tau_F = L_F/R_F$ and $\tau_T = L_T/R_T$. From (3-4) we see that when $\tau_T R_T/KR_F << \tau_F$, the natural time constant of the loop, τ_T, drops out and that the bandwidth is ultimately governed by τ_F.

A more complete solution is obtained using elementary feedback theory. From (3-1) we see that the error current I_E produced by the source voltage V_S is given by

$$I_E = \frac{V_S - I_F(R_F + i\omega L_F)}{R_T + i\omega L_T} \quad . \qquad (3\text{-}5)$$

From this equation and Fig. 7, the block diagram of the feedback loop can be established by inspection and is shown in Fig. 8. In the circuit of Fig. 8 we have included the frequency response of the amplifier chain $A(\omega) = A_o/(1 + i\omega\tau_A)$ and we define $\beta \equiv M\partial V/\partial\Phi$ where M is the mutual inductance between L and the SQUID and $\partial V/\partial\Phi$ is the output voltage of the SQUID detection circuits (i.e. in our case the rf tank circuit) per unit flux change in the SQUID. Defining $G(\omega)$ as the forward transfer function and $F(\omega)$ as the feedback transfer function, the response of the closed loop is given by

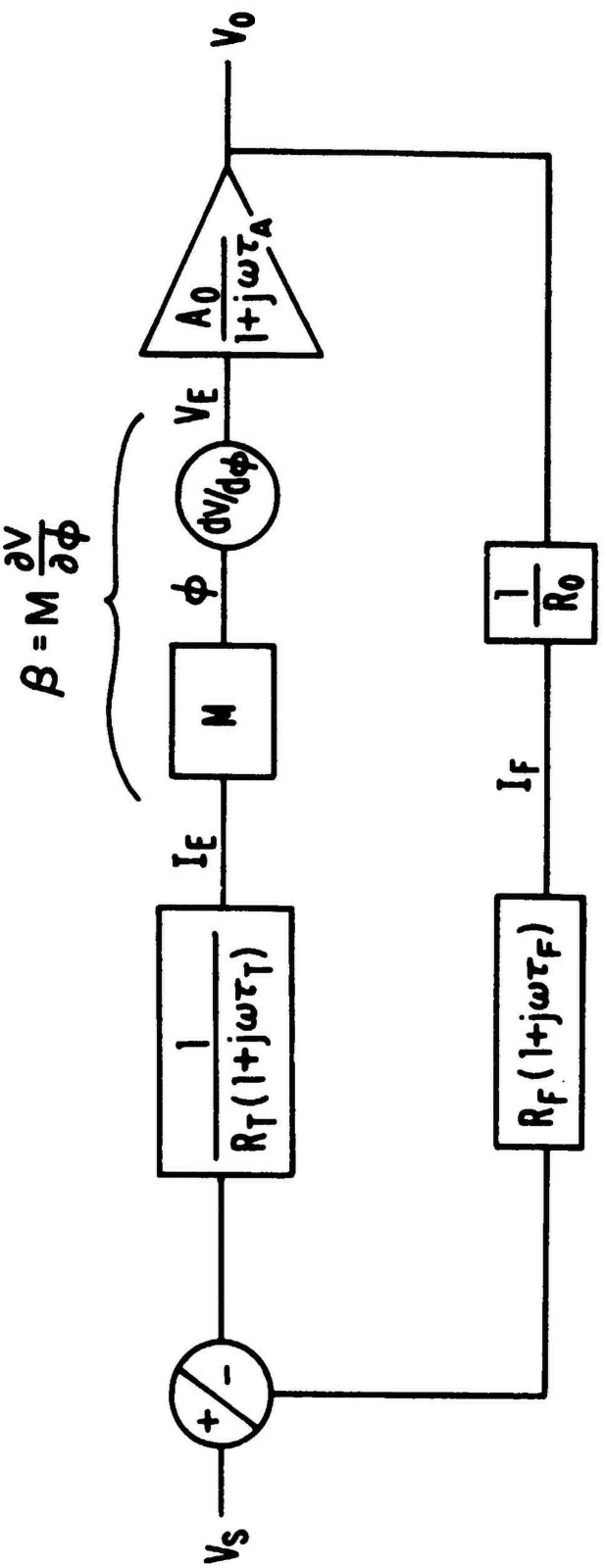

Fig. 8 SQUID amplifier block diagram. The inductive coupling to the SQUID and the frequency response of the amplifier chain are explicitly accounted for.

$$\frac{V_o}{V_s} = \frac{G}{1+FG} = \frac{R_o}{R_F}\left(1+\frac{1}{G(0)F(0)} - \omega^2\frac{\tau_A\tau_T}{G(0)F(0)} + i\omega\left\{\frac{\tau_A+\tau_T}{G(0)F(0)}+\tau_F\right\}\right)^{-1} \qquad (3\text{-}6)$$

where

$$G(\omega) = A_o\beta/R_T(1 + i\omega\tau_T)(1 + i\omega\tau_A)$$

$$F(\omega) = R_F(1 + i\omega\tau_F)/R_o$$

$$G(0)F(0) = KR_F/R_T = A_o\beta R_F/R_oR_T \quad .$$

When $\tau_A << \tau_T$, (3-6) reduces to (3-4), found above. Note, however, that if $\tau_A G(0)F(0)$ is larger than τ_T, the response of the system becomes peaked at a frequency ω_o

$$\omega_o = \sqrt{[G(0)F(0)/\tau_A\tau_T]} \quad .$$

It would be best not to operate in this region, not only since a flat response is usually preferable to a peaked one, but also to avoid instabilities in the feedback loop. (Although the loop as shown in Fig. 8 is completely stable, additional small phase shifts can lead to instability when the response is peaked.) Unfortunately, in practice it is not always possible to make τ_A sufficiently short to avoid these difficulties while simultaneously maintaining sufficient dynamic range in the amplifiers. These practical problems associated with increasing bandwidth are discussed in detail in section 3.2.

C. Noise Temperature of the Amplifier

Although the transfer function bandwidth is a consideration in a sensitive amplifier, its importance is secondary to the amplifier's noise performance. The transfer function may in principle be modified almost arbitrarily; the noise cannot. Poles or zeroes in succeeding stages can cancel zeroes or poles in preceeding stages, and feedback can be used to effectively decrease the response times of the passive components in the input circuit, as we have already seen for the specific case of the SQUID amplifier. None of these, however, can affect the noise characteristics of the amplifier, provided the first stage of amplification has high enough gain. This fundamental distinction between the transfer function and the noise of an amplifier can be made clear with the aid of Fig. 9a, which is the block diagram of a general feedback loop with two stages of forward gain, G_1 and G_2. Three noise sources, N_1, N_2, and N_3, have also been distributed between the stages. These generators specify an equivalent voltage or current noise density in units of volts/$\sqrt{Hz}$ or amperes/$\sqrt{Hz}$. With input signal IN the output of this loop will be

$$OUT = \frac{G_1G_2}{1 + G_1G_2F} (IN + N_1 + N_2/G_1 + N_3/G_1G_2) . \qquad (3-7)$$

It is apparent that only those noise sources that precede the

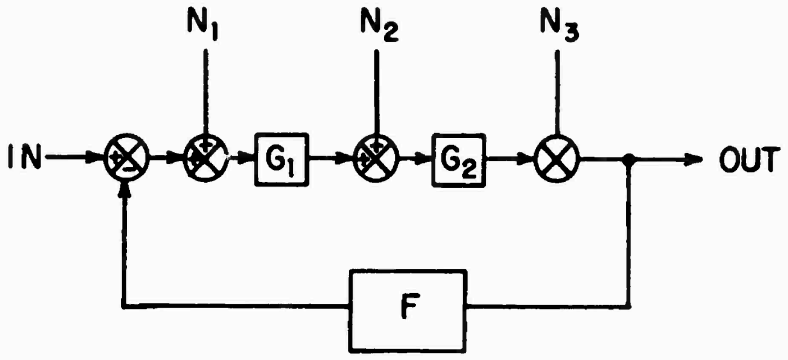

(a)

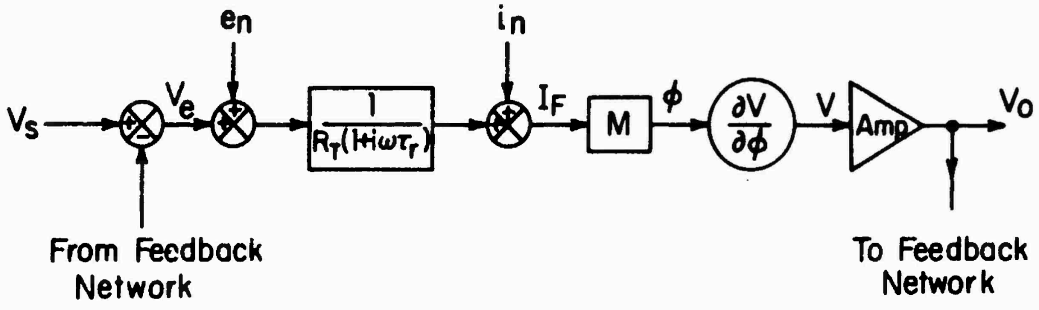

(b)

Fig. 9 a) Block diagram of feedback loop with distributed noise sources. b) SQUID amplifier block diagram with distributed noise sources.

first stage with large gain need be considered in an analysis of the noise of the amplifier. Further, since the feedback network, F, plays no role in determining the relative strengths of the signal and noise at the output, an open loop analysis is all that is required for any values of forward and feedback gain. Hence, the noise properties of the entire system are independent of both feedback and of additional stages of amplification beyond the first stage with high gain.

A convenient parameter used to specify the noise properties of any given amplifier is its noise temperature T_N. This quantity is defined as the extra temperature that must be added to the true temperature T of the source resistance to explain all the noise at the output of the amplifier as arising from Johnson noise in the source resistance. For the block diagram in Fig. 9a we have

$$|OUT|^2 \equiv 4k_B R_S(T + T_N) = 4k_B R_S T + |N_1|^2 + |N_2/G_1|^2 + |N_3/G_1G_2|^2$$

which can be solved for T_N:

$$T_N = (4k_B R_S)^{-1} \left(|N_1|^2 + |N_2/G_1|^2 + |N_3/G_1G_2|^2\right) \qquad (3\text{-}8)$$

Hence the noise temperature depends on the source resistance, the spectra of the noise sources, and the transfer functions

G_1 and G_2. If the noise temperature is less than the true temperature, then the Johnson noise of the source dominates over the amplifier noise, and a quieter amplifier is not ordinarily needed. If, however, the noise temperature of the amplifier is larger than the temperature of the source, then amplifier noise dominates over Johnson noise, and a quieter amplifier would yield increased sensitivity.

SQUID amplifiers can have extremely low noise temperatures. We may use the ideas developed above to obtain an expression for the noise temperature of the SQUID amplifier analyzed in the last section. The block diagram for that amplifier is presented in Fig. 9b with both a current and voltage noise generator present, and with the feedback network absent, since, it will have no effect on the magnitude of T_N. We need include only these two noise generators since they are the only ones to precede the first stage with high gain, which physically is the SQUID. If we identify e_n with N_1 and i_n with N_2, and $1/R_T(1+i\omega\tau_T)$ with G_1, we may substitute directly in (3-8) and obtain

$$T_N(\omega) = \frac{e_n^2}{4k_B R_S} + \frac{i_n^2 R_T^2 (1 + \omega^2 \tau_T^2)}{4k_B R_S} \qquad (3\text{-}9)$$

For the present discussion we will neglect e_n because in regimes where SQUID amplifiers have been operated the current noise term is the dominant one. This current noise generator

takes into account the noise generated physically in the SQUID itself and in the electronics that follow it, all referred back to the point in the block diagram where we have placed our current noise source. We could as well have placed our noise generator after the mutual inductance, M, in the block diagram, which would have made it an equivalent flux noise generator. Indeed, the noise in SQUID's has been conventionally specified as an equivalent flux power density[31] $\langle\Phi_n^2\rangle = \langle i_n^2\rangle/M^2$. We will not follow the convention here because it is an inferior scheme. Specifying the flux noise takes no account of the coupling[32] to the SQUID. A SQUID with very small flux noise but which also has a very small mutual inductance coupling it to the current to be measured may be less useful than a SQUID with slightly more flux noise, but a much bigger mutual inductance. Hence ignoring e_n for now, and making the further assumption that $R_S \simeq R_T$, we have for the noise temperature:

$$T_N(\omega) \simeq \frac{i_n^2 R_S}{4k_B}(1 + \omega^2\tau_T^2) \qquad (3\text{-}10a)$$

The explicit dependence on R_S may be removed by noting that $L/R_S = \tau_T$. Then defining $C \equiv L\langle i_n^2\rangle/4k_B$ we see that the low frequency noise temperature can be written

$$T_N(0) = C/\tau_T \ . \qquad (3\text{-}10b)$$

The quantity C, which we call the action factor after Radhakrishnan and Newhouse,[33] is a function only of the particular SQUID magnetometer used and is a useful figure of merit for the system. Equation (3-10b) shows that for a given SQUID magnetometer (hence a given C), the noise temperature of the amplifier depends only on τ_T. Substituting the representative values $\langle i_n^2 \rangle = (2\text{x}10^{-10}\text{amp})^2$, and $L = 10^{-6}$ H we find that $C \simeq 10^{-3}$ K sec. Note that the current sensitivity quoted above corresponds to a flux sensitivity of only about $10^{-3}\ \Phi_o$, where $\Phi_o = 2.07\text{x}10^{-15}$ weber is the flux quantum. The best SQUID's to date, when operated in a well shielded environment, have demonstrated a noise power density that yields $C \simeq 10^{-6}$ Ksec. For our SQUID at its best, the action factor is $C = 5\text{x}10^{-5}$ Ksec. We expect that better shielding would yield a lower value.

Equation (3-10b) shows that the minimum noise temperature of a given SQUID amplifier is directly proportional to the bandwidth over which that minimum is available, and that the minimum noise temperature is independent of source resistance so long as τ_T is kept constant. Thus if a SQUID amplifier is capable of a 10^{-5} K noise temperature with $\tau_T = 1$ second, it is also capable of a 1 K noise temperature with $\tau_T = 10^{-5}$ second. If τ_T is specified, then (3-10b) specifies $T_N(0)$. One is left, then with the problem of reconciling a given source resistance with the τ_T required by a

desired value of $T_N(0)$. This can be done within limits either directly by physically changing the coil L or indirectly by using impedance matching transformers, as described in the next section. In practice, however, L and the transformer turns ratio cannot be varied continuously but are chosen so as to put τ_T and $T_N(0)$ more or less in the desired range. Once L and the transformer are fixed, $T_N(0)$ is proportional to R_S. Specific contours of $T_N(\omega)$ are discussed later. As we shall see it is possible to get noise temperatures in the sub-Kelvin regime even at source resistances in the tens of ohms range by using transformers. Above ten ohms conventional room-temperature amplifiers with noise temperatures in the liquid helium temperature range are available, although unlike SQUID amplifiers, they have very poor performance at very low frequencies.

D. Impedance Matching Transformers

As indicated above, impedance matching transformers play an important role in extending the range of source impedances over which SQUID amplifiers can be profitably employed. The function of the transformer can be viewed in two equivalent ways. One can view the transformer as stepping the impedance level of the source down (or up) to a level at which, for a given L, τ_T and $T_N(0)$ are in the desired range. Alternatively one can view the transformer as stepping up (or

down) the effective inductance of the SQUID coil. In any case, for a perfect transformer $\tau_T = (N_p/N_s)^2 L/R_s$, where N_p/N_s is the primary to secondary turns ratio of the transformer and (3-10b) remains valid if τ_T is taken as the loop time constant with the transformer present. In practice transformers are not perfect, but if reasonable care is taken in constructing the transformer, (3-10b) remains valid where the action factor C is increased roughly by a factor of two as shown below.

To analyze the operation of the transformer in detail consider the SQUID coil L coupled to the bridge circuit through a transformer with mutual inductance M', primary inductance L_p and secondary inductance L_s. No resistance need be considered, even at dc, since only superconducting components are involved. By elementary circuit analysis a current I_p in the transformer primary produces a current I_s in the secondary given by

$$I_s = -I_p \frac{M'}{L + L_s} = -I_p \, k'\alpha \frac{L_s}{L + L_s} \qquad (3\text{-}11)$$

where $\alpha = (L_p/L_s)^{1/2}$ and k' is the coupling coefficient of the transformer. The effective inductance seen by the current I_p is

$$L_{eff} = \alpha^2 L \left(\frac{L_s}{L + L_s} \right) [1 + (1 - k'^2) L_s/L] \, . \qquad (3\text{-}12)$$

For an ideal transformer in which k' = 1 and $L_s >> L$, $\alpha = N_p/N_s$ and $L_{eff} = (N_p/N_s)^2 L$.

When a superconducting transformer is used in the circuit of Fig. 6, the expression for the noise temperature becomes

$$T_N(\omega) \simeq \frac{\langle i_n^2 \rangle R_S^2 \ (1 + \omega^2 \tau_T^2)}{4k_B \alpha^2 \ k' \ (L_s/[L+L_s])^2}$$

$$\simeq \frac{\langle i_n^2 \rangle R_S}{4k_B} \ (1 + \omega^2 \tau_T^2) \ f(k', L/L_s) \qquad (3\text{-}13)$$

which is the same result found before, in (3-10a), but with a correction factor $f(k', L_s/L) = (1+L/L_s)(1+[1-k'^2]L_s/L)/k'^2$ that accounts for the non-idealities of the transformer. For fixed k', the function f has a minimum for $L/L_s = \sqrt{(1-k'^2)}$. Thus, in order to achieve optimal performance one not only wants to make k' as close to unity as possible, but one also must have $L_s \simeq L(1-k'^2)^{-1/2}$. For real transformers, where with care $0.9 < k' < 0.95$, f is nearly optimized for values of L/L_s in the range $0.25 < L/L_s < 0.65$. Moreover, under these conditions $2.0 < f_{opt} < 2.5$. Thus the requirements for optimization are not demanding, and useful design formulae when a tra sformer is used are:

$$C \equiv T_N(0)\tau_T = 2.25 \ \frac{\langle i_n^2 \rangle L}{4k_B} \qquad \text{K sec} \qquad (3\text{-}14)$$

$$T_N(\omega) \simeq \frac{2.25\langle i_n^2\rangle R_S}{4k_B}\,(1 + \omega^2\tau_T^2) \qquad K \qquad (3\text{-}15)$$

3.2 CONSTRUCTION AND PERFORMANCE OF SQUID AMPLIFIER AND SUPERCONDUCTING TRANSFORMER

A. Construction

A SQUID amplifier divides naturally into two parts: the bridge circuit and impedance matching transformer operating at low temperatures, and the conventional electronic circuits at room temperature used to process the SQUID signal and generate the feedback current. Except for the transformer, which is described in detail below, the construction of the low temperature circuitry is straightforward. The null detector is made by placing a supercondcuting coil in the sensing area of a SQUID magnetometer. For application with high source resistances, this coil should be as large as possible consistent with good coupling to the SQUID. For our system we used a 70 turn single-layer coil wound using 0.01 cm niobium wire on a 0.2 cm diameter coil form. The self inductance of this coil was 1.0 microhenry. The SQUID was a standard double-hole Zimmerman-type rf SQUID.[13] For test purposes R_S and R_F were constructed using short lengths of various types of alloy wire whose lengths were chosen so as to obtain resistances in the range 10^{-3} to 1 ohm. Test signals were generated by driving R_S with a current source. The

null detector and associated low-temperature circuitry were enclosed in a superconducting lead shield and immersed directly in the liquid helium. Further shielding was provided by two concentric mu-metal shields that surrounded the entire liquid helium dewar system. Although all low-frequency signals entering the dewar were routed through low-pass filters, the radio-frequency shielding was not completely adequate for operation outside a screened room, and the performance of the SQUID suffered accordingly. Well shielded or not, the null detector circuit is quite standard and similar to that used widely in voltmeter applications. It is the room-temperature electronics and the impedance matching transformer which must be carefully designed to achieve wide-band, low-noise performance.

Most SQUID voltmeters incorporating feedback have been restricted to dc applications by instabilities in their feedback loops. However, the SQUID amplifier modeled in Fig. 8 is completely stable, since at no frequency is the loop gain unity or larger with a phase shift of 180 degrees. Real SQUID voltmeters, with real instabilities, then, are not perfectly modeled by Fig. 8: they have additional phase shifts introduced at various points in the room temperature electronic circuits which are not accounted for in the model. These additional phase shifts typically arise from the tuned circuit at the front end of the lock-in amplifier. Further,

many commercial lock-in amplifiers have more than a strictly 6 db per octave roll-off in their output amplifiers, and there is an extra phase shift associated with this faster roll-off. Finally, capacitive feed-throughs used as rf filters on cryostat leads may also introduce unwanted phase shifts. If bandwidth is to be preserved, it is necessary to control these stray phase shifts with carefully designed and selected electronics.

The schematic of a SQUID amplifier found to be adequately free of instabilities is shown in Fig. 10. In order to minimize stray phase shifts this circuit incorporates a balanced mixer rf detection scheme, which allows low-noise detection without tuned circuits, and a wide-band lock-in amplifier. This home-made lock-in has an input amplifier that is flat from a few kilohertz to nearly one megahertz and therefore is free of significant phase shifts in the 10 to 100 kilohertz range. Moreover, the output section of the lock-in is a broadband operational amplifier set up as a low-pass filter with a strictly 6 db per octave roll-off. The time constant of this roll-off is adjustable in steps from 1.5×10^{-1} to 1.5×10^{-5} second. There is also a switch to change the op-amp from its usual low-pass filter function to an integrate function for high accuracy, low-frequency applications. An external audio oscillator drives the SQUID and provides a reference for the lock-in amplifier. This

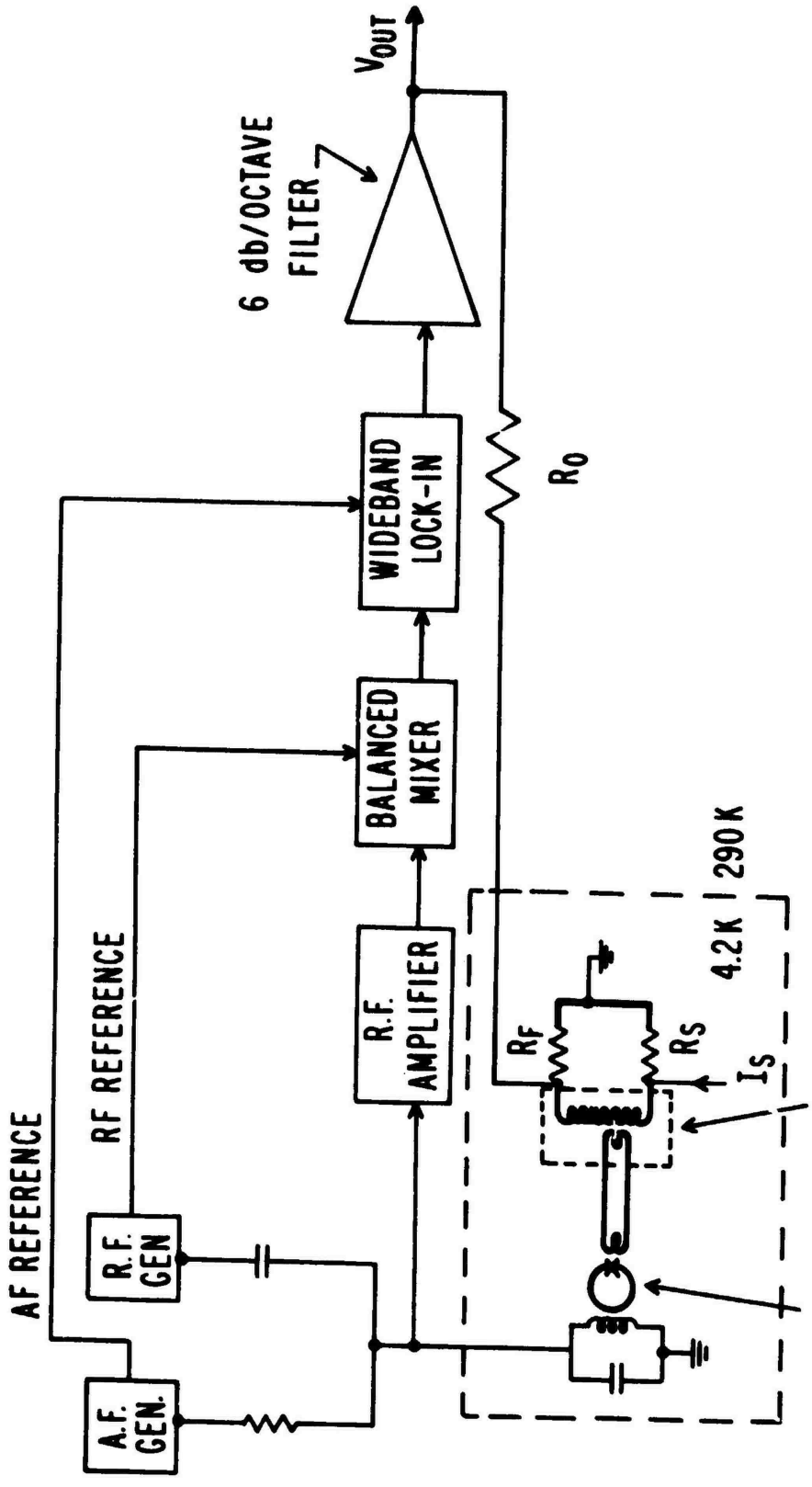

Fig. 10 A practical SQUID amplifier schematic diagram. A wideband lock-in amplifier is incorporated to minimize stray phase shifts.

system was found to be free of instabilities and described very well by the amplifier equivalent circuit analyzed in section 3.1. The detailed comparison of the expected and observed performance is presented later in this section.

While careful attention to the room temperature electronics is necessary for wide-band performance, the superconducting impedance matching transformer is the key to the excellent noise performance of SQUID amplifiers at any but the lowest source resistances. Considerable effort was expended on building a transformer with good performance. The theoretical considerations involved in the design of these transformers were described in section 3.1 D. Here we discuss the practical design considerations and the actual construction. A satisfactory transformer design is shown in Fig. 11. It is an "air core" transformer in which good coupling between the primary and the secondary is obtained by means of a flux conduit formed by a superconducting sheath wrapped around the transformer windings as shown. Because of the perfect diamagnetism (Meissner effect) of the sheath, the flux produced by the transformer coils is constrained to pass through the tube formed by the sheath, assuring good coupling between primary and secondary. It is important that this sheath be singly connected, since if it is multiply connected, circulating currents that cancel the flux produced by the windings will be induced, thereby

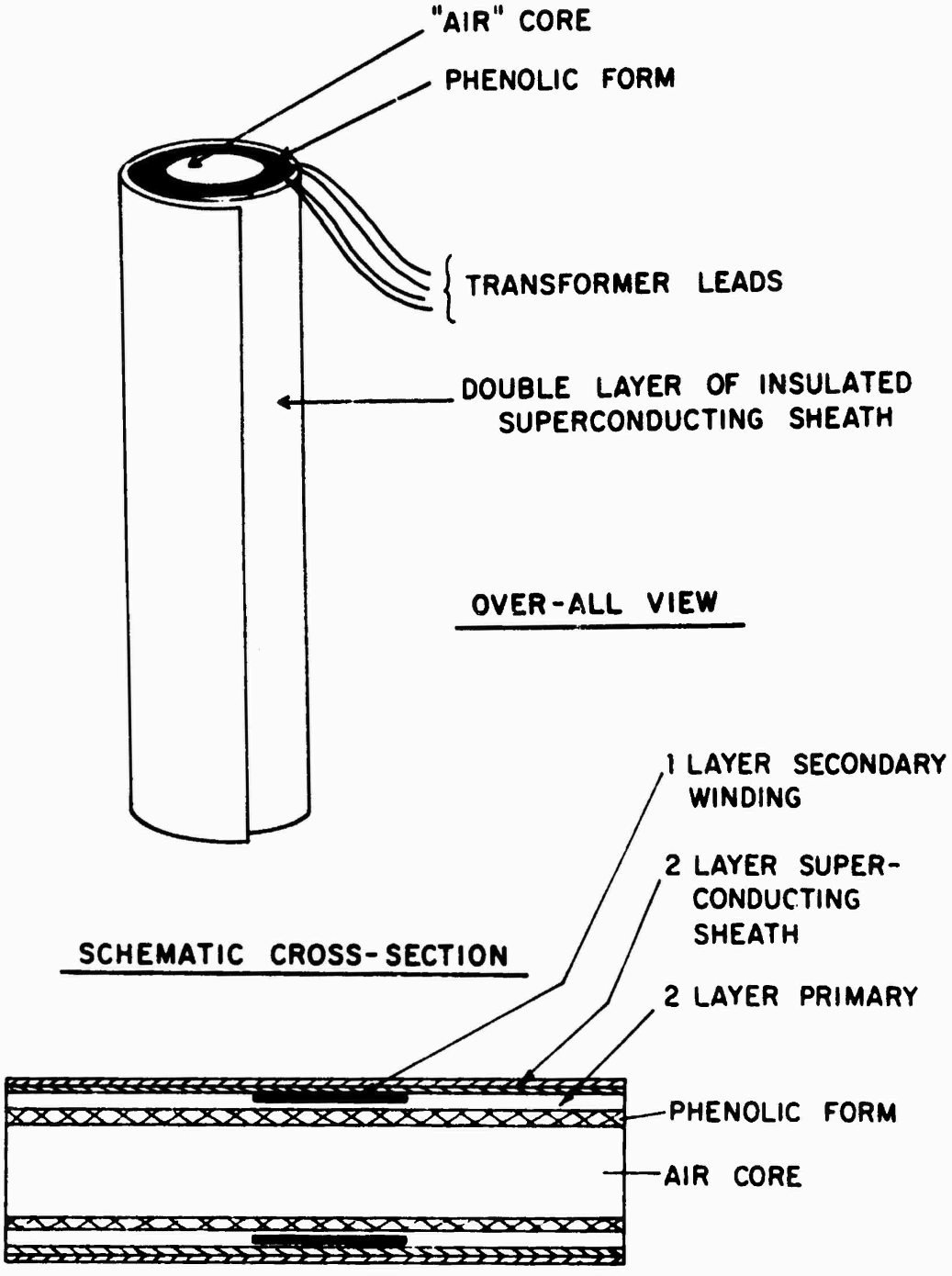

Fig. 11 Construction details of the superconducting impedance matching transformer.

hindering transformer action.

Our most successful transformer, constructed as descibed above, had a 1439-turn, two layer primary and a 30 turn, single layer secondary. The primary was wound using 0.01cm Nb-Ti along the entire length of a 1.27 cm diameter by 7.6 cm long phenolic tube. The secondary, also 0.01 cm Nb-Ti wire, was a shorter coil wound tightly over the primary as shown in Fig. 11. The superconducting sheath was formed by winding two complete layers of 0.0025 cm niobium foil around the entire length of the transformer. Insulation between the layers was provided by a 0.0025 cm thick mylar sheet. The current gain of this particular transformer, when coupled to the one microhenry SQUID coil, was 22, and the coupling constant was measured to be 0.9. The primary self-inductance was approximately 4×10^{-3} henry; the secondary self-inductance was approximately 5×10^{-6} henry; and the effective inductance of the primary when the transformer was coupled to the SQUID was about 7×10^{-4} henry. All these parameters are self consistent in view of the theory presented in section 3.1. Also, according to that theory, this transformer would have been better optimized if the secondary self-inductance were 3×10^{-6} instead of 5×10^{-6} henry. Possible improvements would be the inclusion of a high permeability core for larger current gains and the incorporation of taps along the primary to provide versatility in impedance matching.

Using this transformer we have achieved a 4 K noise temperature over a two-hundred hertz bandwidth with a one ohm source impedance. Improved rf shielding or operation in a screened room should improve this noise temperature by more than an order of magnitude.

B. Performance

Both experimental and theoretical transfer function amplitudes are displayed in Fig. 12. The fit, with no adjustable parameters, is quite good, even for the high-Q situation. The quality of the fit indicates that the feedback circuit is modeled very well by the block diagram in Fig. 8, and that (3-6) and (3-10) may be used with confidence to control and predict the characteristics of the SQUID amplifier. Notice that the lower loop gain corresponds to the lower Q transfer function. The loop gain was restricted to these low values for the parameters given in the figure by a requirement for broad bandwidth with a minimum Q. The Q derived from the model is $Q^2 = F(0)G(0)\tau_A/\tau_T$, under the usual conditions that $\tau_A << \tau_T$ and $\tau_T >> G(0)F(0)\tau_F$. Hence, if we require that $Q = 1$, we have a reciprocal relation $G(0)F(0)\tau_A = \tau_T$ between the loop gain and τ_A. If τ_A were smaller, more gain could have been used while not increasing Q, but this would have required a lock-in whose output amplifier could handle the larger dynamic range required due to

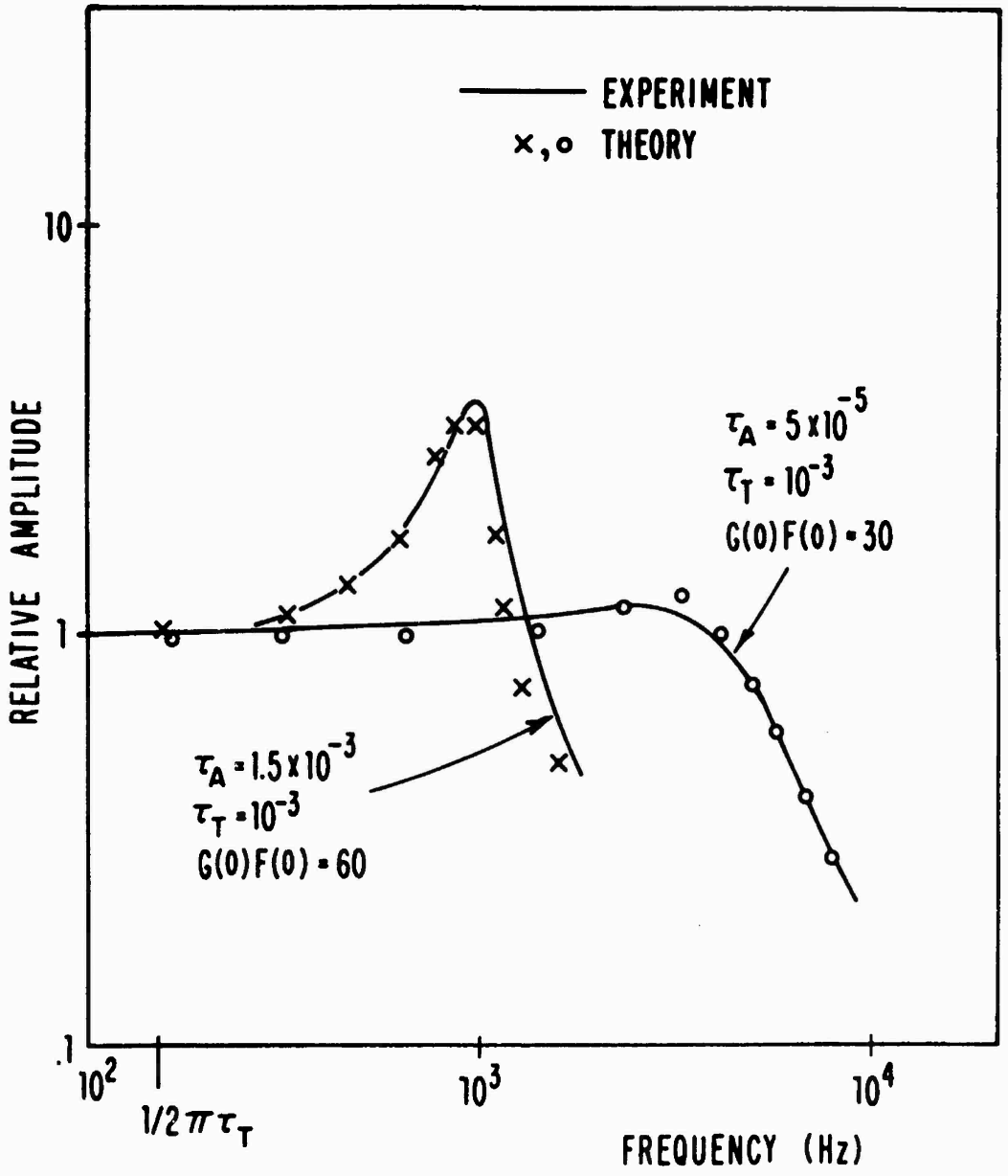

Fig. 12 Frequency dependence of the transfer function on τ_A and G(0)F(0). For the data shown, $\tau_T=10^{-3}$ sec and $R_T=0.11$ ohm.

the extra noise bandwidth. Hence, for the curves shown we were restricted to relatively low loop gain by the dynamic range of the lock-in amplifier. This is not a fundamental limit, however, since with a better lock-in there would be nothing to prevent a bandwidth out to $1/\tau_F$.

Just as the transfer function of the SQUID amplifier follows closely the predictions of the model, so does the output noise spectrum. This spectrum may be written in terms of the noise temperature given by (3-8) in section 3.1:

$$\langle V_N^2 \rangle^{1/2} = [(4k_B R_T (T_N(\omega) + T)]^{1/2} \qquad \text{volts/Hz}^{1/2}$$

where T, the helium bath temperature, is the temperature of the source resistance and R_F. This formula predicts a spectrum with a flat low-frequency region followed by a 6 db per octave rise through the pass band defined by the transfer function,(3-6), and this behavior is precisely what is observed, as shown in Fig. 13. Note that the flat, low-noise region exceeds the intrinsic low-noise bandwidth governed by $1/\tau_T$ by a substantial amount because for the case shown the amplifier noise temperature at low frequencies is substantially below T. If R_T is known and the noise spectrum is measured, the amplifier noise temperature may be calculated from the formula above and contours plotted as a

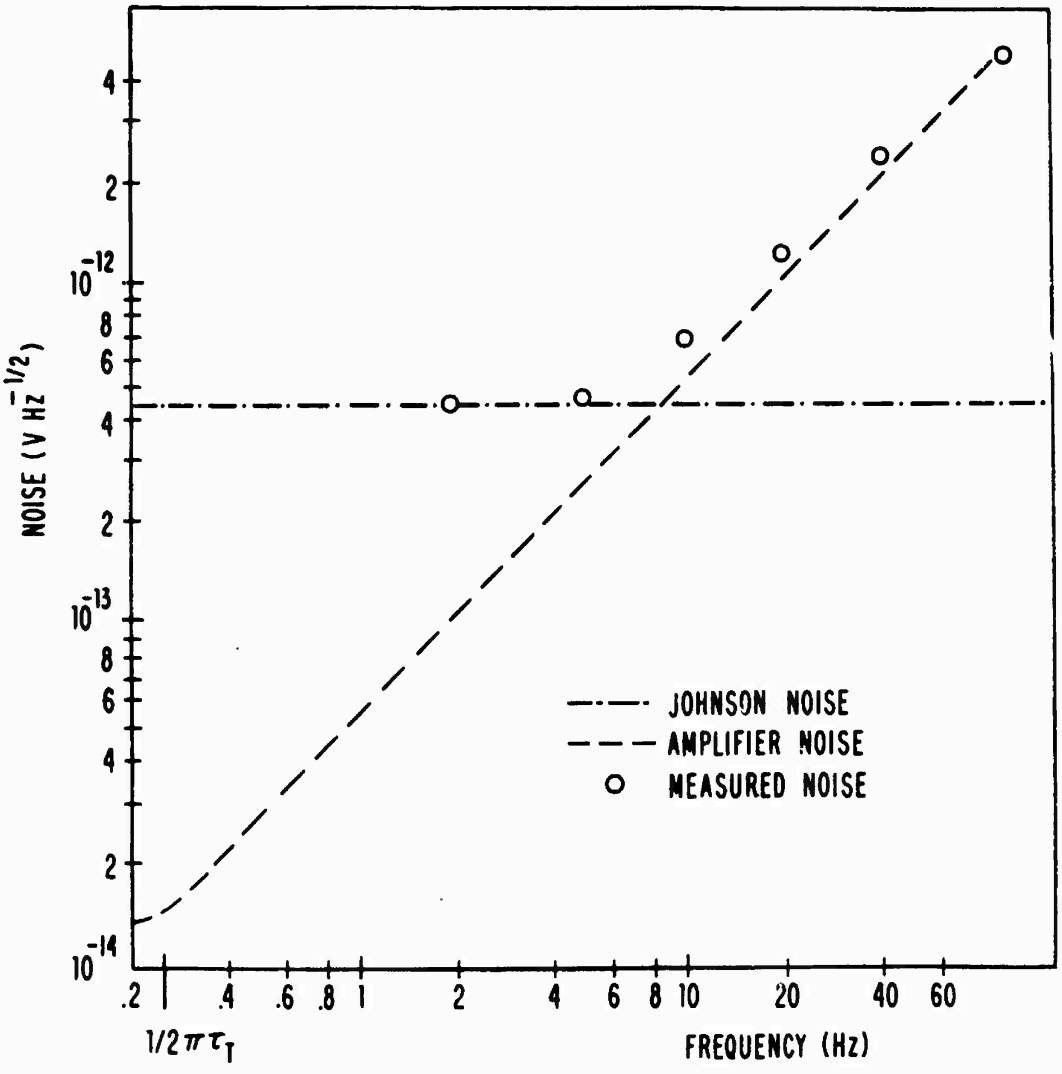

Fig. 13 Frequency dependence of the voltage noise spectral density, referred to the input, for τ_T=0.7 sec and R_T=10^{-3} ohm.

function of frequency and source resistance. These noise contours, crucial for choosing between amplifiers, are shown in Fig. 14. The contours plotted in this figure were calculated from (3-10) with empirical verification at several points. The action factor, C, that these curves imply is about 2×10^{-4} K sec. This figure was achieved without a transformer; when a transformer was used C was found to be larger by an order of magnitude, rather than the factor of two expected on the basis of (3-15). This degradation was caused, we believe, by inadequate shielding of the transformer and we fully expect a well shielded SQUID amplifier to be characterized by a value of C of 10^{-5} K sec or less.

3.3 COMPARISON WITH CONVENTIONAL AMPLIFIERS

We have shown so far that SQUID amplifiers have a list of desirable characteristics for low temperature, low impedance applications, but we have not yet shown over what domains these characteristics provide performance superior to that achieved with conventional semiconductor technology. Perhaps the best way to outline these superior domains is to make a direct comparison to a potentially competing conventional amplifier. To our knowledge the best such amplifier is the Princeton Applied Research (PAR) Model 185. This comparison will cover three broad areas: frequency response, characteritic impedance levels, and noise. It is important

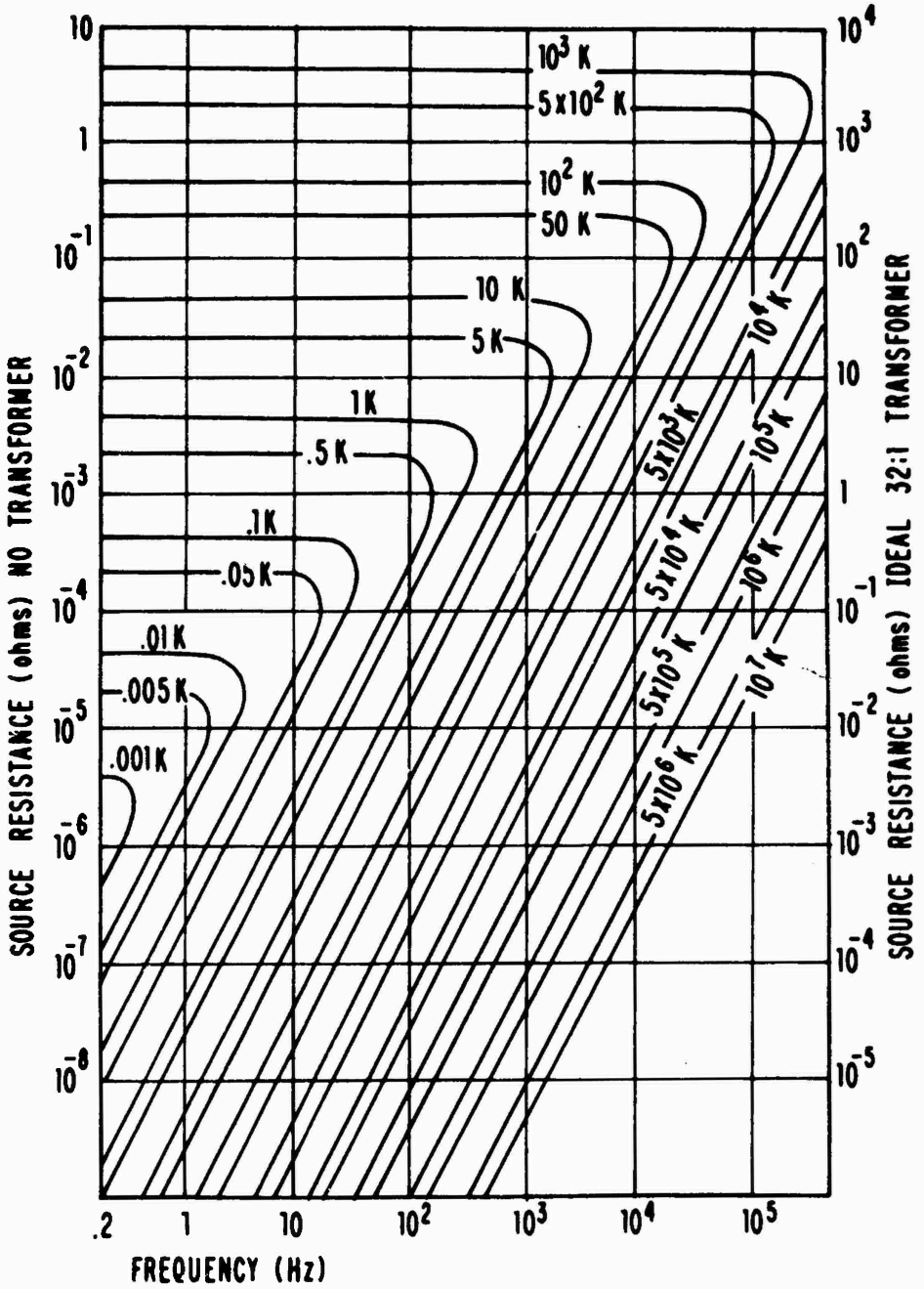

Fig. 14 Typical noise contours of SQUID amplifier. The verical scale is calibrated on the left for coupling without a transformer, and on the right for coupling with an ideal 32:1 transformer.

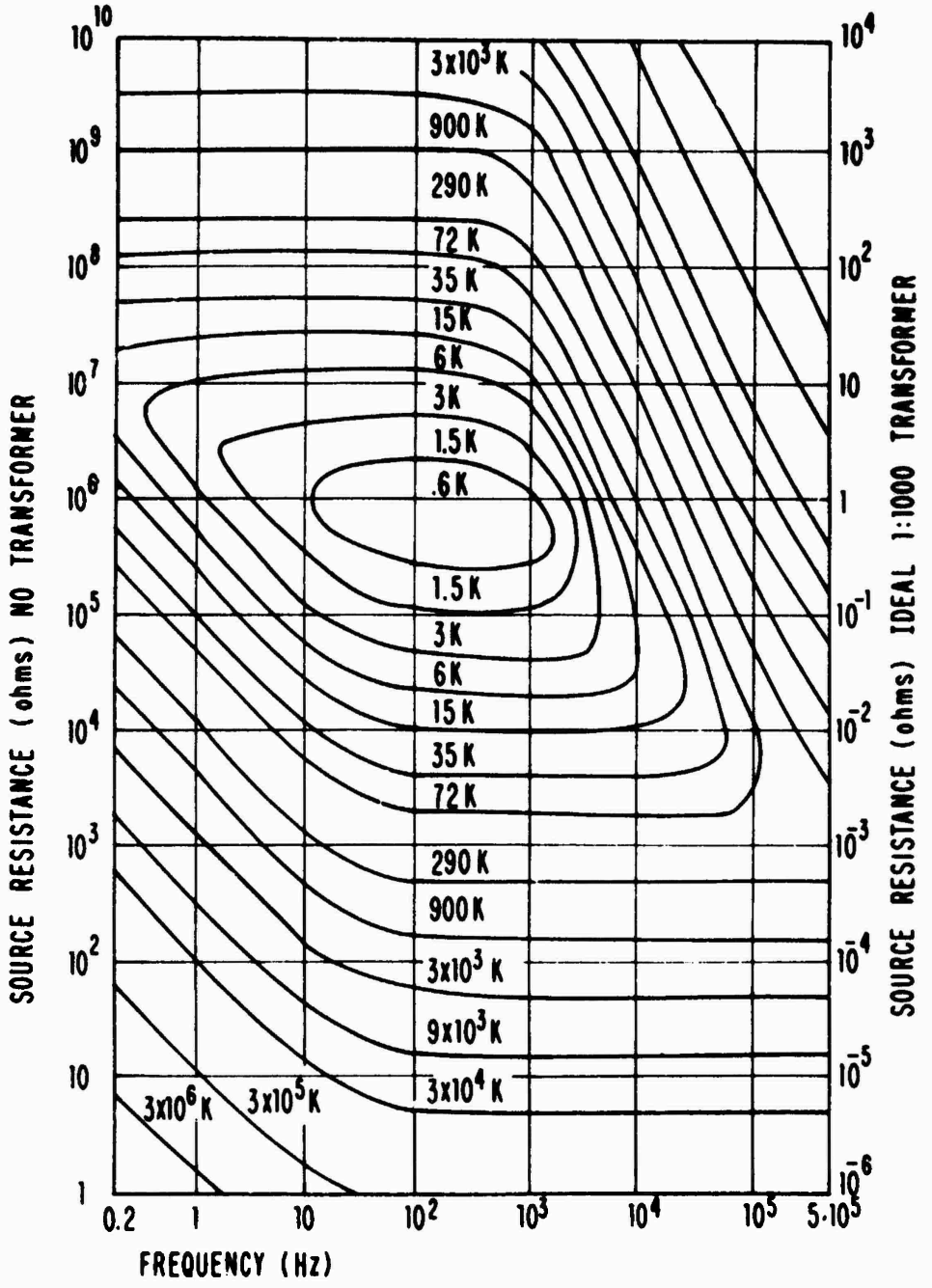

Fig. 15 Noise temperature contours for the PAR 185 amplifier. The vertical scale is calibrated on the left for coupling without a transformer, and on the right for coupling with an ideal 1:1000 transformer.

to clearly state the conditions under which comparisons are made and to realize that different conditions can lead to different conclusions. Since the potential applications of SQUID amplifiers are at low impedance, we will first assume that both the SQUID and PAR 185 amplifiers are coupled through appropriate ideal transformers to handle a one ohm source resistance. We may then compare the frequency response directly; the impedance levels indirectly through the required transformer characteristics; and noise using noise temperature as a parameter. Noise temperature, rather than noise figure, is the most convenient parameter for this comparison since the two types of amplifiers operate at different temperatures and a given noise figure means different things at different temperatures.

If we restrict the comparison to our present imperfectly shielded experimental SQUID amplifier and the PAR 185 commercial amplifier, each coupled with an appropriate ideal transformer to a one ohm source resistance, we may state broadly that the PAR 185 is a broad-band, high impedance, 0.6 K instrument, while the SQUID amplifier is a narrow-band, low impedance, 10^{-6} K device. The noise performance and impedance levels are indicated in Figs. 14 and 15, while frequency response, assuming ideal transformers, may be taken to be the manufacturers rated megahertz for the PAR 185, and several kilohertz for the SQUID amplifier. The

noise temperature contours in Figs. 14 and 15 indicate that for low-noise operation with a source resistance of an ohm or so, a 1:1000 turns ratio is necessary for 0.6 K operation of the PAR 185, which is indicative of the high input impedance of that amplifier, while only a 30:1 turns ratio is necessary for a 0.5 K noise temperature for the SQUID, which similarly follows from its low impedance nature. The PAR 185 is incapable of providing a lower noise temperature than 0.6 K whatever turns ratio is used, while the SQUID amplifier is potentially capable of 10^{-6} K performance over some small bandwidth with a 1000:1 turns ratio. Hence, if ideal transformers were available, the PAR would be superior to the SQUID for source temperatures down to $\sim$0.6 K because of its broader bandwidth. Below 0.6 K, however, the SQUID is unmatched by any conventional amplifier.

If we remove the unreasonable assumption of ideal transformers, the SQUID becomes superior to conventional amplifiers even above 0.6 K. To provide a 0.6 K noise temperature at one ohm the PAR requires a 1:1000 transformer. Such transformers are difficult to wind in any manner approaching the ideal over a broad bandwidth. In practice because of these nonidealities the frequency response of the conventional high impedance amplifier will drop to a few kilohertz at best and the minimum achievable noise temperature may rise slightly due to noise in the non-ideal transformer.[34] Since

the SQUID requires only a relatively small 30:1 ratio transformer, and since transformers of this size may be wound to approximate the ideal over at least several kilohertz, the SQUID's frequency response will not suffer to any large degree and performance at less than 0.6 K is still easy to achieve. Further, the SQUID's excellent performance near zero hertz is unchanged when using superconducting transformers. Hence, for a one ohm source impedance coupled through real transformers the SQUID has a bandwidth comparable to the PAR, with much better noise performance and unhindered zero frequency characteristics.

An additional important way to compare the two amplifiers is to couple them without transformers and map out their performance. If we refer to Figs. 14 and 15 and read noise temperature from the contours at the frequency for each amplifier that provides the best noise performance at a particular source resistance, we derive the graph in Fig. 16. This graph displays clearly the gulf between the two amplifier technologies. Semiconductor technology provides good noise performance at the megohm level, while the superconductor technology provides excellent noise performance at the milliohm level and below. The gulf between these two regions, centered around 30 ohms, may be traversed only with the use of transformers. It is evident, then, that although a SQUID amplifier is not ideally suited to every helium

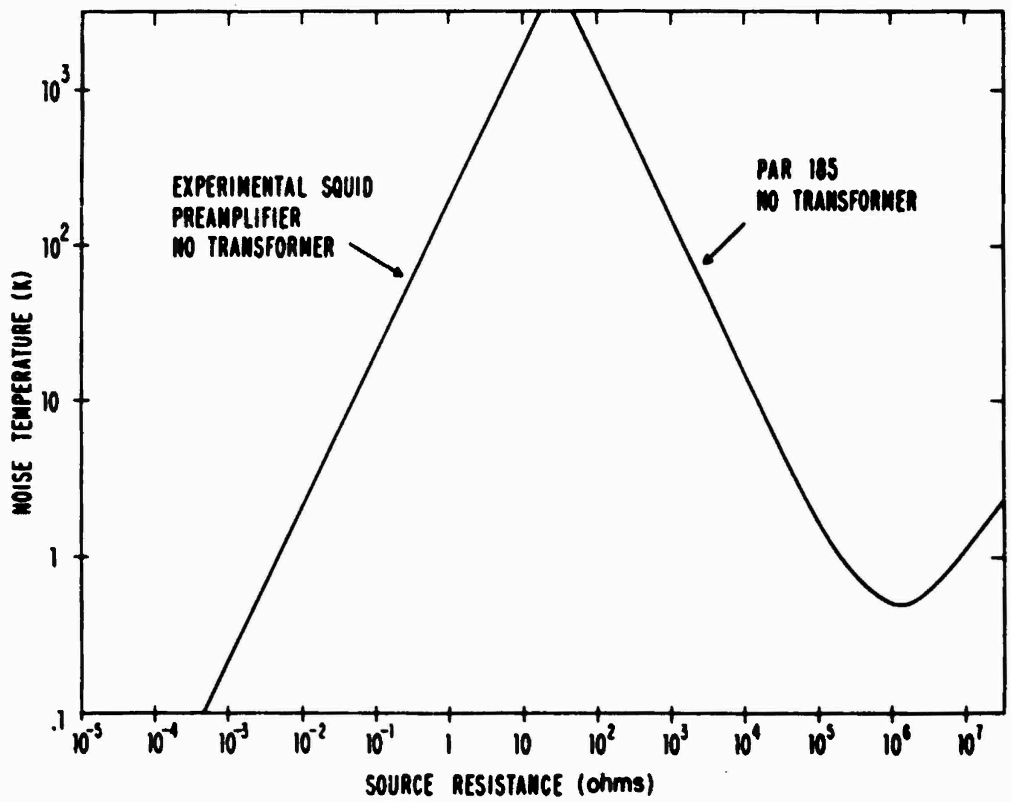

Fig. 16 Minimum noise temperature as a function of source resistance without transformer coupling for a typical SQUID amplifier and the PAR 185 amplifier. For each source resistance the noise temperature indicated corresponds to the frequency at which T_N was minimum.

temperature application, it does provide a versatile and very low noise complement to conventional technology for low impedance applications.

CHAPTER FOUR: DUALITY AND NOISE

The complementary relationship between SQUID and conventional amplifiers is in fact quite formal: the two are duals. This duality puts into perspective both the previous chapter on SQUID amplifier characteristics and some pioneering work of Newhouse[8,33] on cryotrons. We show in this chapter that metal-oxide-semiconductor field-effect transistor (MOSFET) electrometers are precisely dual to superconducting magnetometers; that superconducting voltage amplifiers are dual to MOSFET current amplifiers; and that the noise characteristics of one device are dual to the noise characteristics of the other. The duality principle then suggests that the action factor discussed here and by others in the context of superconducting amplifiers[32,33] also applies to high impedance conventional amplifiers. However, the same principle means that the action factor is not a sufficient characterization of SQUID's, and that a minimum noise temperature and an associated optimum source resistance are other necessary characterizations.

4.1 Duality

Two electrical networks are said to be duals of one another if they obey identical equations, but with the roles of current and voltage reversed. Dual networks may be

recognized or generated by inspection if certain rules are followed: if a given network contains resistances, inductances, capacitances, and voltage and current sources, the dual network contains respectively conductances, capacitances, inductances, and current and voltage sources. Further, a parallel combination of components in one network is replaced by a series combination of dual components in the dual network (in other words, the dual to an impedance is an admittance), and, correspondingly, a series combination is replaced by a parallel combination. For example, a resistive voltage divider network is the dual of a conductive current divider, and a parallel R-C filter is dual to a series G-L filter, where G is a conductance.

If we refer to Fig. 17 and apply the same ideas to the input circuit of a conventional high impedance semiconductor amplifier (Fig. 17a) we obtain the input circuit to a low impedance amplifier (Fig. 17b) with a set of unusual properties. First, it is current sensitive, rather than voltage sensitive. Where stray capacitance, C_s, is important in Fig. 17a, a stray inductance, L_s is important in Fig. 17b. Where the high impedance amplifier may be limited by a parasitic parallel resistance, which ideally should be infinite, the low impedance amplifier is limited by a parasitic series conductance, which, again should ideally be infinite. The high impedance amplifier depends on capacitively coupling an

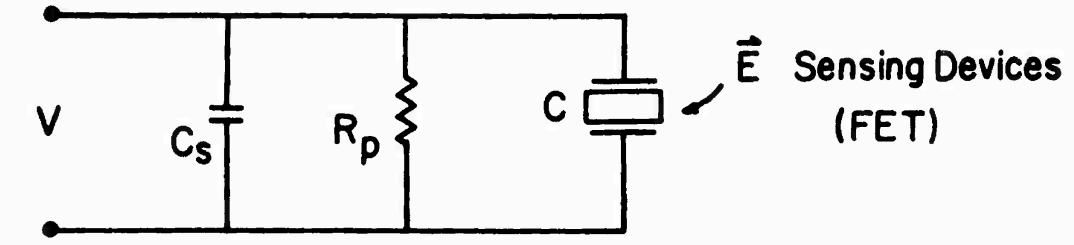

(a)

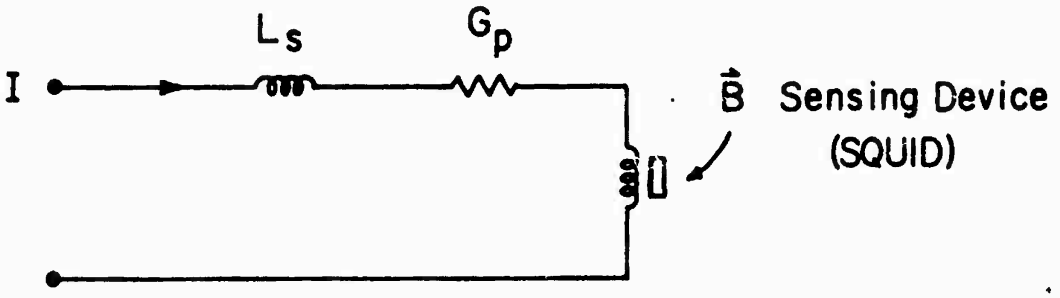

(b)

Fig. 17 a) Lumped MOSFET input circuit model. b) Dual to MOSFET input circuit.

electric field to a suitable sensing device, while the low impedance amplifier depends on inductively coupling a magnetic field to a suitable sensing device. Finally, each circuit functions as a low pass filter (they obey identical differential equations) where the high impedance circuit has a time constant $\tau = RC$, while the dual circuit has time constant $\tau = GL$. The high impedance circuit presented in Fig. 17a is a good description of a MOSFET amplifier, and its dual in Fig. 17b is a good description of a SQUID amplifier. This correspondance is not unique, however, since vacuum tubes would qualify as high impedance amplifiers described by Fig. 17a, while cryotrons or single Josephson junction devices would be well characterized by Fig. 17b.

A. Flux and Charge Transporters

Duality between two devices means that concepts developed for one can be applied in dual form to the other. As an interesting example of this principle, we show that the flux transporter[35] used to couple SQUID magnetometers to a field to be measured, has a dual in FET electrometers. A flux transporter consists of two superconducting inductors connected in a loop with superconducting wire. One coil, say L_1, is coupled to the unknown field, and the other, L_2, is coupled to the SQUID magnetic field sensor. Since the total number of flux linkages in such a multiply connected config-

uration of superconductors must be conserved, a change in the field applied to L_1 is reflected as a change in the field produced by L_2. If N_1 and N_2 are the number of turns in coils 1 and 2 respectively, and Φ_1 and Φ_2 are the net magnetic fluxes, then the conservation of flux linkages requires

$$N_1\Phi_1 + N_2\Phi_2 = 0 \tag{4-1}$$

where we have assumed an initial state of zero flux in each coil. But if Φ_a is the flux applied to L_1 and I is the resulting current flowing in the transporter circuit, then the flux in each coil can be written

$$\Phi_1 = \Phi_a + IL_1/N_1 \tag{4-2a}$$

$$\Phi_2 = IL_2/N_2 \tag{4-2b}$$

Equations (4-1) and (4-2) are sufficient to solve for Φ_2 in terms of Φ_a with the result

$$\Phi_2 = -\frac{N_1}{N_2}\,\Phi_a\,\frac{L_2}{L_1 + L_2} \tag{4-3}$$

Hence if the SQUID sensor cannot be placed directly in the field, the field can be transported from L_1 to L_2 with the SQUID coupled to L_2.

The flux transporter works by conserving flux linkages, and its dual may be found by finding the dual to flux linkages. But the flux linkages are given by $N\Phi = LI$, so the dual quantity must be total charge: $Q = CV$, since C and L and V and I are duals. Indeed, if a field is applied to one of two parallel capacitors a proportional field will be induced in the other capacitor due to the conservation of total charge. Let the capacitor coupled to the unknown field be C_1 with area A_1, and the other, coupled to the electrometer, be C_2 with area A_2. Then, if D_1 and D_2 are the electric displacement fields associated with each capacitor, the conservation of total charge means that

$$A_1D_1 + A_2D_2 = 0 \qquad (4\text{-}4)$$

where we have assumed an initial state of zero charge on each capacitor. But if D_a is the field applied to C_1, and V is the resulting potential drop across the transporter circuit, then the field in each capacitor can be written

$$D_1 = D_a + VC_1/A_1 \qquad (4\text{-}5a)$$

$$D_2 = VC_2/A_2 \qquad (4\text{-}5b)$$

Equations (4-4) and (4-5) are dual to (4-1) and (4-2), and may be solved for the dual to equation (4-3)

$$D_2 = -\frac{A_1}{A_2} D_a \frac{C_2}{C_1 + C_2} \qquad (4\text{-}6)$$

Hence if the electric field sensor cannot be brought to the unknown field, the field may be brought to the sensor using the parallel capacitor charge transporter. Since the gate of a MOSFET is one of the parallel capacitors in a charge transporter, we conclude that there is complete duality between the input circuits of SQUID magnetometers and MOSFET electrometers.

B. Current and Voltage Amplifiers

Not only are SQUID magnetometers and MOSFET electrometers dual, but the circuits that emply them to measure currents or voltages are also dual. The simplest such circuits, in which the MOSFET amplifier is used to measure voltage, and the SQUID to measure current, were shown to be duals at the beginning of this chapter. However, by using feedback, the roles of the two amplifiers can be reversed, so that the MOSFET can be used to measure currents, and the SQUID to measure voltages. The standard MOSFET current amplifier circuit is shown in Fig. 18a and its dual, the SQUID voltmeter circuit in Fig. 18b. In the FET circuit the current to be measured, I_s, is shunted by its own source resistance, R_S. This source resistance is usually so large that a stray

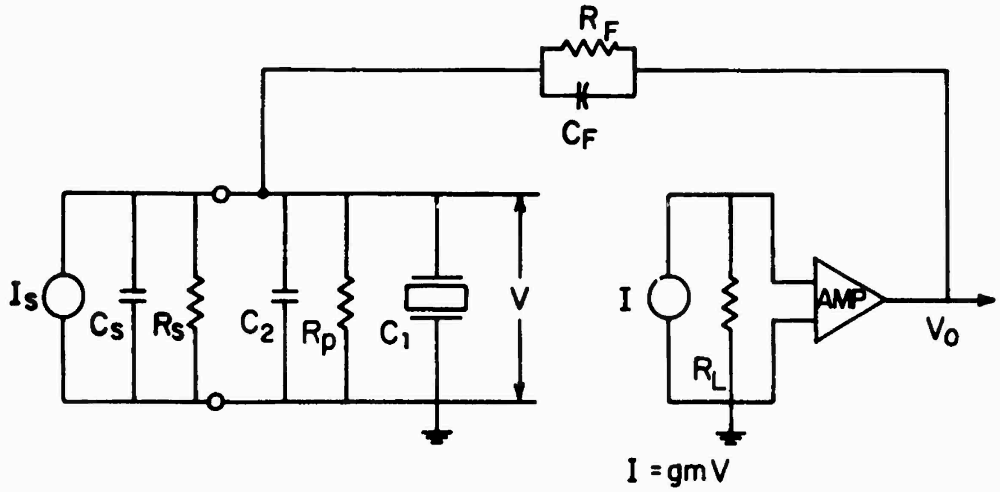

(a)

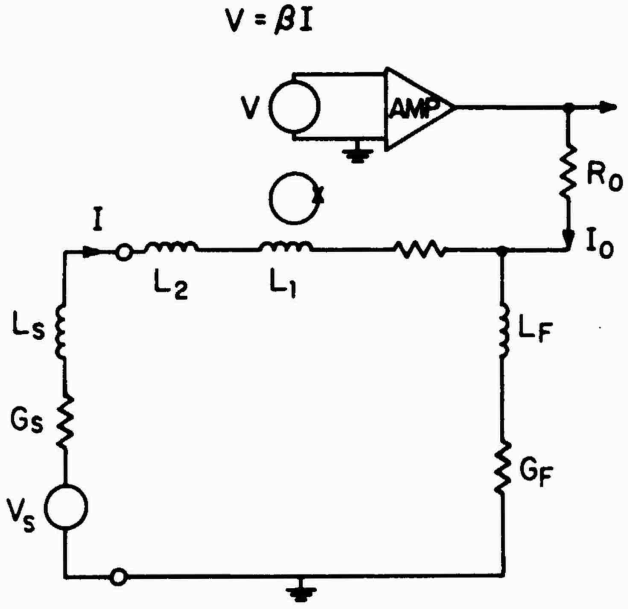

(b)

Fig. 18 a) Equivalent circuit of MOSFET current amplifier.
b) Equivalent circuit of SQUID voltage amplifier.

capacitance, C_S, must be considered for all but the lowest frequencies. Similarly, in the SQUID circuit, the voltage to be measured, V_S, is in series with its own source conductance, G_S, which is typically so large that the series stray inductance, L_S, must be considered for a valid frequency response analysis. In the current amplifier the MOSFET is modeled as a voltage controlled current source with transconductance g_m. The output current is converted to a voltage by R_L, and then further amplified by the remaining stages in the amplifier, and the output voltage V_o is fed back across a large resistor, R_F, to the input circuit. The SQUID in the other circuit is described by exactly dual language: the SQUID is modeled as a current controlled voltage source with transresistance β. This voltage source is amplified by succeeding stages of electronics and the final output current I_o is fed back through a large conductance, G_F, to the input circuit.

In the MOSFET circuit the servo functions by keeping the voltage across the MOSFET input capacitance, C_1, as close to zero as it can. The input current that would ordinarily charge up the capacitor is nulled by a feedback current through R_F. The servo loop in the SQUID circuit behaves exactly the same way. It keeps the current through the SQUID input inductance, L_1, as close to a null as it can. The input voltage that would without feedback drive a cur-

rent through the inductor is nulled by a feedback voltage across G_F. Just as it is desirable in the MOSFET circuit to make the feedback resistance R_F much larger than R_S to minimize the extra current noise originating in R_F, it is desirable in the SQUID circuit to make the feedback conductance G_F much larger than G_S to minimize extra voltage noise. Note that in each circuit we have drawn in the stray capacitance or inductance associated with the large feedback resistance or conductance. Finally, if the amplifier chain in each circuit has enough gain, the output voltage of the MOSFET current amplifier will be $V_o = I_S R_F$, and the output current of the SQUID voltage amplifier will be $I_o = V_S G_F$, each equation valid only for low frequencies. Every detail of operation in one circuit, then, has its dual in the other.

Now if we compare the SQUID circuit generated above to the circuit considered in Chapter Three, and drawn schematically in Fig. 7, we see that they are in fact one and the same circuit. Therefore, by duality, every detail discussed in Chapter Three in the context of SQUID voltage amplifiers should apply also to MOSFET current amplifiers, and all that is known about MOSFET current amplifiers must also apply to the SQUID voltage amplifier. For example, it was shown in the previous chapter that the noise contours for the SQUID amplifier are independent of feedback, so that the same

contours describe both the SQUID voltage amplifier and the SQUID current amplifier. The same rule must then apply to the MOSFET amplifier: identical noise contours apply to the amplifier whether it is used for amplifying current or voltage. Duality, then, can be useful in extending our understanding of both types of amplifiers, and we next explore its implications for the most important aspect of any amplifier: its noise characteristics.

4.2 Noise

The noise performance of a high gain amplifier is a fundamental property of that amplifier, and the duality that exists between the input circuits of superconducting and MOSFET amplifiers means that the noise characteristics of the two amplifiers should also be dual. Noise performance is fundamental because it is essentially independent of transfer function characteristics. It is not ordinarily affected by succeeding stages of amplification or by feedback. The transfer function is not a fundamental characterization of an amplifier because it is determined by the interaction of all stages and feedback. Hence, in comparing the performance of two amplifiers it must be remembered that transfer functions can be manipulated over wide ranges while the noise characteristics, defined as noise figure, noise temperature, or signal to noise ratio, cannot. MOSFET

amplifiers have been characterized by a minimum attainable noise temperature,[36] T_{Nmin}, and an associated optimum source resistance, R_{opt}. The SQUID amplifier, presented in Chapter Three was characterized by the action factor, $C = T_N(0)\tau$. It would then appear, superficially, that a direct comparison between the two types of amplifiers would be difficult. However, since the two amplifiers are duals, this superficial conclusion is wrong, and it must be that all three noise parameters apply to both amplifiers, so that a comparison is simple.

A. Comparison of MOSFET and SQUID Amplifiers

A direct comparison of the two types of amplifiers could not be simpler: all of the analysis of the noise temperature of the SQUID amplifier done in section 3.1C applies in dual form to MOSFET amplifiers as well. In particular, the noise temperature equation, (3-9), is valid for both. We rewrite (3-9) below for SQUID's replacing the source resistance used in 3.1C with reciprocal source conductance, to be consistent with notation of the present chapter. With the further assumption that $G_S \simeq G_T$, we have for SQUID's

$$T_N(\omega) \simeq \frac{\langle e_n^2 \rangle G_S}{4k_B} + \frac{\langle i_n^2 \rangle (1 + \omega^2 \tau_T^2)}{4k_B G_S} \quad . \qquad (4\text{-}8)$$

By duality we can immediately write down the noise temper-

ature for a MOSFET amplifier in terms of current and voltage noise generators:

$$T_N(\omega) \simeq \frac{\langle i_n^2 \rangle R_S}{4k_B} + \frac{\langle e_n^2 \rangle (1 + \omega^2 \tau_T^2)}{4k_B R_S} \quad . \tag{4-9}$$

These two equations generate respectively the two sets of noise contours for the SQUID and MOSFET amplifiers plotted in Figs. 14 and 15. The difference between the two sets of contours is that the voltage noise generator in the SQUID is apparently negligible, which accounts for the SQUID's very low noise temperature at low frequencies and at low source resistances. It is appropriate to point out here, however, that the voltage noise generator in the SQUID input circuit will not be identically zero: there are dissipative events that can occur in the superconducting input circuit such as ac losses or phase slip events that will lead to a very small but finite voltage noise contribution. Further, the feedback resistance, if not negligible compared to the source resistance, will contribute substantial voltage noise, so the voltage noise generator in the SQUID amplifier can be neglected only with caution.

We found in Chapter Three that the SQUID noise temperature contours were characterized by a constant product, $C = T_N(0)\tau$, the action factor, with the condition that the voltage noise source could be ignored. We see now, from

(4-9) that the same will be true for the MOSFET with a low source resistance so that the current noise source can be ignored. From (4-9) we have, for a MOSFET amplifier:

$$C \equiv T_N(0)\tau_T = \langle e_n^2 \rangle C_T/4k_B \quad , \quad \langle e_n^2 \rangle > \langle i_n^2 \rangle R_S^2 \tag{4-10}$$

where C_T is the total input capacitance of the MOSFET amplifier, and $\tau_T = R_S C_T$. For the PAR 185 amplifier, the value of the action factor is about 10^{-5} K sec, which is comparable to the value quoted for the SQUID amplifier in section 3.1C. Not only does the action factor apply to both amplifiers, but the absolute minimum noise temperature that is obvious in the noise contours of the MOSFET amplifier in Fig. 15 also characterizes the SQUID. If we differentiate (4-8) with respect to source conductance, bearing in mind that $\tau_T = G_S L_T$, we find that the noise temperature for the SQUID amplifier has a minimum:

$$T_{Nmin} = \frac{\langle e_n i_n \rangle}{2k_B}\left(\frac{1 + (1 + \omega^2\tau_o^2)^2}{2\sqrt{(1 + \omega^2\tau_o^2)}}\right) \tag{4-11}$$

at an optimum source conductance:

$$G_{opt}(\omega) = \frac{|i_n|}{|e_n|}(1 + \omega^2\tau_o^2)^{-1/2} \tag{4-12}$$

where $\tau_o = G_{opt}(0)L_T$. These formulae are precisely dual to

the usual formulae used to describe the noise in MOSFET amplifiers. Again, the only distinction between the two amplifiers is that the voltage noise source in the SQUID amplifier is very small, while the current noise source in the MOSFET amplifier is not. (Of course, as e_n goes to zero, T_{Nmin} goes to zero and G_{opt} goes to infinity.) The only feature missing from this analysis is flicker noise, which generally has a spectrum resembling 1/f in form. It is this ubiquitous type of noise that is responsible for the closing of the contours evident in the left hand side of Fig. 15, for the MOSFET amplifier. Flicker noise seems to be less of a problem for the SQUID amplifier but it must inevitably become important at some low enough frequency.

B. Basis Parameters for Noise Contours

Except for flicker noise, the noise of both MOSFET and SQUID amplifiers is determined by only three parameters: e_n, i_n, and the input reactance of the amplifier (by reactance we mean the total inductance of the SQUID amplifier input or the total capacitance of the MOSFET amplifier input). The noise is determined by these parameters since they are the only independent parameters in the noise temperature equations, (4-8) and (4-9). (The input reactance comes into these two formulae implicitly through the time constant, τ_T.) The only other variables in these equations are the

source impedance and the frequency which are usually determined independently of the amplifier. We may say, then,that the two noise sources and the input reactance form a basis for describing the noise characteristics of the amplifier. However, the minimum noise temperature, the optimum source impedance, and the action factor, also form a basis for a complete description of noise in both MOSFET and SQUID amplifiers. Moreover, this basis, which we call the noise temperature basis to distinguish it from the noise source basis, is extremely convenient to use.

The parameters of each basis can be derived from those of the other. For the MOSFET amplifier

$$T_{Nmin}(0) = \frac{\langle e_n i_n \rangle}{2k_B} \tag{4-13a}$$

$$T_N(0)\tau_T = \frac{\langle e_n^2 \rangle C_T}{4k_B} \tag{4-13b}$$

$$R_{opt}(0) = \frac{|e_n|}{|i_n|} \tag{4-13c}$$

and

$$\langle e_n^2 \rangle = 2k_B T_{Nmin}(0) R_{opt}(0) \tag{4-14a}$$

$$\langle i_n^2 \rangle = 2k_B T_{Nmin}(0)/R_{opt}(0) \tag{4-14b}$$

$$C_T = 2 \frac{T_N(0)\tau_T}{T_{Nmin}(0)\ R_{opt}(0)} \qquad (4\text{-}14c)$$

We conclude, therefore, that the two bases are completely equivalent. Of course, the same equations and conclusions must be true in dual form for SQUID amplifiers.

The noise temperature basis offers several advantages over the noise source basis. First, its parameters are real and measurable, while the noise sources themselves have a degree of arbitrariness depending on exactly where in the input circuit they are place. Second, the noise temperature basis provides more useful information without ancillary calculations than is provided by the noise source basis. That is, in using any amplifier, the first thing that must be known for sensitive operation is the most favorable impedance level, which is given immediately by R_{opt}. Then, $T_{Nmin}(0)$ will tell you if the amplifier is capable of resolving Johnson noise from the source resistance at a given temperature. Finally, if it is possible to trade off some bandwidth for sensitivity, the action factor tells you immediately how far you can go. By contrast, the noise source basis provides only gross voltage or current level information, and makes no direct comparison to the Johnson noise of the source without calculations. Finally, two of the three quantities in the noise temperature basis are transformer invariant, while none in the noise source

basis are. If an ideal transformer is interposed between the input of an amplifier and the source, only R_{opt}, in the noise temperature basis is changed, while all three parameters in the noise source basis are modified by the transformer. In other words, e_n, i_n, and C_T (for a MOSFET amplifier) are all changed when they are referred to the primary of the ideal transformer attached to the input, but they change in just such a way that $T_{Nmin}(0)$, and $T_N(0)\tau_T$ remain unchanged while $R_{opt}(0)$ transforms as the square of the turns ratio of the transformer, as in the usual ideal transformer impedance transformation. Hence, the noise temperature basis reveals the utility of transformer inputs in a most elegant manner.

4.3 Perspective

Since both SQUID and MOSFET amplifiers have noise characteristics determined (apart from flicker noise) by all three noise temperature basis parameters, we may compare the two types of amplifiers directly, in tabular form. Table 1 lists values for all three parameters, the minimum noise temperature, the action factor, and the optimum source resistance for typical SQUID and MOSFET amplifiers. Notice that a minimum noise temperature has not been measured for a SQUID amplifier, and the upper limit quoted in Table 1 is derived from some careful noise temperature thermometry of Webb, Giffard, and Wheatley[37]. Similarly the optimum source

TABLE 1

Comparison of SQUID and FET Amplifiers

Amplifier	T_{Nmin}	R_{opt}	Action Factor
SQUID	$<1.6\times10^{-4}$ K	$<10^{-6}$ ohm	$\sim10^{-5}$ K sec
PAR 185 (FET)	0.5 K	10^{6} ohm	$\sim10^{-5}$ K sec

A direct comparison of representative SQUID and FET amplifiers. The limits on T_{Nmin} and R_{opt} for the SQUID were derived from reference 37. It should be possible to make SQUID amplifiers with substatially lower action factors than 10^{-5} (Ref. 32)

resistance for the SQUID is only an upper bound based on reports in the literature. The small magnitudes of even these upper bounds are an indication of the small size of the effective voltage generator in the SQUID amplifier input circuit. The rest of the table bears out the general conclusions presented in section 3.3, where the two amplifiers were compared operationally: either amplifier is suitable for sensitive measurements on sources at liquid helium temperatures, but the SQUID is best suited for small source resistances, while the MOSFET amplifier is best for large source resistances. However, where the smallest noise temperatures are required, the FET amplifier is of limited use, while the SQUID amplifier is good down to at least 1.6×10^{-4} K and possibly much lower. The low flicker noise of the SQUID, not covered in Table 1, is an additional advantage at dc and low frequencies. Notice that in terms of time constant-noise temperature trade-offs, as parameterized by the action factor, both amplifiers are about the same, and neither has the advantage.

It is interesting to speculate on how small an action factor is possible in any amplifier. Radhakrishnan and Newhouse[33] have already pointed out that the Heisenberg uncertainty principle sets a lower limit on this quantity of $T_N(0)\tau_T > h/k_B \simeq 10^{-10}$. Radhakrishnan and Newhouse also compare the action factors for SQUID's, SLUG's, and several

other types or room temperature and low temperature amplifiers. It appears that their comparisons are valid, although SQUID's have improved considerably since their article appeared. The only points that Radhakrishnan and Newhouse do not make clear are that, first, the time constant that goes into the calculation of the action factor must be the time constant of the input circuit without feedback, and second, that the action factor is not a complete specification of the noise properties of the amplifiers. We have shown here that a complete noise basis of SQUID and FET amplifiers, at least, requires two more parameters: the minimum noise temperature, and the optimum source impedance.

The noise temperature basis provides an explanation of the distinction between SQUID and cryotron amplifiers, and in so doing, points out new directions for further development of Josephson linear amplifiers. SQUID and cryotron amplifiers have been designed for different extremes in the noise-temperature time-constant trade off governed by the action factor. Radhakrishnan and Newhouse have estimated the action factor to be about 10^{-6} K sec for the best cryotron amplifiers[33], and judging by experiments done in this laboratory and in the literature, the best SQUID's are in the range between 10^{-5} and 10^{-7} K sec, so that the two types of amplifiers have available about the same range

in which to trade sensitivity for bandwidth. The difference is that cryotrons have been optimized for the smallest input circuit time constant, while SQUID's have been optimized for the smallest low frequency noise temperature.

This distinction appears to be only an accident of history. Cryotrons were initially developed with computer applications in mind, and so were designed for the highest possible speed. Noise temperature was a secondary consideration since in digital computer applications the difference between the "on" and "off" signal levels of the device can be orders of magnitude larger than the noise of a device with even a relatively high noise temperature. SQUID's, on the other hand, were initially developed for extremely sensitive static or quasi-static measurements in systems with relatively low source resistances. The static nature of the measurements, along with the low source resistances, encouraged the use of long time constants, and resulted in extremely low noise temperatures. These optimizations, then, are not unique, and one could design a cryotron or SQUID amplifier with arbitrary balances between noise temperature and input circuit time constant. In particular there is no reason why a SQUID amplifier could not be designed with megahertz bandwidths and noise temperatures in the range of a few Kelvin.

In principle one need not design a new SQUID to realize a wide bandwidth with low noise: an ideal transformer interposed between the SQUID and the source would do the same thing. Such a transformer leaves the action factor unchanged, but does change the input circuit time constant by transforming the source resistance as discussed in section 3.1D. Hence an ideal N:1 transformer, with a current gain less than unity, would result in a wider bandwidth but higher noise temperature amplifier, for a given source resistance. The difficulty with this scheme, of course, is that transformers with near ideal characteristics are difficult to construct over bandwidths of more than a few kilohertz, so that any real transformer used will limit the speed of the amplifier. However wideband SQUID amplifiers may be designed with action factors as small or smaller than present SQUID amplifiers. Such redesigned SQUID's would be wideband low noise devices because they would need no transformer.

Wideband SQUID's may be constructed by making them smaller, and so reducing their self inductances. From (4-13c) and duality we may write

$$C \equiv T_N(0)\ \tau_T = \frac{\langle i_n^2 \rangle L}{4k_B} = \frac{\langle \Phi_n^2 \rangle}{4k_B\ k' L_1} \qquad (4\text{-}15)$$

where $\langle\Phi_n^2\rangle = M^2\langle i_n^2\rangle$ is the effective flux noise of the SQUID. Here, $M = k' (L_T L_1)$ is the mutual inductance between the SQUID and the input circuit, L_T is the self inductance of the input circuit, and L_1 is the self inductance of the SQUID. Changing the size of the SQUID changes L_1 roughly in direct proportion to the dimension of the SQUID. The coupling constant k' may in principle be kept arbitrarily close to unity as the SQUID is reduced in size, so it remains to determine the scaling law for the flux noise as the size of the SQUID is changed. Then we can determine how the action factor will change. The flux noise, however, has no universal scaling law. For rf SQUID's the mean flux noise scales scales directly with the SQUID self inductance[38] so that there would be no size dependence of the $T_N(0)\tau_T$ product. For dc SQUID's, however, the flux noise is independent of SQUID inductance provided the noise is predominantly due to the room temperature electronics. For such a SQUID the action factor is increased as the SQUID is reduced in size. For a dc SQUID dominated by self noise (noise generated by the SQUID itself) the mean square flux noise scales with the square of the SQUID self inductance, so the action factor improves as this type of SQUID is made smaller.

Wideband SQUID amplifiers could then be made by cascading small dc SQUID's. Cascading insures that the influ-

ence of the noise of the room temperature electronics would be postponed until later. These small SQUID's would be designed with a minimum inductance, so that thin film integrated circuit technology should be appropriate, and the resulting integrated amplifiers could find use in high speed radiation detectors and the new breed of Josephson tunnel junction computer elements[15] now being developed.

PART II

MICROCOMPOSITE WIRE

CHAPTER FIVE: INTRODUCTION TO SUPERCONDUCTING MATERIALS

In Part I of this report we considered the application of superconductive devices to the problem of handling data and information in linear amplifiers; in Part II we consider the application of superconductive materials to the manipulation of energy on an industrial scale. We will briefly outline the history of superconductive materials from the efforts of H. Kamerlingh Onnes[40] to the state of the art today, and then concentrate on an extension of the state of the art. This extension, which has yet to prove practical but has certainly proved interesting, is the process invented by C.C. Tsuei[41,42,43,44,45] at the California Institute of Technology for producing a microcomposite superconductive wire. The bulk of Part II will then concentrate on our measurements of the properties of wire made by Tsuei's process, and an interpretation of some of the results in terms that have been used to describe conductivity in normal metal composites.

5.1 History

H. Kamerlingh Onnes realized soon after his discovery of superconductivity that superconductors could play an import-

ant role both in creating high magnetic fields and in carrying large currents with miniscule dissipation. The first efforts at winding high field solenoids were Onnes' but he was frustrated by a lack of theoretical understanding of the physics of superconductivity. Onnes found, for example, that an isolated section of Pb superconductor could carry very large currents, but when the same wire was wound into a solenoid the coil would go normal before even a 0.1 tesla field was reached. Onnes originally felt the problem was due to impurities in the material, but Silsbee[46] pointed out that the problem was more fundamental; that the critical current and critical field of a superconducting wire are related. The critical current is that current required to make the critical field at the conductor's surface. For Pb the critical field is about 0.08 tesla. It was still felt nevertheless that the purer a material the better its superconductive properties would be, that if extremely pure and strain-free Pb wire could be formed into a solenoid, superior performance could be achieved. But no matter what efforts were made in that direction, no higher critical fields ensued, and applied superconductivity remained dormant for fifty years after these early strenuous efforts.

Fundamental research into superconductivity continued in an increasing number of laboratories throughout the world despite the apparently poor prospects of practical appli-

cation. In 1933 Meissner and Ochsenfeld[47] discovered that the magnetic flux was expelled from the bulk of a pure superconductor as it was cooled below T_c, the transition temperature. This discovery showed that superconductivity was not just the absence of resistance, but a new thermodynamic state of matter. The thermodynamic two fluid model or Gorter and Casimir[48] soon followed, and the London[49] phenomenological theory of the electrodynamics of superconductors emerged in 1935. Pippard,[50] in 1953, refined the work of the London brothers by showing that the electrodynamics of superconductors was generally non-local, and introduced the idea of the coherence length to characterize the range of nonlocality. Ginzburg and Landau[51] introduced their famous phenomenological theory of superconductivity in 1950, and showed it to be the logical extension of the work of the Londons'. Their theory produced two coupled differential equations governing the behavior of a complex order parameter, ψ, which is generally given a quantum mechanical interpretation as the wave function for the center of mass motion of the superconducting electron pairs in the metal. The Ginzburg-Landau theory thus emphasizes the quantum nature of superconducting phenomena within a convenient formalism, and therfore has proved very useful in the development of superconducting technology.

In 1956 A.A. Abrikosov[52] showed, using the Ginzburg-Landau (GL) equations, that there were two types of superconductors possible, now generally called type I and type II. The pure superconducting elements studied by most physicists since the time of Onnes were type I, and were generally characterized by critical fields the order of 0.1 tesla or so. But Abrikosov's theory showed that the type II materials, which had been largely avoided by physicists because they appeared hard to characterize, would not necessarily be limited to a critical field equal to the thermodynamic field, and that zero resistance superconductivity could persist in these materials to very large fields. Unlike type I materials, the type II materials do not exhibit a complete Meissner state at high fields. Rather, magnetic flux is admitted to their bulk in discrete bundles called fluxoids (or fluxons or vortices) and superconductivity is destroyed only at the core of each fluxoid, and not in the entire volume of the superconductor.

Abrikosov used his theory to explain experimental data taken twenty years earlier by Shubnikov, et al[53] on the magnetic behavior of superconducting alloys. (Shubnikov recognized at that early date that the behavior of the alloys was essentially different from that of most of the pure elements.) The work of Shubnikov, Ginzburg, Landau, and Abrikosov remained relatively obscure in the West, however,

and was overshadowed in 1957 when Bardeen, Cooper, and Schrieffer[54] published their famous microscopic theory of superconductivity. However, in 1959, Gorkov[55] showed that the microscopic theory reduced to the Ginzburg-Landau-Abrikosov theory near T_c, and thus gave the phenomenological theory and the idea of type II superconductivity a firm foundation.

This fifty years of pure research finally meshed with an applied effort in the early 1960's. In 1961 J.E. Kunzler[56] and a group at Bell Laboratories discovered that Nb_3Sn would remain superconducting in fields of at least 8.8 tesla. It was quickly pointed out by B.B. Goodman[57] that Nb_3Sn was a type II superconductor, and therefore subject to Abrikosov's theory. Thus it became clear in 1961 that the key to industrial applications of superconductivity was not in the ultra-pure elemental superconductors that had been the preoccupation of physicists since Onnes, but in carefully treated and prepared compound and alloy superconductors of the type described by Abrikosov. Despite this firm theoretical understanding won after fifty years of study, the problem of high field high current applications was not yet solved. The performance of solenoids always fell short of that expected from short sample tests of these new type II materials, just as had been found for the old type I materials. There was a difference, however. The theory that

Onnes lacked was now in hand.

5.2 Type II Superconductivity

It is not the purpose of this chapter to present the theory of type II superconductivity, which is well covered in several texts.[58] Rather, the fundamental concepts needed to understand the differences between short sample tests and actual solenoid performance will be presented and the criteria for stability of high field superconducting magnets will be developed from the concepts. It is these criteria, and the methods used to make practical superconducting wires that possess them that lead to the kind of wire produced by Tsuei's process.

The fundamental concept of type II superconductivity is the fluxoid. A fluxoid is a whirlpool of supercurrent surrounding a core of essentially normal material and enclosing a certain discrete amount, or quantum, or magnetic flux. It is easy to give a simple picture of the structure of a fluxoid. The basis of our picture is the quantum nature of the superconducting fluid: the center of mass motion of all the superconducting paired electrons is characterized by a single valued complex order parameter, or wave function. We may use the standard quantum mechanical gauge-invariant form for a current of particles with charge e* and mass m* (the charge and mass of a Cooper pair) just

as we did in the discussion of Josephson phenomena in Part I:

$$\vec{J}_s = \frac{e^*\hbar}{2m^*i}(\psi^*\vec{\nabla}\psi - \psi\vec{\nabla}\psi^*) - \frac{e^{*2}}{m^*}|\psi|^2\vec{A} \qquad (5\text{-}1a)$$

$$= \frac{e^*}{m^*}|\psi|^2(\hbar\vec{\nabla}\theta - e^*\vec{A}) \qquad (5\text{-}1b)$$

where θ is the phase of the wave function. Since the closed line integral of the vector potential gives the enclosed magnetic flux, we may use (5-1b) to find the quantity of flux associated with each vortex, if a path of integration with zero current on it can be found. If each fluxoid is surrounded by others with the same sense and magnitude of circulation, then a path surrounding each fluxoid can always be found along which the current density is zero. Midway between identical fluxoids the circulating currents oppose each other and cancel out, providing our integration path. Integrating (5-1b) around such a path we find

$$\frac{\hbar}{e^*}\oint\vec{\nabla}\theta\cdot d\vec{l} = \oint\vec{A}\cdot d\vec{l} \equiv \Phi \qquad (5\text{-}2)$$

$$\text{or} \qquad \Phi = nh/e^* \qquad n = 0,\pm1,\pm2,....$$

where we have set the line integral of the gradient of the phase equal to an integral multiple of 2π since the complex order parameter must be single valued. Hence the flux

enclosed by the circulating currents of a vortex must be quantized, with a flux quantum $\Phi_o = h/e^* = h/2e \simeq 2\times10^{-15}$ weber.

If instead of integrating around a path on which the supercurrent density is zero, we choose a path close in to the vortex we obtain

$$\oint \frac{m^*}{e^*|\psi|^2} \vec{J}_s \cdot d\vec{\ell} + \Phi = n\Phi_o \qquad (5\text{-}3)$$

in place of (5-2). If we choose a symmetric path very close to the core we may neglect the magnetic flux term in (5-3) compared to the current density term, and if the radius of the integration path is r, (5-3) becomes

$$\frac{2\pi r m^* J_s}{e^*|\psi(r)|^2} = n\Phi_o \quad , \quad r \to 0 \quad . \qquad (5\text{-}4)$$

Hence $J_s/|\psi(r)|^2 \propto 1/r$ for small r. Therefore, as r goes to zero, $J_s/|\psi(r)|^2$ must go to infinity. But J_s at best remains finite, always less than some critical value, J_c. It must therefore be concluded that the magnitude of the order parameter goes to zero at the core of each fluxoid. Our picture of a fluxoid is then a whirlpool of supercurrent centered on a thin core of normal material, and enclosing a single quantum of magnetic flux. (Our arguments above do not show that each fluxoid contains only a single quantum of

magnetic flux. A detailed analysis of the GL equations are required for that.[58])

A type II superconductor containing vortices is said to be in the mixed state. The breakdown of the Meissner state and the entry of the first vortices occurs at a field $H_{c1} < H_c$, where H_c is the thermodynamic critical field. As the field is increased, superconductivity in type II material persists until the fluxoids are packed so tightly together that the average magnetic field inside the material becomes identical with the applied field, and the value of field for which this occurs is called H_{c2}. This behavior can be illustrated with the schematic magnetization curves in Fig. 19, which show curves for a type I and a type II material with identical thermodynamic critical fields. It can be shown that the areas under each curve must be equal, but superconductivity in the type II material can persist well beyond the cut off for the type I, and it is this type of behavior that Kunzler[56] and others in the early 1960's showed could be used for high field and high current applications.

Although fluxoids permit the superconducting order parameter to exist in very high fields, they also provide a complication: the motion of fluxoids is dissipative, and they tend to move under the influence of transport currents. The situation for fluxoids in the presence of a transport

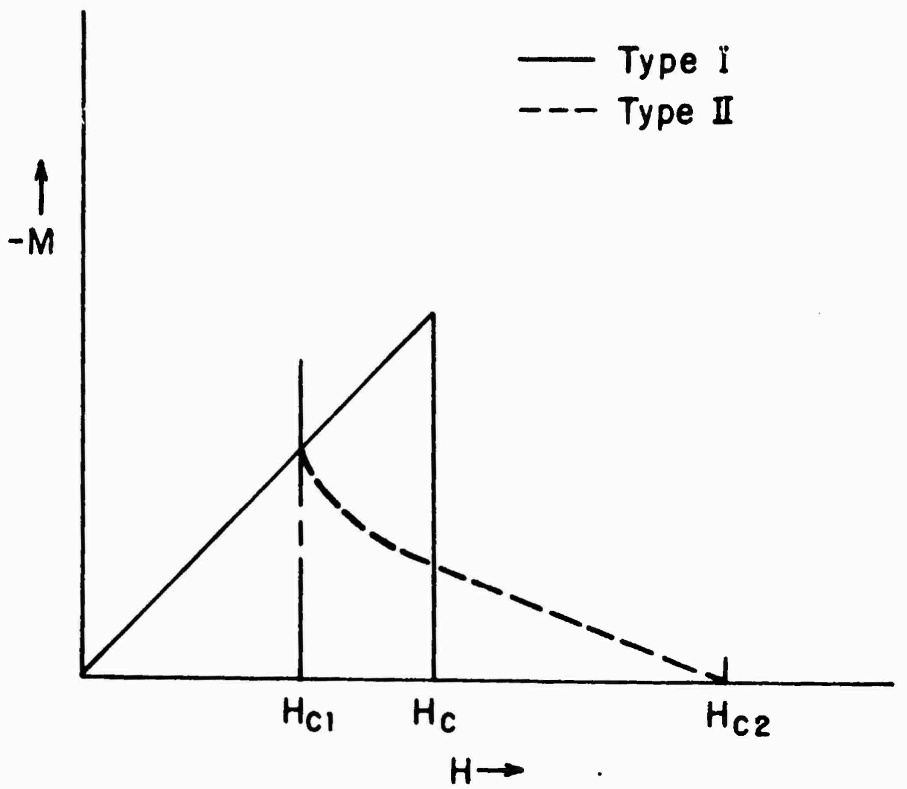

Fig. 19 Schematic magnetization curves for a type I material and a type II material with identical thermodynamic critical fields, H_c.

current is shown schematically in Fig. 20. The transport current, J_t, creates a net Lorentz force per unit length $J_t\Phi_o$, acting transversely on each vortex. Thus a vortex gains energy when it moves in response to a transport current, but this energy can only become heat. When the fluxoid moves, its associated magnetic field moves with it, creating an electric field parallel to the direction of current transport. This electric field acts on both the superconducting electrons and the normal electrons and any energy thus imparted to the normal component eventually becomes heat. Hence motion of the fluxoid will be opposed by a viscous force, and a voltage drop will appear across the ends of the conductor. It can be shown that at high currents and fields the net resistance of the wire will approach its normal state value, and a material in which flux motion is resisted by a viscous force alone will be useless as a high field high current superconductor.

Fortunately, viscous drag is not the only force available to impede the motion of fluxoids. Various kinds of material defects in the superconductor itself can trap, or pin, flux, allowing currents to pass without resistance until the forces that tend to propel the fluxoid overcome the pinning forces.[59,60,61] Pinning can occur at lattice defects, voids, grain boundaries, or at any inhomogeneity of the superconducting material. The free energy of a flux-

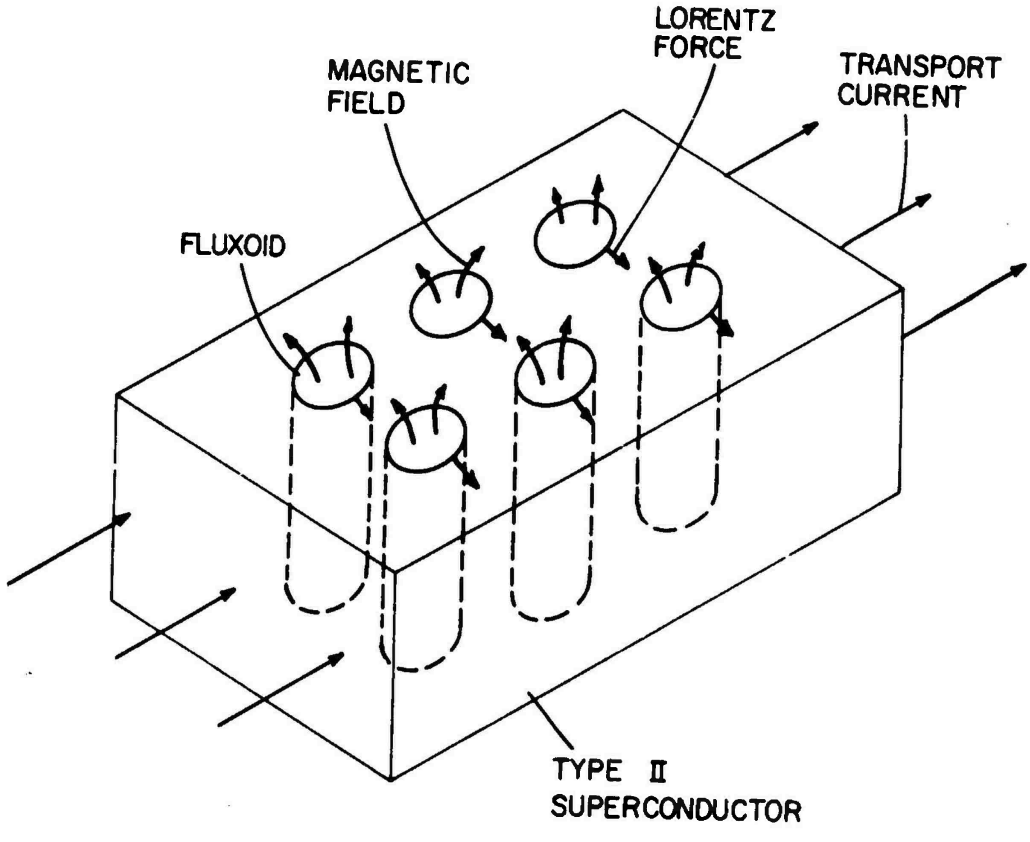

Fig. 20 Schematic representation of fluxoids in a type II superconductor.

oid is then a function of position in a superconductor with such inclusions, and fluxoids will move around until they settle into free energy minima (where the total free energy must take account of interactions between fluxoids). Then further motion of the fluxoid will be postponed until the depinning force due to the transport current and applied field (and thermal activation) become strong enough to force the fluxoid out of its well. If just a few fluxoids in a localized segment of superconducting wire in a solenoid wound with thousands of meters of wire suddenly shift their positions for whatever reasons, enough heat could be released to drive that segment normal. Once the segment is normal, ordinary joule heating due to the transport current would not only keep it normal, but would propagate the boundaries of the normal region until the whole solenoid was normal. Then, the high resistance of the now normal solenoid would overwhelm the energizing power supply, so the magnetic field of the solenoid would collapse, dumping its energy into the coil, sometimes causing the conductor to melt. Since such a catastrophe could be precipitated in any small region of the very long superconductor, it is clear that the conductors must somehow be made stable against the original small perturbation of fluxoids. In other words, it is impossible to prevent occasional fluxoid motion, but it may be possible to prevent that motion from driving the

superconductor in the immediate vicinity permanently normal. Several schemes for stabilization have been successfully developed, and all present superconducting magnets use one or another of them. Present commercial techniques for producing stable superconducting wire are difficult, expensive, and work poorly for the materials with the best superconducting characteristics. Tsuei's process, the general topic for Part II of this report, has the potential of simplicity, economy, and utility for the better materials.

5.3 Stable Superconducting Wire

Three techniques have been developed to stabilize the zero resistance state of high field high current type II superconductors.[62] These techniques are called cryostatic stabilization, dynamic stabilization, and intrinsic stabilization. All three require the construction of a composite of a superconductor and a highly conductive normal metal, usually copper. It is also required by all three that the superconductor in the composite be in the form of a multitude of fine filaments, rather than a few large superconducting strands with the same total cross section. The only distinction between the three kinds of stabilization is the role played by the copper.

The first method for stabilizing superconducting wire was proposed in 1965 by Kantrowitz and Stekly,[63] and by

Laverick,[64] and their technique is now usually called cryostatic stabilization, though sometimes it is referred to as steady state stabilization. The idea is to embed the superconducting wire in copper enough to handle the full current when some segment of the superconductor goes normal due to a large fluxoid jump. In properly designed wire the temperature increase in the copper when carrying the full current will not be enough to prevent the reestablishment of superconductivity when the flux jump has relaxed. Hence cryostatic stabilization demands

$$J^2 \rho A_m < h(T_{ch} - T_b)\ P \qquad (5\text{-}5)$$

where J is the current density in the dopper

ρ is the resistivity of the copper

A_m is the cross sectional area of the copper matrix

h is the heat transfer coefficient from the copper to the bath, in watts/cm^2 K

P is the perimeter of the matrix subject to cooling by the bath

T_{ch} is the critical temperature at zero current, but in the applied field

T_b is the temperature of the bath.

But J in (5-5) is related to the desired critical current density in the superconducting portion of the composite, J_{ch}, by

$$J = J_{ch}A_s/A_m$$

where A_s is the total superconducting cross section, and J_{ch} is the critical current density at T_b in the applied field.

The geometry of the copper-superconductor composite is then governed by

$$\frac{A_s^2}{A_m P} < \frac{h(T_{ch} - T_b)}{J_c^2 \rho} \quad . \tag{5-6}$$

The way in which the left hand side of this inequality scales implies that may small conductors of a fixed geometry will work better than a single large composite conductor of the same geometry. It is possible to refine this analysis further (see refernce 63) and consider the heat that must be removed from the superconducting part of the composite as well as the joule heat generated in the copper matrix, and find a condition on the maximum thickness of the superconducting material in the composite. The approximate condition is

$$d < \frac{2}{J_{ch}} \left[\frac{k(T_{ch} - T_b)}{\rho} \frac{A_m}{A_s} \right]^{1/2} \tag{5-7}$$

where d is the superconductor filament thickness (or diameter) and k is the thermal conductivity of the supercon-

ductor. Equation (5-7) should be viewed as an engineering rule of thumb, rather than as an exact expression. It yields filament sizes of less than 100 micrometers for typical NbTi alloy-copper composites. Equations (5-5) and (5-6) stress having a large value of P, to maximize the effectiveness of the bath in keeping the conductor cold, so that coils wound using cryostatic stabilization criteria must allow for circulation of the bath within the coil. This requirement, together with the need for large amounts of copper, generally restricts cryostatically stabilized coils to overall current densities less than 10^4 amp/cm^2. Hence they are not suitable for compact or high field magnets.

A more sophisticated stability condition, called dynamic stability,[65] was worked out around 1967. Coils designed for dynamic stability have a reduced cooling requirement and less copper than coils designed for cryostatic stability and therefore have larger overall current densities. Dynamic stability takes advantage of the fact that a clean copper matrix can not only conduct heat away from a flux jump location quickly, but can also impede the diffusion of magnetic flux through the conductor. Slowing the flux limits the power dissipated in a flux jump, and if that power can be removed quickly, the wire will never go completely normal and the copper will never have to conduct the full current load. A detailed analysis along these lines places a

premium on a multifilamentary construction with the maximum filament thickness given again by (5-7). The minimum cross sectional area of copper required is difficult to find analytically, but empirically much smaller amounts than for complete cryostatic stability have been used, and magnets relying on dynamic stabilization are among those with the highest achieved overall current desities.

Between 1967 and 1970 it was realized that a multifilamentary conductor could be made stable against fluxoid jumps without relying on the presence of any copper at all. Such conductors are thus called intrinsically stable, or, since the analysis assumes that no heat is carried away by the copper, adiabatically stable.[66] The analysis of adiabatic stability makes use of the cycle of events that would without stabilization lead to a catastrophic flux jump. Such a cycle is shown schematically in Fig. 21. Suppose there is some initial small impulse of flux, $\Delta\Phi$. This flux jump releases some amount of heat, thus raising the temperature of the superconductor by ΔT. But this higher temperature results in a reduced local value of critical current, and hence increased flux penetration. This additional flux motion releases additional heat and the cycle is repeated. However, both the magnitude of any initial flux motion and the resulting temperature increase are reduced as the superconducting filament size is reduced. Hence, for small

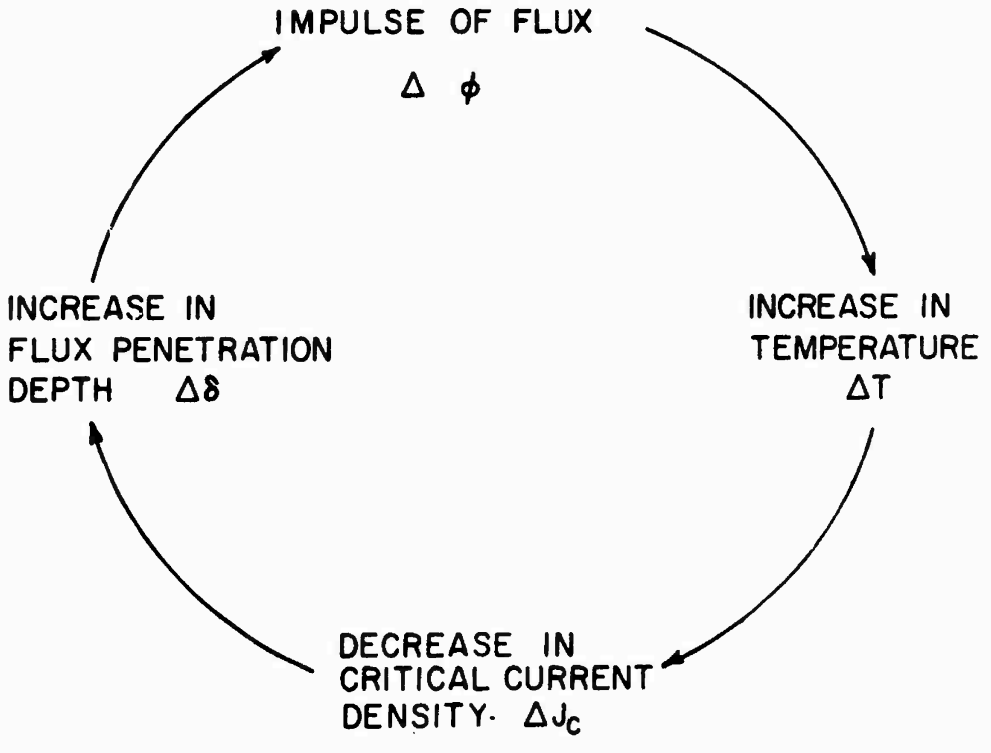

Fig. 21 Instability cycle in a type II superconductor.

enough filaments repeated instability cycles will result in only a finite net temperature rise, where the condition on filament size is

$$d \leq \frac{\pi}{2J_{ch}} \left(\frac{\gamma c}{\mu_o} J_{ch} (dJ_{ch}/dT)^{-1} \right)^{1/2} \simeq \frac{\pi}{2J_{ch}} \left(\frac{\gamma c (T_{ch}-T_b)}{\mu} \right)^{1/2} \quad (5\text{-}8)$$

where γ is the density of the superconductor in (kg/m^3), c is the specific heat of the superconductor in (J/kg K), and $\mu_o = 4\pi x 10^{-7}$ is the permeability of free space. The condition (5-8) usually requires filaments somewhat smaller than those indicated in (5-7), the order of 25 micrometers. Using adiabatic stabilization relieves some of the requirements on the copper. It need not have the high thermal and electrical conductivity required by cryostatic or dynamic stability, nor must it be present in large amounts. Some sort of matrix must be used, however, if only for mechanical support of the separate superconducting filaments. The copper matrix also provides a degree of extra stability, which can not be ignored when considering the overall reliability of the system.

No multifilamentary superconducting system will be reliable, however, unless the filaments are twisted into a helix. Cryostatic, dynamic, and adiabatic stabilization all require the use of many small filaments in a copper matrix, but an implicit assumption in all of the analysis has been

that the separate filaments act separately. If they were all coupled together, as they could be by eddy currents in the copper due to a time dependent applied magnetic field, their independence would be lost and they would act as one large strand rather than as a multitude of filaments. Twisting the multifilamentary composite into a helix limits the magnitude of these eddy currents. For a given rate of change of field there will be a critical twist pitch, above which the filaments will behave separately, and below which they will not. Hence the final criterion for a reliable superconductor is that it be twisted at a steep enough pitch to ensure the independence of its filaments for the highest rate of change of field to be encountered. Tinkham[67] gives a clear account of the physics involved in this twisting requirement.

The list of requirements for making a stabilized superconducting wire reduces to a few simple ideas, but making real materials that are both consistent with these ideas and have large critical currents and fields is difficult. A stable superconducting wire must consist of a large number of very fine filaments embedded without touching one another in a copper matrix. This matrix should have good thermal and electrical conductivity, and the whole composite should be twisted to accomodate dynamic magnetic fields. At present, the only class of conductors that have been suc-

cessfully developed using these ideas have been the class of ductile superconductors. The material used in virtually all applications is an alloy of niobium and titanium. The wire is made by first manufacturing solid rods of the NbTi alloy each about one centimeter in diameter, and perhaps 30 or 40 centimeters long. These rods are then slid into closely fitting copper tubes of the same length, but with an hexagonal outside perimeter. These copper tubes, with the NbTi rods in their centers, are then stacked in arrays to form a billet with axial symmetry perhaps 50 centimeters in diameter and 30 or 40 centimeters long. This array is encased in a copper jacket and drawn into wire. Area reduction ratios of 10^6 are not hard to achieve but the drawing process must have various intermediate anneals and heat treatments to form the required pinning sites in the NbTi alloy. The twisting of the composite can be achieved as an integral part of the drawing. Magnets made from this type of wire have proven robust and reliable, but they are restricted to fields of less than 10 tesla by a low value of H_{c2}. At present, hopes for an intrinsically stable wire with higher field capability rest on finding a process for producing multifilamentary Nb_3Sn.

Nb_3Sn conductors cannot be formed in the same way as NbTi because Nb_3Sn has an A-15 crystal structure, which is quite brittle. Nb_3Sn will therefore crumble if an attempt

is made to draw it into wire, so that it must be formed only after the material is drawn, or in some process which does not require any drawing, like vapor deposition. Nb_3Sn superconductors have been made which are suitable for high field magnets, but usually in the form of a vapor deposited tape which is not adiabatically stable. Hence these conductors must be ramped slowly, and kept well below their critical fields for reliable operation. Progress toward a multifilamentary structure for Nb_3Sn has been made recently,[62] however, by drawing pure niobium rods in a copper-tin alloy (bronze) matrix. Both of these materials are ductile enough to allow considerable drawing, and a high temperature anneal after the drawing reacts the tin with the niobium to form an interfacial layer of Nb_3Sn on the surface of each niobium filament. This process has several difficulties. First, control over the final reaction is poor, so it is hard to make uniformly high quality (stoichiometric) Nb_3Sn. Performance therefore seldom matches theory. The second problem is that the Nb_3Sn layers on each filament are still brittle so that bending the wire to wind a solenoid can ruin the conductor. Finally, the process is more complex and expensive than that used for the ductile Nb alloy superconductors.

C.C. Tsuei has proposed a new technique for manufacturing multifilamentary superconductors, which is easily

applied to Cu-Nb_3Sn composites. The process is strictly metallurgical, avoiding the costly manipulation of each individual filament which is intrinsic to all present processes, yet it produces filaments with thicknesses of a micrometer or less, with perhaps 10^5 filaments in the cross sectional area of the composite wire. The filaments are so fine that they may be sharply bent without breaking, and the quality of the Nb_3Sn should ultimately match that possible with present multifilamentary techniques. The only fundamental distinction (apart from filament size, and hence flexibility) between the results of Tsuei's process and those of the conventional techniques is that the array of filaments in Tsuei's wire is random, and the filaments themselves are discontinuous. It is the purpose of the rest of Part II to examine the effects of this disorder on the superconducting properties of Tsuei's wire. Chapter 6 describes the process by which the wire is made. Chapters 7 and 8 present the results of our experiments with the wire. Chapter 9 covers a theoretical model for estimating the resistive properties that were observed in some of the experiments. The model also explains data on other inhomogeneous media. Finally, Chapter 10 summarizes our conclusions and lists directions for further research.

CHAPTER SIX: TSUEI'S MICROCOMPOSITE WIRE

6.1 The Process

Tsuei's technique[41] for manufacturing superconducting A-15 filaments in a copper matrix uses a microscopic metallugical process, rather than mechanical stacking of macroscopic arrays. The structure resulting from Tsuei's process is shown in Fig. 22. The copper was etched from the end of a piece of microcomposite wire and the freed filaments photographed in a scanning electron microscope. The technique used to produce these filaments evolved from some experiments by Newkirk and Tsuei.[44] They were studying the process by which high purity copper becomes superconducting after being melted in a niobium crucible. Controlled amounts of Nb were dissolved into molten Cu, and when cooled, the microstructure and superconducting properties of the resulting composite were studied. Tsuei and Newkirk found, in accordance with the phase diagram of the Cu-Nb system, that the Nb did not remain dissolved in the Cu as the system cooled, but instead would precipitate out and form discrete particles with a range of size determined by the cooling rate and by the Nb concentration. Particles of characteristic dimension less than one micrometer resulted from rapid quenching or form Nb concentrations of less than 1.5 atomic %. Ten micrometer particles seemed to dominate

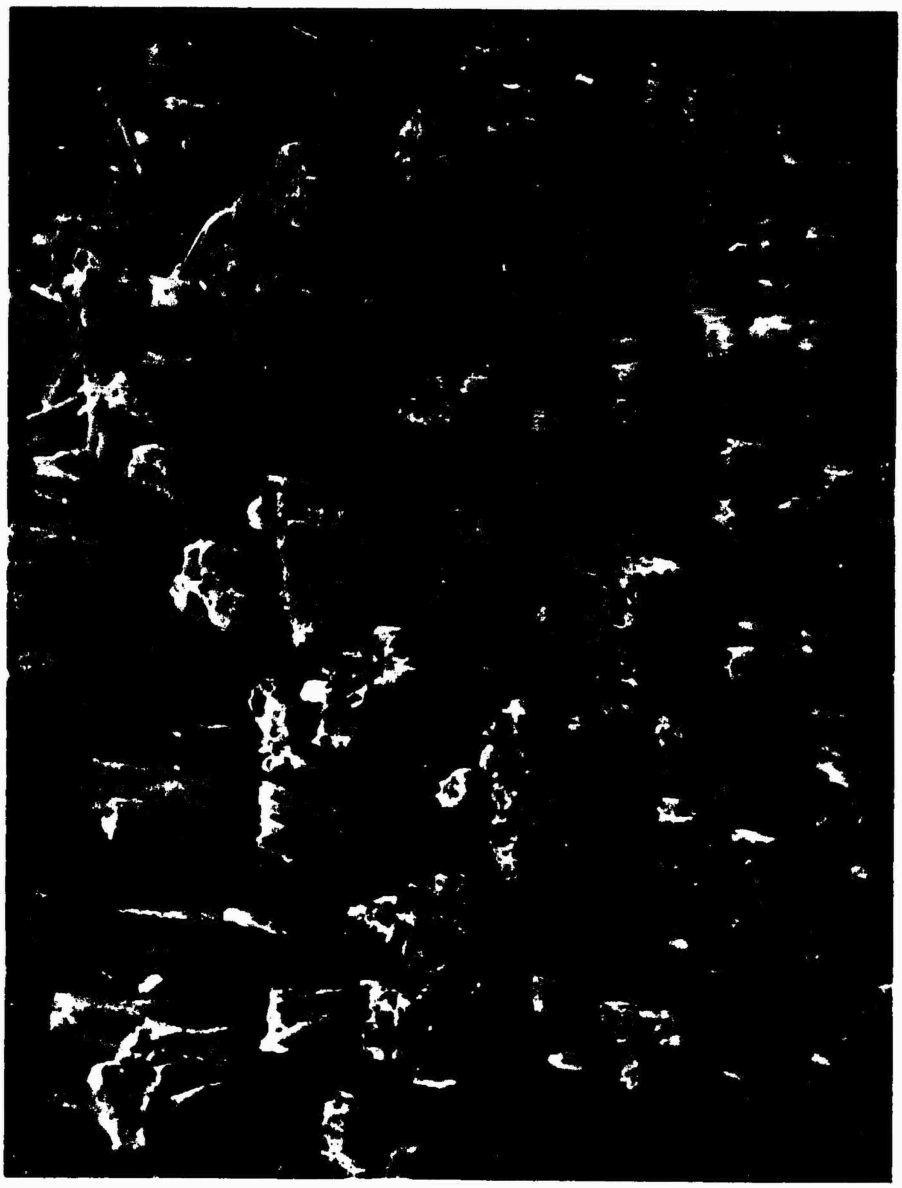

Fig. 22 Scanning electron micrograph of filaments in Tsuei's microcomposite wire. The copper has been etched away from the end of the wire, exposing the filaments. The wire had a reduction ratio of about 40, and the magnification here is about 1500.

the microstructure for larger concentrations and for longer cooling times.

The microstructure of this Cu-Nb composite not only explained the superconductivity of "pure" copper that had been melted in a niobium crucible, but also provided a very simple and direct means of producing a multifilamentary composite. Clearly, the melted copper dissolves some small amount of the niobium crucible, and as the sample is cooled, the niobium precipitates in the form of small or large particles, and these discrete Nb particles account for the observed superconductivity of the composite. It was also clear that these same Nb particles could be drawn into filaments if the ingot were drawn into wire. Studies of such wire, pursued by Tsuei,[42] confirmed the existence of these filaments in the drawn wire, and further showed that the superconducting properties of the material tended to improve with increased reduction (drawing) of the wire. These studies used as much as 10 atomic % Nb in the composite, and other studies have shown 20 atomic % composites to be workable.[68]

With these encouraging results in hand, Tsuei next added a small amount of Sn to the Cu-Nb melt, to form a bronze, rather than copper, matrix around the Nb particles in the undrawn material. Then, after drawing, a high temperature anneal (600 to 800 ^{0}C) reacted the Sn in the bronze matrix

with the Nb filaments to form a layer of Nb_3Sn at the Cu-Nb interface, in the same manner as in conventionally constructed Cu-Nb_3Sn composites.[41,43] The resulting superconducting transition temperature of 15 to 18 K together with X-ray studies confirmed the formation of Nb_3Sn at the interfaces.

The final Cu-Nb_3Sn microcomposite superconducting wire has several advantages over conventional macrocomposites. First, the wire is inexpensive to produce since the process is not much different from that used to make simple Cu wire. Second, the composite could have excellent superconducting stability. The filaments typically have sub-micrometer diameters and should be in particularly clean contact with the copper matrix; thus both adiabatic and dynamic stability conditions are met, with the additional possibility that the finite length of each filament might play a role in ac stability similar to that played by the twist pitch in conventional composites. Finally, the small diameter and good metallurgical bond of the filaments to the Cu mean that the composite should be quite flexible. Studies[43] of this last feature have shown that bending the wire repeatedly around a one inch mandrel tends only to increase the critical current of the composite. These three factors make the microcomposite technique quite attractive, but there are problems.

Tsuei's microcomposite superconductors have two distinct disadvantages. First, the Nb concentration is restricted to values less than 20 atomic %, so that overall current densities may not be quite as large as conventional techniques could allow. Second, and more fundamentally, the filaments, though uniformly aligned, are disordered in size and position. The effects of this disorder are by no means clear, and they are the principal concern of Part II of this report. We present evidence in later chapters suggesting that the effects of the disorder are that any remnant resistance of this wire will diminish roughly as the inverse cube of the area reduction ratio of the drawn wire; that superconduction in these disordered materials is a percolation process; and that the fundamental obstacle to application of this wire may be a lack of ac stability due to percolative clusters of filaments. We will also use the insight gained from considering this novel composite as a percolation system to propose a modification of an old but currently popular theory of conduction in disordered normal conductors for the case in which conductivities differing by orders of magnitude are involved.

6.2 The Technique

A process for producing microcomposite superconducting wire of Tsuei's type has been developed at Harvard Univer-

sity by J. Bevk and J. Harbison. They begin with a block of pure Cu, with a typical volume of one cubic centimeter, and wrap the desired weight of pure Nb foil around it. They use these bulk materials rather than powders to minimize oxidation. The Nb wrapped Cu is then placed in a levitation coil energized by a high power radio frequency generator, and the sample is induction melted in an argon atmosphere but without physical contact to any boat. This levitation technique minimizes the chance of contamination and maximizes the power available to heat the sample. When the sample is completely molten, it is dropped into a mold by smoothly reducing the radio frequency power until the sample falls through an opening in the bottom of the levitation coil. This process is repeated several times to be sure that the ingot is well mixed, and then Sn in the required amount is added to the sample. The whole process is repeated with the Sn several more times to assure uniform mixing of all three components. This process results in a high quality well mixed sample, but one which has been quenched by falling into a cold mold. To control the cooling rate the sample is remelted in a water cooled Cu boat, and cooled relatively slowly (100 K/sec) to the solid state. The final ingot has a diameter of about 0.8 cm. It is swaged to about 0.1 cm and then drawn to about 0.05 cm in diameter, for an area reduction ratio of roughly 300. The advantages of this

levitation technique are: first, the levitation coil can handle relatively large masses, the order of ten grams; second, the samples can be raised to a higher temperature than with a boat technique, and mixed more thoroughly; and third, the final controlled cooling can be optimized independently for minimum thermal and hence compositional gradients.

Other techniques have been used to make the same kind of Cu-Nb-Sn microcomposites, and we list them here without attempting evaluations. The initial work of Tsuei and Newkirk[44] involved melting the Cu and Nb by induction in a glassy carbon crucible, though later Tsuei used a water cooled silver boat and induction melting to make the multifilamentary Nb_3Sn composites.[41] Callaghan and Toth,[69] at the University of Minnesota, have studied electrical resistivity as a function of reduction and current density on samples made by arc melting powders. The microstructure evident in their composites look qualitatively no different from Tsuei's. R. Roberge and R.D. McConnell,[70] at the Institut de recherche de l'Hydro-Quebéc, however, also prepared samples by arc melting, but reported a microstructure somewhat different from that observed by Tsuei. They reported a nearly continuous sponge-like network of Nb precipitates rather than discrete particles. They suggest that the same structure could also be present in Tsuei's

material but that it was not observed by Tsuei because of the way his samples were prepared for microscopic study. Roberge and McConnell report only scanty electrical data, however, so it is impossible at this time to decide if their samples behave electrically like Tsuei's. Finally, Tsuei has suggested that a zone melting scheme might be possible,[71] should it prove desirable to produce this wire on an industrial scale. That is, the Nb and Sn could be dissolved into a small stationary molten zone of Cu. Pure Cu would be continuously fed into the molten region from one side and the microcomposite withdrawn from the other. When a suitable length of microcomposite has been produced, it could be cut off and drawn into the desired size wire.

The microcomposite samples we have studied for this report were made only by the induction melting techniques. Some of the wire was made at the California Institute of Technology with the silver boat technique, and some made at Harvard with the levitation technique. Our experiments to date have not revealed any microstructural distinction between the wires.

CHAPTER SEVEN: MAGNETIZATION OF MICROCOMPOSITE SUPERCONDUCTORS

If wire made by Tsuei's process is to have any utility, an understanding of the mechanism for coupling current between filaments is essential. If the filaments are strongly coupled, one would expect current transport properties much like those of conventional multifilamentary composites. If, however, the filaments are only weakly coupled, then in high fields and currents one would expect a certain amount of resistance to appear due to current flowing through normal copper. Since the magnitude of this resistance would have to be extremely small for practical microcomposite wire to compete with conventional composites, an investigation of the coupling mechanism is in order. Our investigation has been conducted with two techniques: resistance measurements treating current and temperature as independent parameters; and magnetization as a function of applied field and temperature. The magnetization experiments suggest a proximity effect[72] coupling mechanism, while the resistance data are consistent with a percolation model for filament coupling. We shall discuss the magnetization of our disordered microcomposites in this chapter, and their resistivity in the next.

7.1 Magnetization Measurements

Magnetization measurements of a multifilamentary superconducting wire in a longitudinal field are a direct probe of transverse coupling between filaments. The magnetization $\vec{M}$, of a long cylinder of material in a uniform axial field is defined by the relation

$$\vec{B} = \mu_o(\vec{H} + \vec{M}) \quad . \tag{7-1}$$

The Meissner effect, described by the equation $\vec{B} = 0$, occurs in the bulk of pure superconducting materials in weak fields. These materials are said to perfectly diamagnetic since, from (7-1), the magnetization $\vec{M}$ exactly cancels the applied field $\vec{H}$, or $\vec{H} = -\vec{M}$. For inhomogeneous materials, however, the Meissner effect may occur partially or not at all, and the magnitzation is described better in terms of the magnetic flux Φ in the sample instead of the applied field $\vec{H}$. From (7-1), the flux enclosed in any cross section of the cylindrical sample is

$$\Phi = \int\vec{B}\cdot d\vec{A} = \mu_o\int\vec{H}\cdot d\vec{A} + \mu_o\int\vec{M}\cdot d\vec{A} \quad .$$

But the integral of $\mu_o H$ is the applied flux, Φ_a, that would be in the sample area if the magnetization were zero. The integral of M can be written as the average magnetization of

the sample, $\bar{M}$, multiplied by the cross sectional area of the cylindrical sample, A. Hence we may write

$$\bar{M} = \frac{\Phi - \Phi_a}{\mu_o A} \quad . \tag{7-2}$$

Inhomogeneous materials can generate curves of magnetization versus temperature with two branches. If the field is applied only when the sample is already below the transition temperature, then screening currents flowing around the circumference of the sample can prevent the entrance of magnetic flux. From (7-2), this leads to a large diamagnetic response, $\bar{M} \simeq -\Phi_a/\mu_o A = -H$. However, if the magnetic field is applied before the sample is lowered through its transition temperature, some magnetic flux may be trapped by inhomogeneities and not expelled, thus reducing the magnitude of the average magnetization in (7-2) from the full Meissner value. A two-branched magnetization curve as a function of temperature for an inhomogeneous superconductor is shown in Fig. 23. The curve A-B arises from the screening of applied flux, and is called the screening response. The branch B-C resulting from a partial expulsion of flux is called the expulsive response. The whole curve is termed irreversible, since the screening response cannot be repeated unless the applied field is removed and the sample cooled through T_c again.

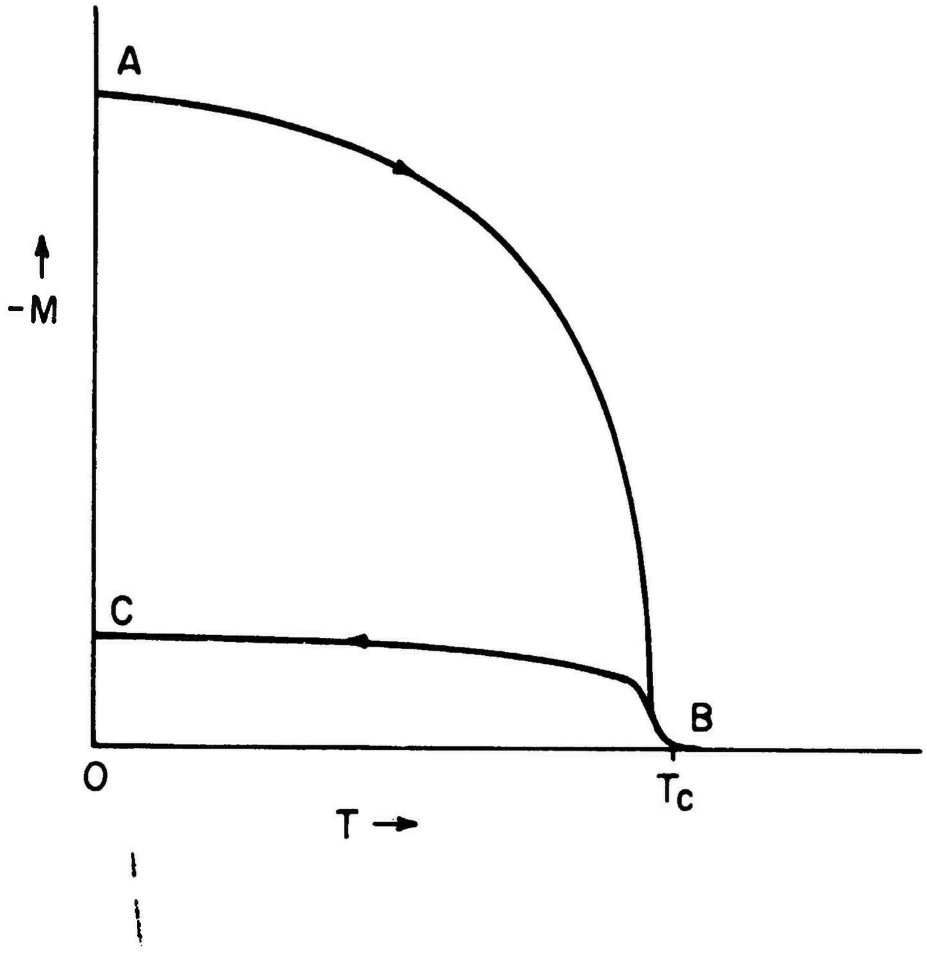

Fig. 23 Schematic irreversible magnetization curve. A-B is the screening response, and B-C is the expulsive response.

The screening part of an irreversible magnetization curve contains the information we need about the lateral coupling of filaments in the microcomposite wire. Well coupled filaments will allow supercurrents to screen weak applied fields from the bulk of the sample. The screening magnetization will then be about $\bar{M} = -H$ for low enough temperatures and applied fields. On the other hand, filaments with weak coupling could admit some flux thus reducing the magnitude of $\bar{M}$ below $|H|$. The expulsive part of the irreversible curves contain very little information useful for determining the coupling strength between filaments. The ability to expel flux has no simple relation to the interfilament coupling but instead depends on numerous metallugical parameters. Measurements of screening magnetization, then, are a direct probe of interfilament coupling. If the filaments are coupled by supercurrents we expect to measure a large screening response. If the current between filaments is strictly normal we expect only a small amount of screening.

The instrument we used to measure this screening was the SQUID magnetometer developed by J.P Gollub[74] for this laboratory, and modified by D.E. Prober.[75] This instrument measures the temperature dependence of the quantity of flux inside a cylindrical sample in a parallel field. The apparatus as used for these measurements was capable of resolving about 10^{-2} flux quanta (2×10^{-19} weber). Data were

taken by first cooling the sample below T_c in an ambient field less than about 10^{-7} tesla. Then a field parallel to the axis of the sample was applied and the sample temperature slowly raised above T_c. As the sample warmed, flux moved in and was detected by a superconducting pickup coil and flux transporter which was coupled to the SQUID, and the SQUID output as a function of temperature recorded on an x-y plotter. Finally the field was removed and the sample cooled below T_c again, so that it would be ready for application of a new field. Hence we measured the initial part of a classical magnetization curve starting at the origin of the M-H plane, even though the raw data were taken as a function of temperature. Data could not be taken directly as a function of H because the superconducting solenoid that produced the field had to be kept in its persistent current mode for stable operation of the SQUID.

7.2 Magnetization of Wire with Five Atomic Per Cent Niobium

The magnetization curves of microcomposite wire containing 5 atomic % Nb reveals that the superconducting filaments are weakly coupled by supercurrents over a wide range of reduction ratio. All of the samples available for testing were manufactured at the California Institute of Technology by Wilkie Y-K Chen by the induction melting technique (see Chapter Six) in a water cooled silver boat.

Four samples were tested, with reduction ratios of approximately 10, 40, 200, and 800. These reductions correspond to wire diameters of 0.20 cm, 0.10 cm, 0.05 cm, and 0.025 cm. All samples contained 1.5 atomic % Sn, and after drawing were annealed at 600 ^{o}C for 48 hours to form the interfacial Nb_3Sn. The presence of filaments was confirmed by examination of polished and etched specimens in the scanning electron microscope in the Gordon McKay Laboratory at Harvard. The persistence of superconductivity to nearly 16 K in these samples was taken as sufficient evidense for the presence of Nb_3Sn on the filaments. Detailed compositional analysis by X-ray or microprobe techniques was not carried out, but such analysis performed by Tsuei[41] has always revealed the presence of Nb_3Sn.

As discussed in section 7.1 the raw data from the magnetometer is magnetization as a function of temperature, but it can be replotted as magnetization versus applied field. To illustrate this feature we have plotted the data from the 0.05 cm sample (R = 200) both ways in Figs. 24 and 25. Figure 24 shows the magnetization normalized by the applied field (that is the susceptibility) as a function of temperature for two applied fields of 10^{-4} and 10^{-5} tesla. Both the screening and expulsive branches of the curve are shown. Note that the weaker field produces a larger screening response in this normalized plot, but a smaller expulsive

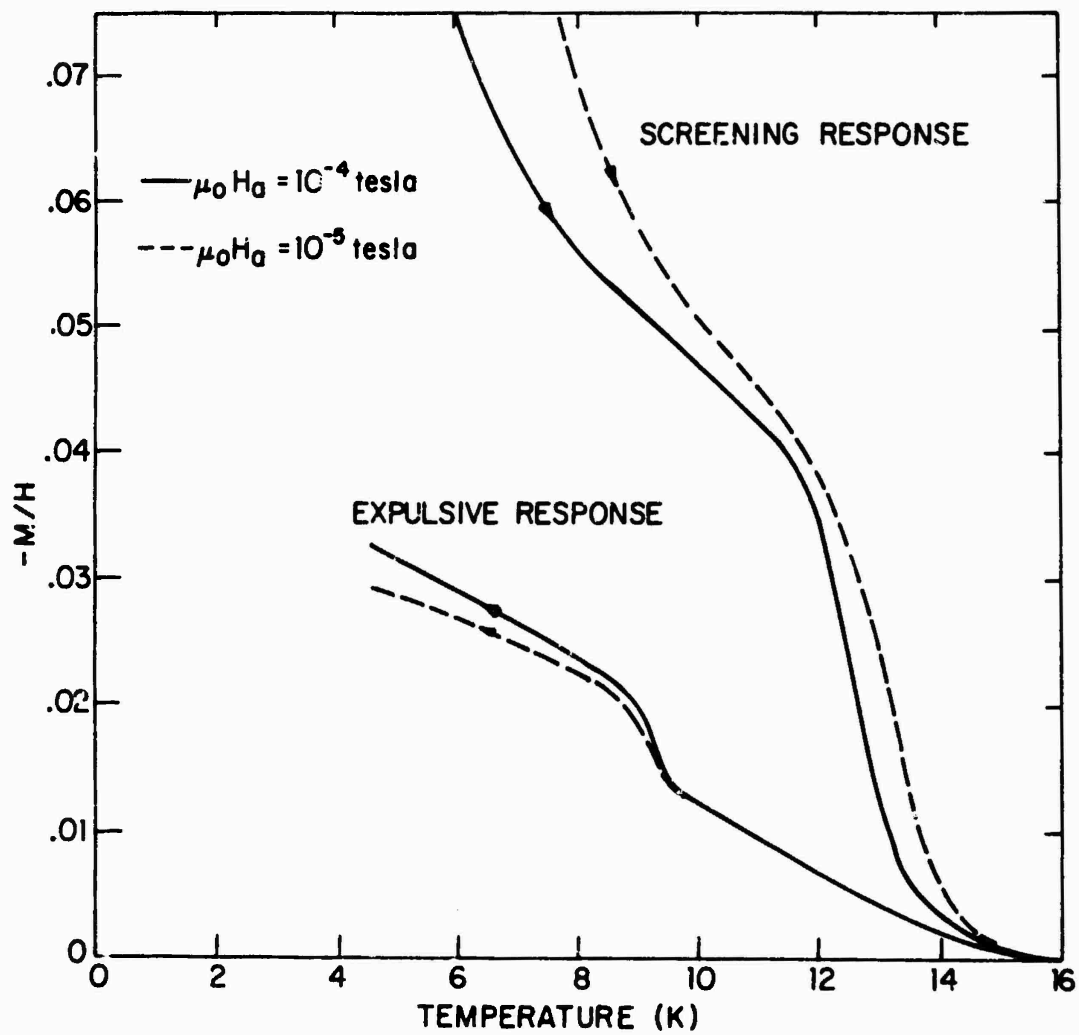

Fig. 24 Normalized magnetization versus temperature for 0.05 cm 5 atomic % Nb wire, R=200.

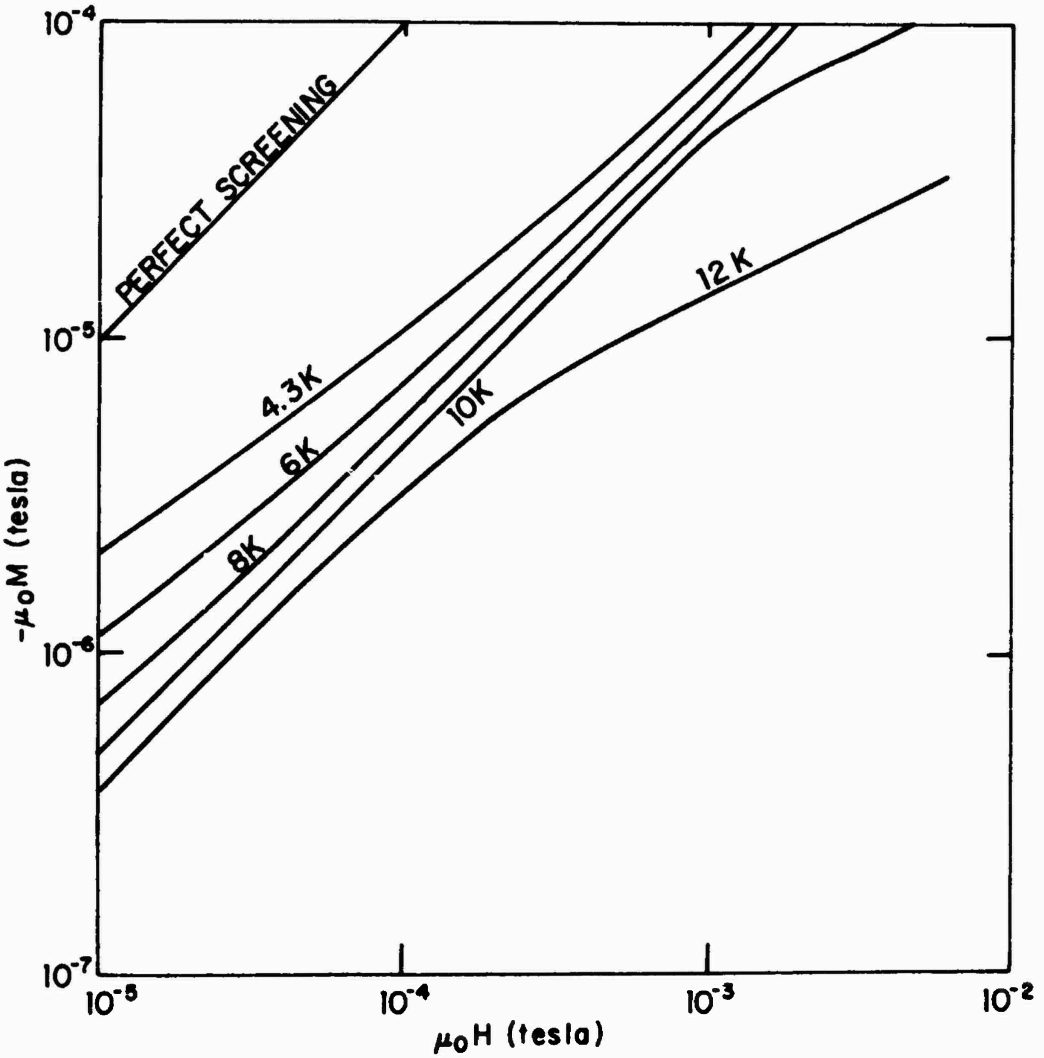

Fig. 25 Magnetization versus field for 0.05 cm 5 atomic % Nb wire, R=200

response. Hence the screening part of the curve behaves as expected: the sample becomes more diamagnetic in weaker fields. The expulsive response is less predictable, however. That less of the weaker field is expelled is an example of the difficulty in interpreting this part of the data, and for most of what follows we ignore the expulsive response. Accordingly, in Fig. 25, all screening data for the same 0.05 cm wire have been transposed to the M-H plane, and plotted for several different temperatures. The trends in this plot are quite clear. Lower fields and lower temperatures yield increased screening. Yet the lowest fields and temperatures do not yield perfect screening. A field of 10^{-5} tesla (0.1 gauss) evokes only 20 % of the full screening response at 4.3 K. At 10^{-6} tesla, not shown in Fig. 25, the response is only about 30 %. The data on this sample, then, indicate that its filaments are semi-isolated. Screening currents can flow between some filaments at low temperatures and fields, giving some regions a large diamagnetic response, but other filaments presumably are completely isolated, allowing the applied field to penetrate the copper around them. The strong temperature dependence of the screening response even at $T \simeq T_c/4$ is suggestive of a proximity effect coupling mechanism.

If the proximity effect is responsible for coupling supercurrents between filaments then one would expect the

screening response to increase with increasing reduction ratio. That is, filaments in wire with a large reduction ratio are closer together and proximity effect superconductivity in the copper would be correspondingly stronger. To test this correlation we have plotted in Figures 26 and 27 the screening magnetizations of samples with reductions smaller and larger than the reduction value of 200 for the 0.05 cm diameter sample. Data on the 0.20 cm sample, with a reduction ratio of 10, is shown in Fig. 26. The screening response here approaches a level of only 5 % at 4.3 K, compared to about 20 % for the 0.05 cm wire that was reduced a factor of 200. These two samples compare qualitatively as we expected: the wire with more reduction has a larger screening response. The screening response also correlates with reduction ratio for the 0.025 cm sample. The screening curves for this wire, with a reduction of 800, are displayed in Fig. 27. Here the screening exceeds 40 % at 4.3 K and 10^{-5} tesla, and, at an extra data point taken for this sample the screening approaches 70 % at 2.3 K and 10^{-5} tesla. At low fields and temperatures, then, there is positive correlation between a large reduction ratio and a large screening response.

This low temperature and field correlation, however, does not hold at high temperatures or fields. For example, a direct comparison between the 4.3 K curves in Figures 25,

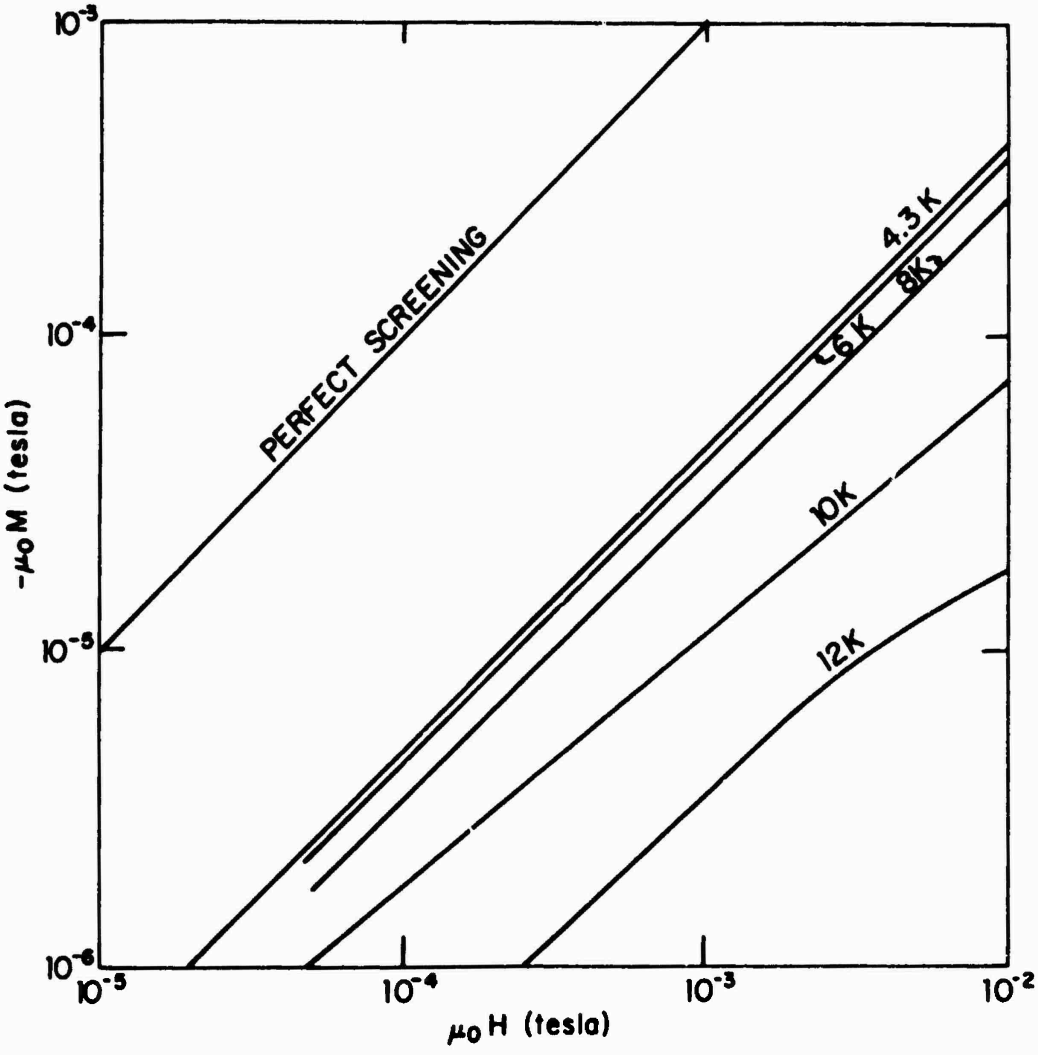

Fig. 26 Magnetization versus field for 0.20 cm 5 atomic % Nb wire, R=10

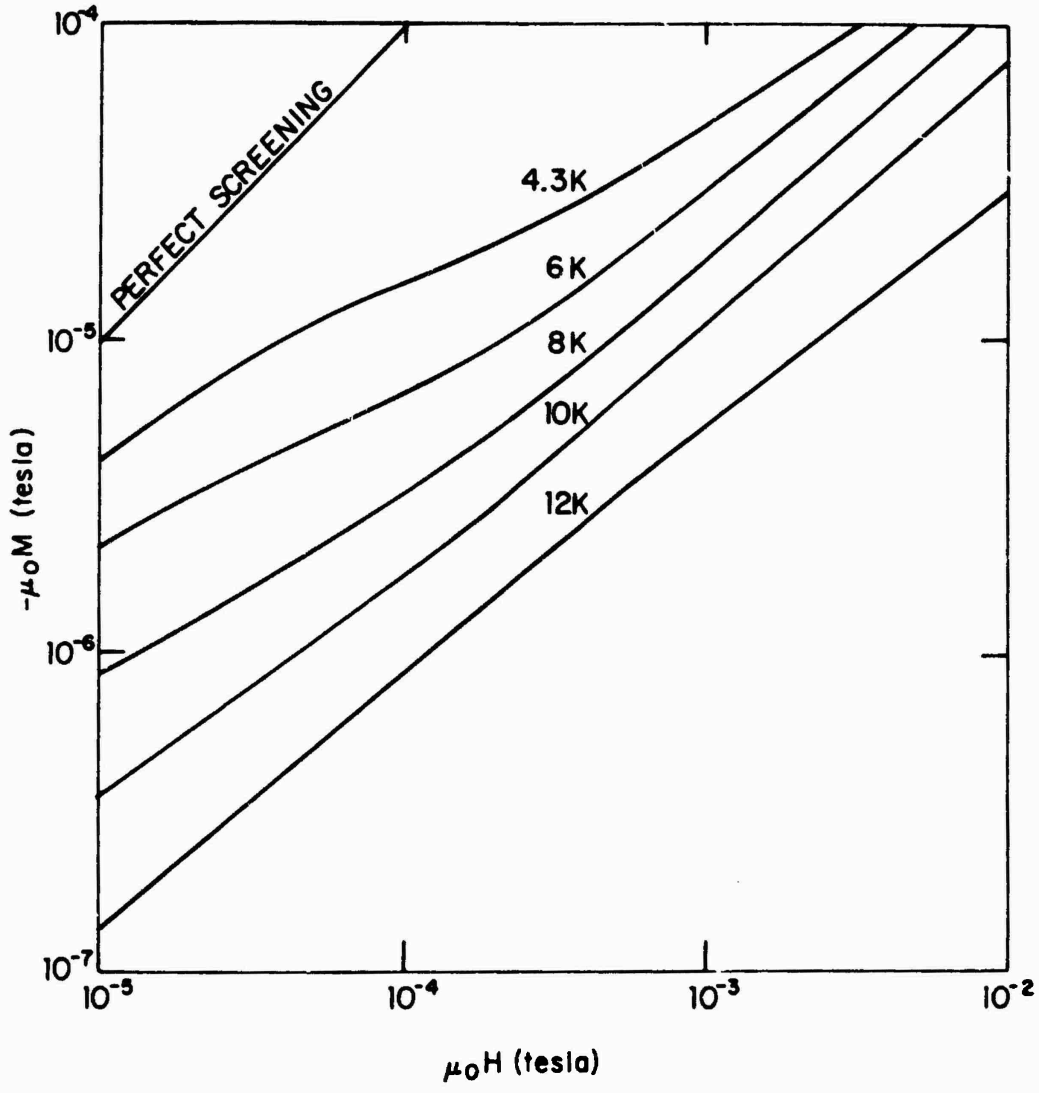

Fig. 27 Magnetization versus field for 0.025 cm 5 atomic % Nb wire, R=800.

26, and 27 reveals that the curve for the sample reduced a factor of 800, Fig. 27, crosses over the other two curves near $3x10^{-4}$ tesla and 10^{-3} tesla. This phenomenon is shown explicitly in Fig. 28, which graphs the 4.3 K curves for all three samples. It is as if the flux penetrates the copper of the R = 800 sample rather quickly as the field is raised, but then continues to penetrate the filaments themselves. There is apparently less penetration of the filaments in the two samples with thicker filaments. Even in weak fields and at low temperatures, however, none of the 5 atomic % Nb samples show complete screening, and the general behavior of the screening curves as a function of reduction ratio suggests that the filaments are only weakly coupled. Strong direct contact between filaments can be ruled out as a coupling mechanism in the 5 atomic % Nb samples.

7.3 Magnetization of Wire with Ten Atomic Per Cent Niobium

The magnetization of microcomposite wire containing 10 atomic % Nb reveals that the filaments are more strongly coupled than in the 5 atomic % Nb samples. We have had two specimens of 10 atomic % wire available for testing and both display a near perfect screening response at low fields and temperatures. The first sample was made at the California Institute of Technology by induction melting in a water cooled silver boat, and had a reduction ratio of about 600.

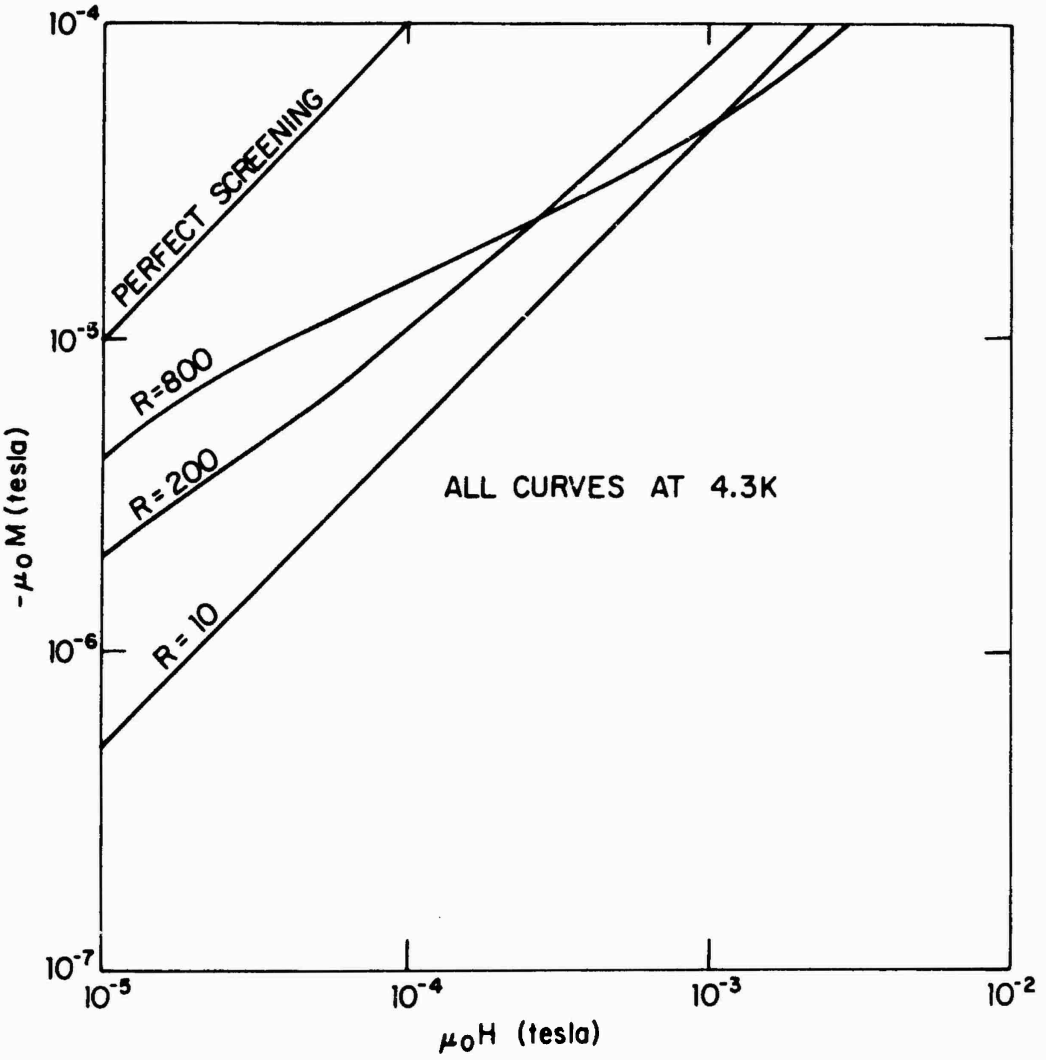

Fig. 28 Magnetization versus field for three reductions of 5 atomic % Nb wire, all at 4.3 K.

The second wire was made at Harvard University by the levitation technique, and was reduced in area a factor of roughly 300. In what follows we distinguish the two wires with the symbols CCWR600 and HCWR300, which stand for "California (Harvard) Composite Wire, Reduced a factor of 600 (300)." Both samples contained 1.5 atomic % Sn, and were annealed at 600 ^{o}C for 48 hours. Cursory microscopic surveys with the scanning electron microscope failed to reveal any obvious microstructural distinctions between the two wires. The superconducting critical temperature as measured from the magnetization curves was about 15.5 K for CCWR600 and about 14.5 K for HCWR300. The magnetization curves for CCW are plotted in Fig. 29, and those for HCW in Fig. 30. The nearly perfect screening evident in both figures at low temperatures and fields implies that supercurrents can flow easily between filaments. By definition, therefore, the filaments are well coupled, in contrast to the 5 % case.

The magnetization curves of the two 10 atomic % samples not only differ qualitatively from the 5 atomic % samples, but also differ between themselves. They both exhibit strong screening in small fields and at low temperatures in contrast to the weak screening of the 5 % wires, but in higher fields and temperatures the screening response decays differently in each. The CCWR600 sample in Fig. 29 loses its

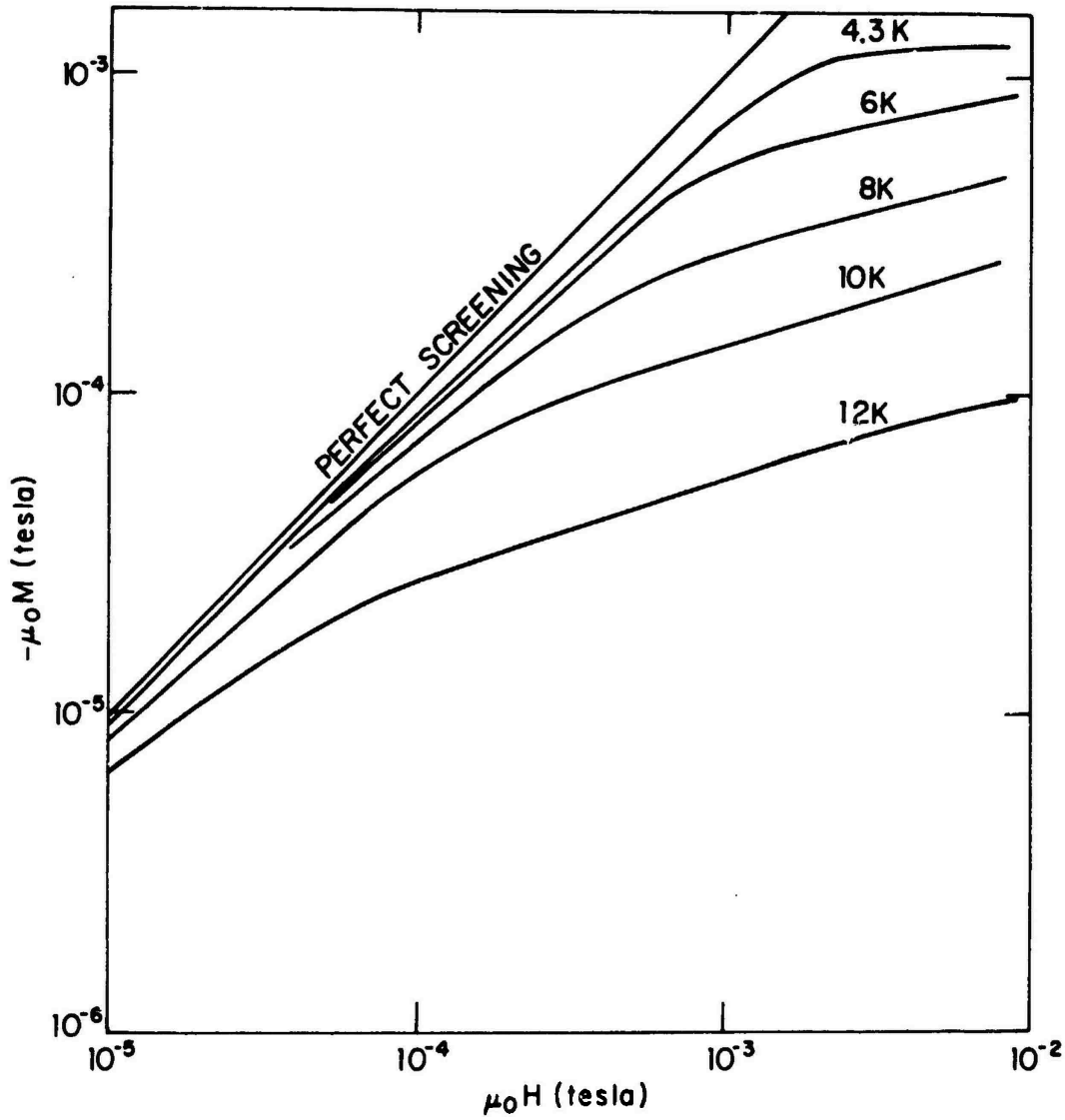

Fig. 29 Magnetization versus field for CCWR600, 10 atomic % Nb wire, R=600

shielding rather gradually. For the fields and temperatures plotted, the screening response is always monotonically increasing. In high fields the rate of increase does not keep up with increasing applied field, and the result is the admission of flux to most of the sample. At 4.3 K there is a relatively abrupt change in slope of the screening curve at a field of about 2×10^{-3} tesla, indicting that flux moves into the sample after that point, but never so quickly that the screening curve would begin to decrease. At higher temperatures, the change from low field to high field behavior is more gradual, but qualitatively the same as the 4.3 K curve. All of the curves for the CCW sample, then, increase monotonically. The HCW sample in Fig. 30, however, does not have a monotonic screening curve. In small fields and low temperatures this sample exhibits the same large screening response as the CCW specimen, but at high fields, the magnetization turns around and begins to decrease. The 6 K curve, for example, turns around at about 3×10^{-3} tesla, and thereafter magnetic flux enters the sample rapidly. The negative slope of the high field magnetization of HCW distinguishes it from the monotonic behavior of CCW, but both are distinguished from the 5 atomic % specimens by a virtually complete screening response at low fields and temperatures.

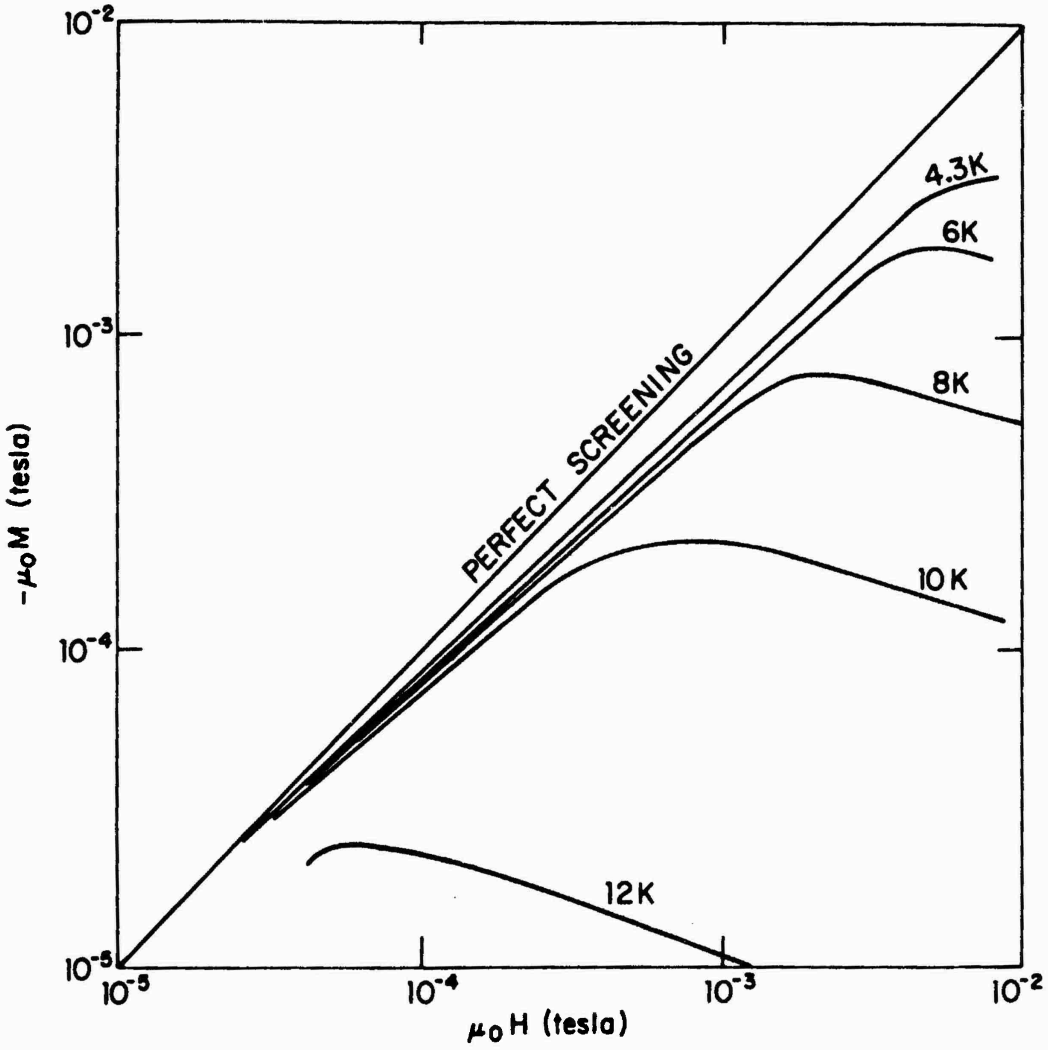

Fig. 30 Magnetization versus field for HCWR300, 10 atomic % Nb wire, R=300.

7.4 Discussion

A proximity effect model for interfilament coupling can qualitatively account for the observed screening magnetization in each of our samples. The proximity effect[72] is the induction of superconductivity in an ordinarily normal metal by a superconducting material in close proximity. The same term, however, can also apply to the destruction or abatement of superconductivity in a superconductor in intimate contact with a normal metal. Both effects can occur at the same time. Superconductivity in the normal metal extends away from the normal-superconducting (NS) interface for a distance determined by the normal metal properties. The characteristic length is called the normal coherence length, ξ_N. In a clean metal that ordinarily remains normal down to extremely low temperatures, the normal coherence length is given by

$$\xi_N = \frac{\hbar v_N}{2\pi k_B T} \qquad \text{(clean)} \qquad (7\text{-}3a)$$

where v_N is the fermi velocity of the normal metal. For a dirty metal (where the mean free path is much shorter than the clean coherence length) the normal coherence length becomes

$$\xi_N = \left(\frac{\hbar v_N \ell_N}{6\pi k_B T} \right)^{1/2} \qquad \text{(dirty)} \qquad (7\text{-}3b)$$

where ℓ_N is the mean free path. While superconductivity extends into the normal metal a length characterized by the normal coherence length, it is depressed within the superconductor near the NS interface for a length the order of the ordinary Ginzburg-Landau temperature dependent coherence length:

$$\xi_{GL}(T) \simeq \xi_o(1 - T/T_c)^{-1/2} \qquad \text{(clean)} \quad (7\text{-}4a)$$

$$\simeq (\xi_o \ell)^{1/2} (1 - T/T_c)^{-1/2} \qquad \text{(dirty)} \quad (7\text{-}4b)$$

where ℓ is the mean free path in the superconductor, and ξ_o is the BCS coherence length.

The proximity effect has been studied theoretically by de Gennes,[72,76] and experimentally by Clarke[20], and by others. Clarke's experiments involved an SNS structure, rather than a single NS interface. He was able to show that the SNS junction could support a supercurrent between the S layers of the sandwich, and that the structure generally behaved like a very low impedance Josephson tunnel junction. Unlike tunnel junctions, however, SNS junctions can have a very thick barrier. Clarke managed to get supercurrent coupling through dirty normal regions of thickness approaching one micrometer, at low temperatures. The critical current was found to increase roughly exponentially at low

temperatures, in contrast to tunnel junctions, which have approximately constant critical currents at low temperatures. The ability of SNS junctions to pass supercurrent through thick barriers is the feature we propose to exploit in a proximity effect model of our microcomposite wire.

A model that assumes isolated filaments in a sea of copper, with supercurrent between filaments supported strictly by the proximity effect, can account for the low field and low temperature screening characteristics of our samples of microcomposite wire. Superconductivity in the copper extends away from a filament for a distance characterized by the normal coherence length. This length is much shorter in the 5 atomic % samples than in the 10 atomic % samples. Resistivity measurements above T_c show the 5 % samples to have a mean free path[77] of about 200 Å, compared to 3000 Å and 6000 Å in the 10 % CCW and HCW samples respectively. The clean coherence length at 4 K, however, is about 5000 Å, assuming a fermi velocity of 1.5×10^6 m/sec. Hence the 5 % samples have ξ_N = 1000 Å and are in the dirty limit, but the 10 % samples are marginally clean. It is simple to explain qualitatively the relative cleanliness of the 10 % samples, since their larger concentration of Nb pulls more Sn out of the copper matrix during the final high temperature anneal (The Sn concentration was 1.5 atomic % in all our samples). The longer mean free path in HCW compared to

CCW could be due to a slight difference in Nb concentration between the two samples. For any sample, clean or dirty, we expect good proximity effect coupling of adjacent filaments when the normal coherence length becomes comparable to half the average filament separation.

Simple calculations show, and microstudies confirm, that typical separations in these microcomposites are approximately two micrometers. Further, the separation varies inversely as the square root of the area reduction ratio and directly as the square root of the volume concentration of filaments (for well drawn wires). Hence the two micrometer value holds within a factor of two for our samples with reduction ratios between 200 and 600. Sample CCWR600 alone has a typical interfilament spacing closer to one micrometer, due to a combination of high reduction and large Nb concentration.

Hence the proximity effect model provides a qualitative explanation of the behavior of our samples in small fields and at low temperatures. The 5 % samples typically have normal coherence lengths much smaller than half the interfilament spacing, and so have relatively little suppercurrent coupling between filaments. Further, what coupling there is, scales with the reduction ratio as one would expect: closer filaments yield better coupling. The 10 % samples, on the other hand, have normal coherence lengths close to the clean

value of 0.5 micrometer, which is comparable to half the filament spacing, so the strong coupling observed in the magnetization measurements is to be expected.

The proximity effect model may also provide an explanation of the different behaviors in high fields of the two 10 % samples. That the screening curves for the CCW sample remain monotonic after complete screening breaks down, if put in terms of the Bean model of flux penetration,[58] would imply that the critical current density within the copper was independent of field. But a field-independent critical current in the copper would be expected only if superconductivity in the <u>filaments</u> was not depressed by the penetrating field. This last statement could hold in fields of 10^{-2} tesla or so if the copper was not too clean. That is, superconductivity in the S side near the NS junction is suppressed less as the mean free path of the N side becomes shorter.[78] Presumably, the CCW sample was dirty enough so that superconductivity was not greatly reduced in the filaments. However, the HCW sample was cleaner than CCW by a factor of two. Superconductivity in the filaments in HCW might then have been weakened sufficiently by the clean copper to have become susceptible to the applied fields, and so cause a field dependent critical current in the copper. Such a critical current, in the Bean model, would account for the change in sign of the slope of the magneti-

zation of HCW after screening first breaks down.

To put the above analysis on a firm footing would require a detailed analysis of the proximity effects in clean materials. To the author's knowledge, such a study has not yet been done. We can give some support to the Bean model picture of flux penetration in our microcomposites, however. We note that using the Bean model[58] to interpret the measured screening magnetization implies a critical current density in the copper at 4.3 K of about 10^3 amp/cm^2. This is a reasonable value, and provides some justification for our conjectures.

As a final topic in this chapter, we consider the possibility that the proximity effect lowers the transition temperature of the composite. One might suspect a reduction in T_c in some of these microcomposites because of their fine filaments in good electrical contact with clean copper. However a large effect is not likely, as can be inferred from a formula by Deutscher and de Gennes.[72] They obtain for T_{cNS}, the transition temperature of the composite:

$$T_{cNS} = T_{cS} - \frac{\pi^2 \hbar^2}{8m\alpha' (d_s + b)^2} \qquad (7\text{-}5)$$

where T_{cS} is the transition temperature of an isolated filament, d_s is the thickness of the Nb_3Sn layer on the

filament, b is the extrapolation length[72,78] in the copper, and α' is the slope of the Ginzburg-Landau parameter $\alpha(T)$ at T_{cS}. But α' is given by $\alpha' = \hbar^2/(2m\xi_{GL}(0)T_{cS})$, where $\xi_{GL}(0)$ is the low temperature coherence length of the Nb_3Sn. Substituting this into (7-5) we have

$$T_{cNS} = T_{cS}\{1 - [\pi^2/4][\xi_{GL}(0)/(d_s + b)]^2\} \qquad (7\text{-}6)$$

The coherence length of the Nb_3Sn is typically the order of 100 Å, d_s is conservatively estimated to be no less than 1000 Å, and the smallest possible value of b is zero. If T_{cS} = 18 K then (7-6) with the above parameters yields $T_{cNS} \simeq 17.5$ K. We have chosen the values of the parameters conservatively, so that this reduction of 0.5 K is probably too large. Since we have observed no transition temperature above ∿16 K we conclude that we have not seen directly any effect of the proximity of copper on the transition temperature of the Nb_3Sn filaments. It is much more likely that the general magnitude of T_{cNS} and its variations from sample to sample are caused primarily by fluctuation in the stoichiometry of the Nb_3Sn. We note that had the proximity effect theory predicted values of T_{cNS} lower than those actually observed, all predictions based on this theory would have to be questioned.

In summary, we state the following broad conclusions. The Nb_3Sn filaments in the 5 atomic % Nb wires are only weakly coupled, and certainly not connected by direct contact between filaments. The 10 atomic % Nb wires, however, show evidence of much stronger interfilamentary coupling. All of the magnetization results discussed in this chapter are at least qualitatively consistent with a proximity effect coupling mechanism for wires of both compositions. The 5 atomic % Nb wire with weak coupling has dirty copper which restricts the range of the proximity effect, while the 10 atomic % Nb wire with relatively strong coupling has cleaner copper, with a correspondingly longer range proximity effect. The estimated ranges, based on normal resistivity measurements, are consistent with the observed coupling strength of each wire. Finally, the reduction in the observed transition temperatures from the nominal value of 18 K normally expected for Nb_3Sn, is larger than would be expected from the theory of the proximity effect. This discrepancy suggests that several mechanisms are involved in determining T_{cNS}, the proximity effect among them.

CHAPTER EIGHT: RESISTANCE OF MICROCOMPOSITE SUPERCONDUCTORS: EXPERIMENTS

In this chapter and the next we show experimentally and theoretically that the simple proximity effect model discussed in the last chapter is not sufficient to explain all aspects of the interfilamentary coupling of our microcomposite wire. The proximity effect model does not recognize the fundamentally statistical nature of the problem. The random positions of the filaments must result in a finite probability for very close contact between filaments. If the density of filaments is large enough, random contacts will become important as an interfilamentary coupling mechanism. Magnetization measurements, however, will not be sensitive to a few direct contacts, since they will be only a small perturbation on the volume screening currents. Hence we have used resistance measurements to probe for the effects of touching filaments. In this chapter we present experimental evidence that our 10 atomic % Nb samples are at or near a concentration threshold for dominance of random contacts over the proximity effect in electrical conduction. In the next chapter we present two theories of electrical conduction; one for these particular materials and the other a phenomenological theory for inhomogeneous media in general. Finally we will put into perspective the relative importance

of the proximity effect compared to random contacts in microcomposite materials.

8.1 Conductivity Measurements

Conductivity measurements are more sensitive to microstructural details than magnetization measurements. As discussed in Chapter Seven, a magnetometer measures an average magnetization, where the average extends through the cross section of the sample. Hence small variations in the magnetization due to localized variations in the microstructure will not be picked up. A voltage measurement, on the other hand, can be very sensitive to local variations: a single superconducting path, no matter how tortuous, will render the sample resistanceless (for small currents). Yet this same path need contribute almost nothing to the bulk diamagnetism of the specimen. Thus magnetization measurements are only a partial probe of the interfilamentary coupling, and conductivity measurements provide complementary information which is essential for an accurate characterization of random inhomogeneous materials.

Our conductivity measurements were of two types, distinguished primarily by their sensitivities. We have made low sensitivity measurements with a conventional chopper-stabilized amplifier capable of resolving 10^{-8} volts under optimal conditions. Our high sensitivity measurements used

a SQUID amplifier, of the type discussed in Part I of this report. The ultimate sensitivity of this instrument for the essentially dc measurements involved was about 10^{-14} volts/$Hz^{1/2}$, limited by the Johnson noise of the normal voltage contacts. The relatively insensitive conventional measurements were easy to apply to tests involving high magnetic fields or large currents. The high sensitivity measurements, on the other hand, were essential for following the resistive transition through several decades of voltage to seek out the initial superconducting path as the sample cooled.

The technique used for the conventional measurements was very direct. All the measurements reported here were done in the helium bath. There was no provision for raising the temperature above 4.2 K, but the temperature could be lowered by pumping on the bath. All measurements were made using a standard four-probe technique, with the voltage tabs inside the current tabs. Due to the limited quantity of wire available for testing, our measurements were done on short samples, the order of 2 or 3 cm long. The voltage probes were kept one to two cm apart, so of necessity they were quite close to the current leads. All connections were soldered, and care was taken to prevent the solder at adjacent current and voltage leads from running together. For high current measurements, above 5 amperes up to 200 amperes,

a special cryostat was constructed to reduce heating effects at the current contacts. The high current equipment, including a special high current power supply, are described in Appendix A.

There is an intrinsic difficulty with these measurements due to the highly anisotropic composition and relatively short length of our samples. In samples with a reduction ratio of several hundred, the length of the filaments is a significant fraction of the length between voltage probes. Hence, in these samples, the measured voltage can be sensitive to the precise location and configuration of the probes. We have noticed occasional anomalous results, such as regimes of negative resistance, which we attribute to such problems. The results presented here, however, are reproducible within 50 % so we have assumed that the effects of the anisotropy are at most to multiply the measured voltages by a factor the order of unity. Montgomery[79] has developed a technique for taking account of the anisotropy of a material in a resistance measurement that involves placing the four electrodes at the corners of a parallelepiped-shaped sample, and permuting the current and voltage leads. This procedure is difficult to apply to our cylindrically shaped specimens, and was not used. Hence our technique for the low temperature measurements were the simplest possible, though not the most accurate.

Our techniques for sensitive measurements on the SQUID amplifier, while limited in accuracy by the same phenomena as the low sensitivity measurements, were a good deal less direct. The problems here were not due to any difficulty with the SQUID itself, but instead resulted from the extremely small resistances sought with the high sensitivity available with the SQUID. The range of resistance typically covered by the SQUID amplifier was from 10^{-6} ohm down to less than 10^{-13} ohm. At the same time the inductance of the sample was typically about 10^{-8} henry. The time constant $\tau = L/R$ associated with the sample then ranged from 10^{-2} second to 10^{5} seconds. Hence, for resistance levels less than about 10^{-8} ohm, the voltage developed across the sample with a one second or shorter time scale would be dominated by inductive, and not resistive effects. Therefore, in the most sensitive measurements, the current supplied to the sample could not be changed, and it was impossible to sweep out the I-V characteristic of the specimen.

We used two techniques to get around this roadblock. The first was to apply the sample voltage to the SQUID amplifier circuit through a superconducting switch while holding the sample current constant. The change in the output of the amplifier as the switch was closed corresponded to the voltage across the sample. The second technique was to leave the amplifier connected with the sample current

constant, but sweep the temperature of the sample. That way we could measure the resistance of the sample as a function of temperature. Since there were no time dependent currents there were still no inductive effects to interfere with detection of the smallest voltage. This technique was especially useful when the sample was completely superconducting at the lowest temperatures, since in that case an absolute resistance, instead of merely a resistance change, could be measured.

Other problems associated with making a SQUID amplifier function with the highest possible sensitivity over the temperature range of 2 K to 18 K required by these samples, are discussed in Appendix B. The specific design of the amplifier and cryostat that we used are also presented in Appendix B. Here we note only that the practical limit to the sensitivity of the SQUID measurements was about 10^{-12} volts, rather than the 10^{-14} volts/$Hz^{1/2}$ due to thermal noise in the voltage contacts. This reduction by two orders of magnitude of the available sensitivity was caused by thermal voltages generated by temperature gradients across the normal voltage contacts. Evidently, extreme voltage sensitivity without superconducting contacts is a difficult proposition.

8.2 The Five Atomic Per Cent Samples

Our relatively insensitive conventional measurements were enough to reveal a small remnant resistance in our 5 atomic % Nb samples. They all showed a large drop in resistivity below T_c, but some still had a measurable resistance in zero field, while others had a measurable resistance in fields larger than 0.1 tesla. As a group they showed little variation in resistance for fields between 0.3 and 1.0 tesla and temperatures between 2 and 4.2 K. That this resistance appears constant implies that it is associated with normal material, presumably the copper, and not with something like flux flow in type II superconductors.

The results of the tests on the 5 % samples are summarized in Table 2. All numbers quoted here were inferred from voltage measurements taken in a 1.0 tesla field and were shown to be temperature independent. The maximum current used was 5 amperes. Of main interest are the experimental results for the remnant resistivity, listed in the fourth column. Samples taken from different locations (end or middle) of the same wire differ by as much as an order of magnitude. Even ratios of remnant resistivity for samples cut from corresponding locations on different wires do not agree very well. Nevertheless there is substantial correlation with the reduction ratio,R, in the second column. The larger reductions tend to produce smaller remnant resistance.

TABLE 2

Comparison of Resistivities

for Five Atomic Per Cent Nb Samples

Sample Diameter	R	ρ_o	ρ_{rem}	$\rho/f_s R^3$
0.20 cm	10	4.5×10^{-6}	4.2×10^{-9}	4.5×10^{-8}
0.10 cm (end)	40	4.4×10^{-6}	4.3×10^{-8}	6.9×10^{-10}
0.10 cm (middle)	40	4.3×10^{-6}	5.5×10^{-9}	6.7×10^{-10}
0.05 cm (end)	200	3.3×10^{-6}	4.0×10^{-11}	4.1×10^{-12}
0.05 cm (middle)	200	2.0×10^{-6}	2.5×10^{-10}	2.5×10^{-12}

R is the area reduction ratio of each sample. Resistivity units are ohm-cm. ρ_o is the measured resistivity for $T > T_c$. ρ_{rem} is the measured remnant resistivity at 4.2 K and B = 1.0 tesla. The last column is a predicted remnant resistivity.

The last column in Table 2 is a prediction for the measured remnant resistivity. The theory that generated the predictions will be discussed in Chapter Nine. We note here that there is rough agreement in the general order of magnitude of the predictions and the data. In view of the large spread in the data this is perhaps the best that could be hoped for.

The evident variability of the remnant resistivity of these wires is disturbing. All the samples were made from nominally identical ingots, so the wide spread in results must reflect either small variations in the manufacturing process, or else an uncontrolled inhomogeneity in each individual sample. On the other hand, our cursory microscopic examination of the samples failed to reveal any clear distinctions between them. There are, however, solutions to the problem of obtaining consistent data short of tracking down the origins of the problem in the manufacturing process.

One solution is to work with only a single sample, and measure its properties between successive stages of area reduction. This technique has actually been carried through by Callagan and Toth[69] for small reduction ratios. We shall examine some of their results in section 9.2E, but we note here that they indeed obtained consistent trends as their sample was reduced. Our own samples, variable as they were, nevertheless allow us to state the following broad conclusions from the conventional resistivity tests. The

5 % samples, when superconducting at all, were only weakly so, and fields less than one tesla were enough to restore a temperature independent resistance to them. This remnant resistance tends to grow smaller as the wire is drawn out (reduced in area), in qualitative agreement with a theory to be presented in Chapter Nine.

The conventional voltage measurements allowed us to measure the remnant resistance in the presence of fields, but they were not capable of detecting the first signs of resistance as the sample is warmed, or as the field is increased from zero. For such sensitive measurements a SQUID amplifier, of the kind described in Part I must be used. A number of factors dictate this choice. First, the samples have very low source impedances, from 10^{-3} ohms down to zero. No combination of conventional amplifiers and transformers have a noise temperature in the liquid helium range for such low impedance.[34] Second, the large L/R time constant of the samples in a low resistance state require a nearly dc measurement. Only SQUID amplifiers have the low flicker noise to make such a measurement possible without the use of noise prone choppers.

The results of the SQUID investigation for the 5 atomic % sample that was reduced a factor of 200 are presented in Fig. 31. This is a logarithmic plot of resistance against a linear temperature scale. There is a relatively steep

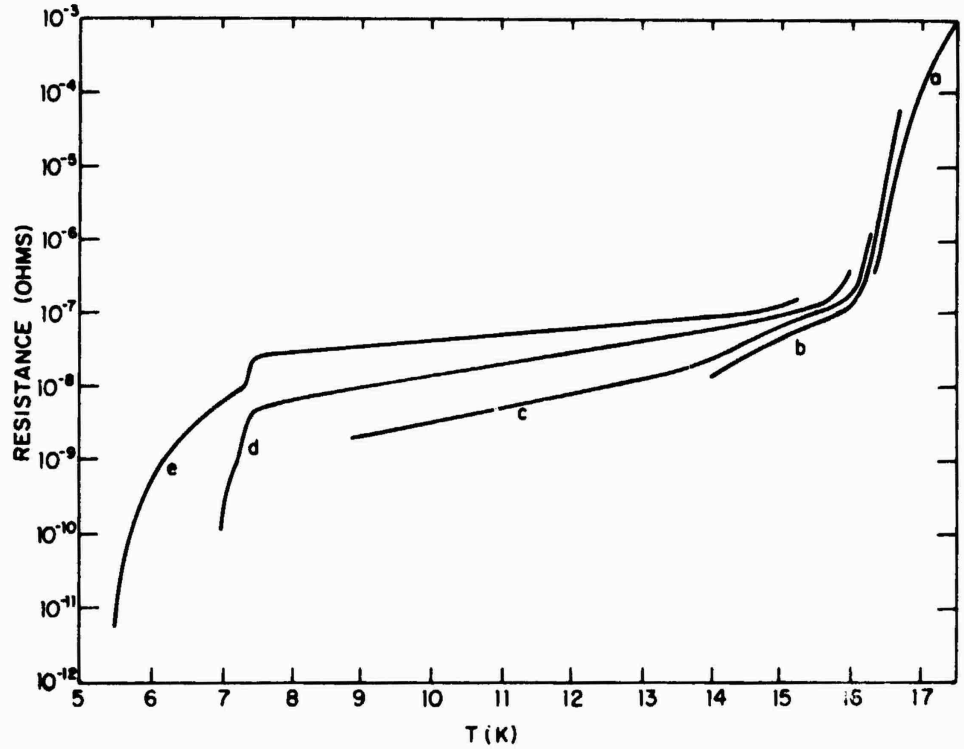

Fig. 31 Resistive transition of the 0.05 cm 5 atomic % Nb wire, R=200. Curves a through e are measurements made with different current levels, ranging in decades from 6×10^{-5} amp for curve a to 0.6 amp for curve e.

drop in resistance over a temperature interval of about 1.5 K as the temperature drops below 17.5 K. This precipitous fall in resistance ends abruptly, on this logarithmic scale, after four orders of magnitude. Thereafter the resistance fans out with dropping temperature in a manner that depends on the amount of current used in the four probe measurement. The larger the current, the more level the slope. At the largest current available for these measurements, 0.6 ampere, the sample remains in the low resistance state down to a temperature slightly less than 6 K. Thereafter, a second precipitous drop occurs, and the SQUID amplifier loses the resistance in noise below about 10^{-13} ohms as the sample evidently goes completely superconducting. The steps that are apparent on the two highest current curves between 7 and 8 K are probably the result of the soldered voltage probes becoming superconducting and causing a redistribution of currents. We note that the resistance level after the initial drop at about 16 K, is 10^{-7} ohm. The sample diameter was 0.05 cm, and the distance between voltage probes was about 1.0 cm, so the 10^{-7} ohm level leads to a resistivity of about 2×10^{-10} ohm cm, which is consistent with the resistivity measured conventionally in the 0.05 cm (middle) sample in Table 2.

The clear implication is that the resistances are due to the same mechanism, which we have supposed to be current

flowing through normal copper to get from one filament to the next. Hence we account for the remnant resistivity measured in both the conventional and SQUID experiments by assuming that the filaments are isolated over a large temperature range, as well as in high fields. The disappearance of resistance in low fields, low currents, and at low temperatures is quite plausibly due to the waxing strength of the proximity effect under those conditions.

Now let us compare the SQUID resistance data in Fig. 31 to the SQUID magnetization data for a similar piece of wire in Fig. 25. Assuming the wires would behave similarly in each test, they would appear to become resistanceless at temperatures where screening is incomplete, even for very small applied fields. This observation supports our idea that the resistivity measurements are more sensitive to microscopic structural variations than are the magnetization measurements.

In conclusion, we may say that individual samples of the 5 atomic % Nb microcomposite wire show a fairly well defined level of resistance, called the remnant resistance, evidently due to current flow in the normal copper. The disappearance of this resistance with decreasing current, field, and temperature, is consistent with a proximity effect coupling mechanism. In our picture of competition between the proximity effect and random contact, the conclusion is that the

5 atomic % Nb samples do not have enough contacts to dominate the proximity effect as the primary interfilamentary coupling mechanism.

8.3 The Ten Atomic Per Cent Samples

Our 10 atomic % Nb samples behaved qualitatively differently from the 5 atomic % Nb samples in our electrical measurements, just as they did in the magnetization measurements. In the conventional measurements they never showed a temperature independent resistance below T_c, even with currents in excess of 100 amperes, or in fields of 1.0 tesla. In the SQUID amplifier measurements, the resistive transition was relatively steep down to a level of 10^{-12} ohm, and never showed an extended plateau, in sharp contrast to the 5 % samples, where a resistance plateau at 10^{-7} ohms was a pre-eminent feature.

Two 10 % samples were available for these experiments, as in the magnetization experiments. The samples were the same CCWR600 and HCWR300 discussed in the last chapter. Unfortunately, a substantial fraction of the CCW specimen was destroyed in some high current tests, and there was not enough left to test in the subsequently developed SQUID apparatus. Hence we report here conventional measurements on both wires, but detailed SQUID measurements on only the HCW samples. Performance in the conventional experiments

were sufficiently similar, however, that we expect no fundamental distinctions between CCW and HCW in the SQUID measurements.

Conventional data on CCWR600 is presented in Fig. 32. This figure displays the voltage across the sample as a function of current through it, in a four probe arrangement, as a function of transverse magnetic field. The temperature was nominally the bath temperature, approximately 4.2 K. However, the sample was too short for a proper arrangement of current contacts, so heating may have been a problem. See Appendix A. The voltage zero in Fig. 32 was offset for each curve for the sake of clarity. The zero field curve is remarkable in that no discernable voltage appears until nearly 120 amperes are flowing in the sample, after which the voltage appears in a continuous though non-linear manner. There is no reason to believe that this resistance is due to anything else than flux flow resistance in the Nb_3Sn. There is no linear region, and, in higher fields, the voltage begins to increase quite rapidly toward the normal resistance of the sample. It is most likely, then, that the resistive phenomena measured in Fig. 32 are due to ordinary superconductive properties of the filaments, namely flux flow resistance.

For comparison, some conventional data on HCWR300 are presented in Fig. 33, in approximately the same format. The

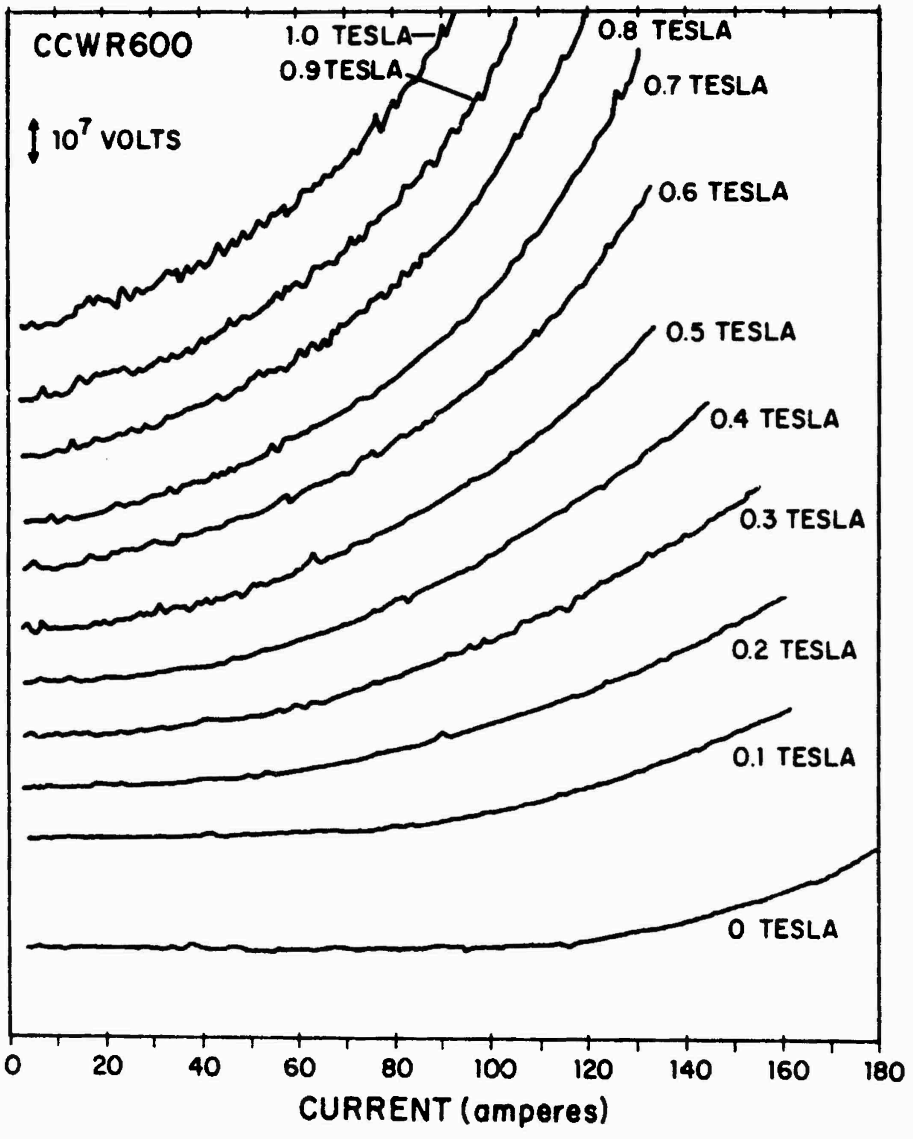

Fig. 32 I-V curves for CCWR600, as a function of field. All curves measured at 4.2 K, with zero offset for clarity.

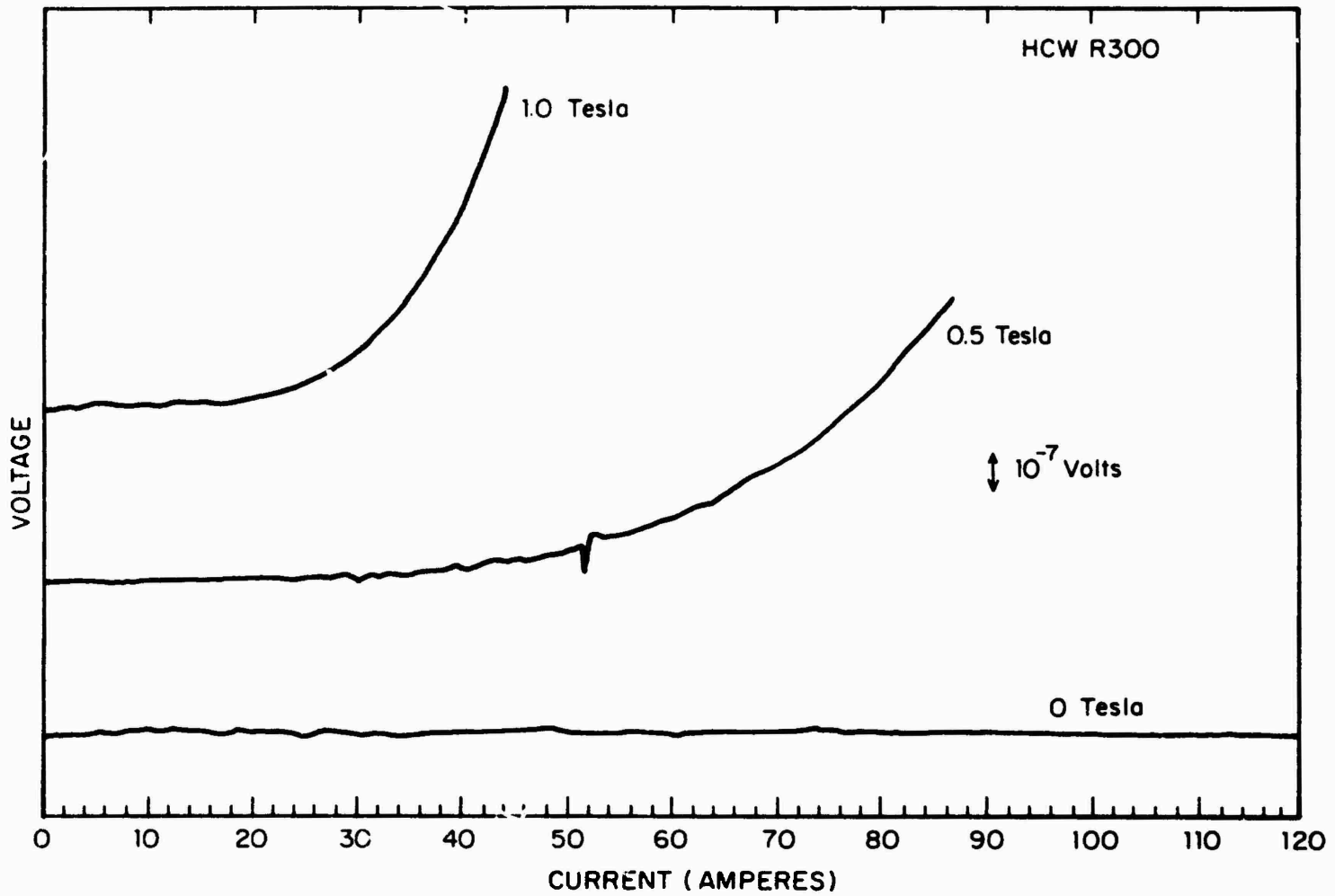

Fig. 33 I-V curves for HCWR300 as a function of field. All curves measured at 4.2 K with the zero offset for clarity.

details are different, but the qualitative features are the same. HCW seems to have a better defined critical current than CCW, and a more steeply rising voltage for a particular field. This sample was long enough for good current connections (see Appendix A)and this might explain some of the differences. In any event, the critical current in zero field is over 120 amperes, and when the voltage does appear in the higher fields, it does so in a steeply non-linear manner.

The dichotomy between the 5 and 10 % samples that exists in the magnetization measurements and the conventional voltage measurements persists in the SQUID voltage measurements. Data on HCWR300 taken with the SQUID amplifier are shown in Fig. 34. The contrast to the 5 % case in Fig. 31 is stark. Over a range of about 3 K the 10 % sample drops about 8 orders of magnitude in resistance, with no feature that could convincingly be called a plateau in resistance. The smallest detectable resistance in this measurement was $2x10^{-12}$ ohm, for an upper limit on resistivity of $4x10^{-15}$ ohm cm at about 13 K. (In an early experiment using the switching technique described earlier with the sample immersed directly in a superfluid helium bath, we were able to set an upper bound of $3x10^{-17}$ ohm cm for the CCW sample.) It is tempting to ascribe this behavior to the predominance of touching filaments that we have hypothesized. However,

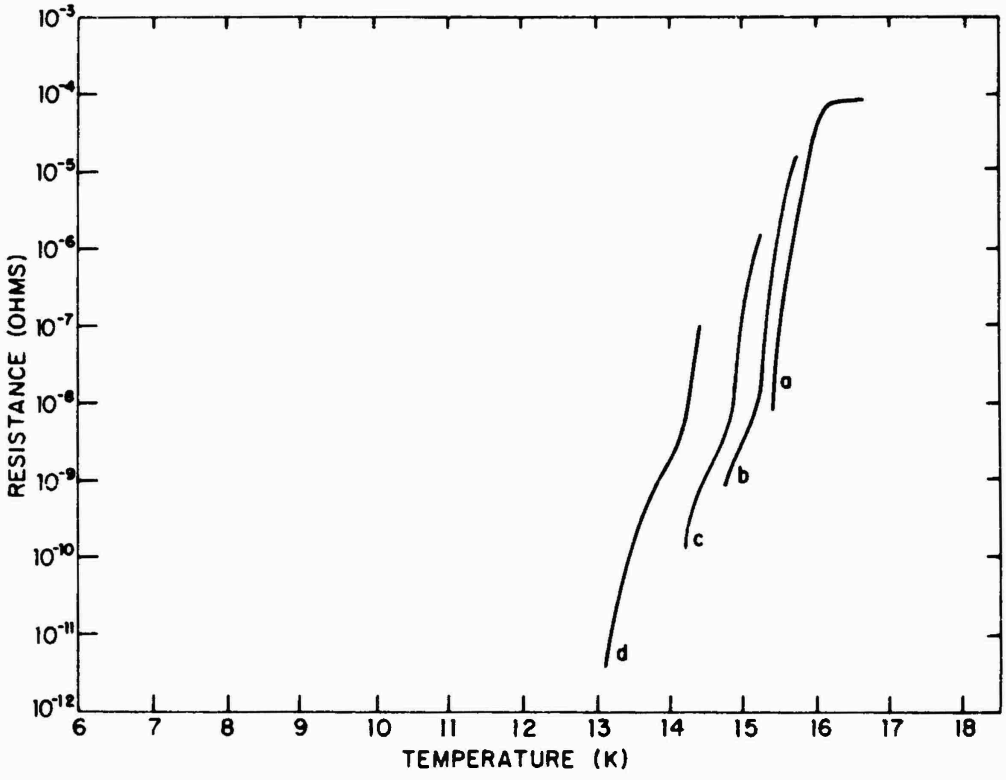

Fig. 34 Resistive transition of HCWR300, 10 atomic % Nb wire, R=300. Curves a through d are measurements made with different current levels, ranging in decades from 6×10^{-4} amp for curve a to 0.6 amp for curve d.

we must be careful. The magnetization curves for this type of sample (the magnetization and resistance measurements were done on different samples) are plotted in Fig. 30. They show nearly perfect screening of small longitudinal magnetic fields. This behavior was deemed in Chapter Seven to be consistent with the proximity effect model. Hence it could still be that the relatively sharp transition in HCW follows from the proximity effect model. Although the SQUID measurements show clearly the distinction between the 5 and 10 % samples, they do not by themselves require interfilamentary coupling by random contacts to play a large role in the behavior of the microcomposites.

To sum up: we have learned experimentally that the 10 atomic % Nb samples behave qualitatively differently from the 5 atomic % Nb samples. The 5 % samples all show a finite resistance in small magnetic fields, and currents less than 5 amperes. In contrast, the 10 % samples require in excess of 100 amperes in zero field before a resistance is developed. The resistive transition of the 5 % material has a prominent resistance plateau over a wide range of temperature after an initial drop of four orders of magnitude. The 10 % specimen, on the other hand, drops quickly by eight orders of magnitude in resistance without showing any similar plateau. The persistance of these distinct behaviors in all our measurements suggests that the proximity effect

interfilamentary coupling model that was sufficient for the 5 % wire, may not be sufficient for the 10 % wire. In the next chapter, we seek to shed light on the distinction between 5 and 10 % wire by considering theoretically the general problem of conduction in inhomogeneous media.

CHAPTER NINE: RESISTANCE THEORIES

We shall present two theories to explain the resistance of wire made by Tsuei's process. The first is specific to the case of superconducting filamentary segments in a normal matrix. The second is more general and applies to any two phased inhomogeneous material. Our assumptions throughout are that the copper between filaments is fully normal, and that the only property of the superconducting filaments is that they have zero resistance. If, in the real wire, the dominant interfilament coupling mechanism is the proximity effect, then these theories should predict the resistance of the wire in fields or temperatures high enough to suppress the proximity effect, but low enough to leave the filaments unaffected. If, on the other hand, the dominant coupling mechanism is random contacts, then these theories should show at what concentration of filaments such an effect is important.

9.1 Estimate of Remnant Resistance

Our initial theory was really more of an estimate of the resistance of wire made by Tsuei's process. The original calculation was made by Tinkham,[80] and has been published in a paper by Davidson, Beasley, and Tinkham.[4] We give a simplified version of the calculation here.

The a priori consequence of discontinuous filaments is that current must flow through possibly normal copper to get from one filament to the next. We characterize the resulting dissipation with an effective resistivity, which we call the remnant resistivity, ρ_{rem}. An estimate of the magnitude of ρ_{rem} may be obtained with the aid of Fig. 35. In this model current flows into each filament along half its length and out along the other half. The current flow is transverse between overlapping filaments to both minimize dissipation and satisfy boundary conditions. If there is a total current, I_t, flowing through the wire, and n filaments per unit area, then the current density in the copper, J_{Cu}, flowing out radially from a filament is

$$J_{Cu} = \frac{I_t}{nA\pi rL} \quad . \tag{9-1}$$

Here, A is the cross sectional area of the wire, r is the radial distance out from a given filament, and L is the length of the filament. If d is the filament diameter and s their center to center separation, then the voltage drop between filaments may be approximated by

$$V = 2\int_{d/2}^{s/2} \rho_o J_{Cu} dr = \frac{2I_t \rho_o}{nA\pi L} \ln(s/d) \quad . \tag{9-2}$$

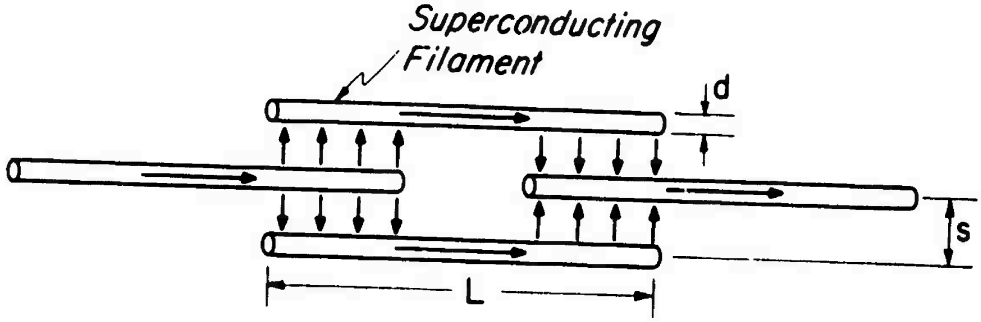

$$\rho_{rem} \approx \frac{\rho_0}{f_s}\frac{d^2}{L^2} = \frac{\rho_0}{f_s}\frac{1}{R^3} = 10^{-14}\,\Omega\,cm$$

Where

ρ_{rem} = Remnant resistivity

ρ_0 = Resistivity for $T > T_c = 10^{-7}\,\Omega\,cm$

R = Cross section reduction ratio = 600

Fig. 35 Model for estimating remnant resistivity in Tsuei's microcomposite wire.

The remnant resistivity may be extracted from this voltage by using the definition: $V/I_t \equiv \rho_{rem}\, L/A$. Further we note that the number density of filaments, n, is related to the volume fraction of superconductor, f_s, by $f_s = n\pi d^2/4$. Also, the macroscopic reduction ratio is related to the microscopic filament geometry by $d^2/L^2 = 1/R^3$. Using all these relations we may finally write for the remnant resistivity

$$\rho_{rem} = \frac{\rho_o}{2f_s R^3} \ln(s/d) \quad . \tag{9-3}$$

In this rough estimate, the logarithm and the factor 2 are not reliable, and in any event combine to make a factor of order unity, so they are ignored hereafter. The final result is compared to the conventional data on the 5 atomic % wire in the last two columns in Table 2. As noted in section 8.2, there is only agreement in the general order of magnitude of the remnant resistivity. But the theory predicts correctly that the largest reductions lead to the smallest resistivity, even with completely normal copper. We note as an interesting feature of this theory, that a wire that obeys (9-3) will actually lose total <u>resistance</u> as it is drawn into finer and finer wire. Ordinary wire, of course, <u>gains</u> in total resistance as the square of the reduction ratio.

If we choose parameters for (9-3) appropriate for the 10 atomic %Nb wires, in particualr a value for ρ_o of 10^{-7} ohm cm, we obtain a remnant resistivity between 10^{-14} and 10^{-13} ohm cm. A value this small could explain the behavior of the conventional measurements at high fields, since resistivities of this size could not be resolved in our conventional measurements. Hence the non-linear shape of the I-V curves in high fields could be explained as flux flow resistance in the superconducting filaments added on to an immeasurably small remnant resistance.

Equation (9-3), however, cannot explain the sensitive SQUID measurements on the 10 atomic % Nb wire. Those measurements were capable of resolving almost an order of magnitude less resistivity than 10^{-14} ohm cm. Since one would expect proximity effect superconductivity in the copper to become important only after most of the filaments are superconducting, there should be a plateau in resistance corresponding to dissipation in the normal copper. Such a plateau is evident for the 5 atomic % Nb samples, Fig. 31, even for currents as small as 6×10^{-4} amperes. Yet 1000 times more current in the 10 % wire, Fig. 34, fails to reveal any such plateau. This is the strongest evidence we have that the proximity effect is not sufficient to explain the resistivity of the 10 % wire. We therefore consider next a theory that allows for a superconducting threshold in Nb concen-

tration without a proximity effect coupling mechanism.

9.2 A Phenomenological Theory

Our more general theory is a phenomenological theory of electrical conduction in microscopically inhomogeneous materials. The theory remains valid if the material is drawn into wire, and for some interesting cases improves on the effective medium theory[81,82,83] (EMT) result near the percolation threshold. The theory was constructed to reconcile data on Tsuei's wire with both the EMT and with percolation theory;[73] hence our phenomenological ideas are an amalgamation of the results of these theories. The EMT, which works poorly for drawn wire, defines a homogeneous effective medium to replace the real heterogeneous mixture by demanding that a suitable average of the effects of inclusions in the effective medium must be zero. For the case where one constituent material is superconducting the EMT predicts that below a critical concentration of superconducting material, the composite is resistive. Percolation theory also predicts a critical volume fraction, but the two theories predict different values. Our phenomenological theory is constructed to satisfy the percolation result for the threshold while retaining important aspects of the EMT result far from the critical region. The theory not only helps explain the difference between our 5 atomic % Nb and

10 atomic % Nb microcomposite wires, but also fits data from totally different materials. We present it here as a guide to both theorists and experimenters concerned with disordered systems.

A. Effective Medium Theory for Aligned Prolate Spheroids

The effective medium theory for electrical conduction in disordered materials defines self-consistently a homogeneous effective medium that replaces the real heterogeneous medium surrounding a particular inhomogeneity. The problem is simplified (but still physically interesting) if we confine our attention to real hetergeneous media composed of only two materials. We have then a mixture of two real media, material one with bulk resistivity ρ_1 and material two with resistivity ρ_2, and an imaginary effective medium whose bulk resistivity ρ_m is to be calculated. The condition we used to set the value of ρ_m is generated as follows:

1. Let the homogeneous effective medium surround an inclusion of either real material.
2. Calculate the total current flowing through the mid-plane of the inclusion and subtract off the total current that would have flowed there if the inclusion were replaced by the effective medium.
3. We demand that the average value of this excess current be zero, where the average is taken over the

different possible compositions and orientations of the inclusions. ρ_m is adjusted until this condition is met.

We have already simplified the problem by allowing only two possible compositions for the inclusions, and ordinarily the problem is further simplified by assuming the inclusions are all spherically shaped, eliminating the orientational average. We will be slightly less simple, and assume that the inclusions are prolate spheroids with their symmetry axes aligned in the direction of the applied field. This removes the isotropic degeneracy of the problem but does not introduce an orientational average. It is also physically relevant for inhomogeneous material drawn into wire, as in Tsuei's process.

The calculation then proceeds as follows. The total current I_i flowing through an inclusions is[84]

$$I_i = \frac{1}{\rho_m}\pi b^2 E \frac{u_i}{1 + (u_i - 1)X} \qquad (9\text{-}4)$$

where b is the semi-minor axis of the prolate spheroid

u_i is ρ_m/ρ_i, $i = 1,2$

E is the applied elctric field

X is the depolarization factor for the prolate spheroid.

The value of X is given by[85]

$$X = \frac{1 - \varepsilon^2}{\varepsilon^3} \left((1/2) \ln \frac{1 + \varepsilon}{1 - \varepsilon} - \varepsilon \right) \qquad (9\text{-}5)$$

where ε is the eccentricity of the prolate sphereoid. Note that for a sphere, the eccentricity is zero, b is the radius and X = 1/3. If we $u_i = 1$ (the inclusion has the same resistivity as the effective medium) the current would be $\pi b^2 E/\rho_m$, so that the excess current is

$$\Delta I_i = (\pi b^2 E/\rho_m) \frac{(u_i - 1)(X^{-1} - 1)}{(X^{-1} - 1 + u_i)} \quad . \qquad (9\text{-}6)$$

Now let the concentration of material one be C_1 and that of material two be C_2. Then the average value of the excess current is

$$\langle \Delta I \rangle = C_1 \Delta I_1 + C_2 \Delta I_2 \qquad (9\text{-}7)$$

where $C_1 + C_2 = 1$. The condition that this average be zero leads to a quadratic equation for ρ_m whose solution is the effective medium theory result:

$$2\rho_m = \rho_1 \left(1 - \frac{C_2}{X}\right) + \rho_2 \left(1 - \frac{C_1}{X}\right) + \left\{ \left[\rho_1 \left(1 - \frac{C_2}{X}\right) + \rho_2 \left(1 - \frac{C_1}{X}\right) \right]^2 - 4\rho_1 \rho_2 \left(1 - \frac{1}{X}\right) \right\}^{1/2} \qquad (9\text{-}8)$$

Equation (9-8) may be put into an equivalent form by changing from resistivity to conductivity as the parameter describing the constituents of the system. If $\sigma_i = 1/\rho_i$, where $i = 1,2,m$, then

$$2\sigma_m\left(\frac{1}{X}-1\right) = \sigma_1\left(\frac{C_1}{X}-1\right) + \sigma_2\left(\frac{C_2}{X}-1\right) + \left\{\left[\sigma_1\left(\frac{C_1}{X}-1\right)+\sigma_2\left(\frac{C_2}{X}-1\right)\right]^2+4\left(\frac{1}{X}-1\right)\sigma_1\sigma_2\right\}^{1/2} \tag{9-9}$$

Equations (9-8) and (9-9) emphasize two limits in the behavior of ρ_m or σ_m. If the conductivity of one constituent goes to zero the system is best described by the conductivity form, (9-9). If the resistivity of one constituent goes to zero, then we are served better by (9-8). This distinction will be useful to us later.

Equations (9-8) and (9-9) fit data in situations where the conductivity ratio σ_1/σ_2 is close to unity[73,81,86] but when this ratio becomes very large or very small a serious deficiency develops for the EMT. If, for example, we let σ_1 go to zero in (9-9) (we adopt the convention that material two is always the material with the higher conductivity) we have

$$\sigma_m/\sigma_2 = \begin{cases} (X^{-1} - 1)\{[C_2/X] - 1), & X < C_2 \leq 1 \\ 0, & 0 \leq C_2 \leq X \end{cases} \tag{9-10}$$

Hence the EMT predicts that the composite will act like an insulator until a critical volume fraction of conducting material is reached, and that the critical value is exactly the depolarizing factor for the particular shape inclusion. For spherical inclusions, where X = 1/3, this threshold comes at a not unreasonable value. If the material is drawn into wire, however, so that the depolarizing factor for the inclusions approaches zero without a change in topology, the EMT predicts the unlikely result that the threshold approaches zero. A similarly unphysical result occurs if, instead of letting σ_1 go to zero, we let ρ_2 go to zero. From (9-8) we have

$$\rho_m/\rho_1 = \begin{cases} 1 - C_2/X, & 0 \leq C_2 \leq X \\ 0, & X < C_2 \leq 1 \end{cases} \tag{9-11}$$

Equation (9-11) is the EMT description of resistivity in a composite of normal and superconducting materials. Again, there is a critical volume fraction of superconducting material required for bulk superconducting behavior, and this

concentration threshold is none other than the depolarizing factor of the inclusions. This false prediction of close coupling of the critical volume fraction to the shape of the inclusions is a serious problem for the EMT, and one must go outside the EMT to resolve the dilemma.

B. Percolation Theory

The problem of correctly assigning this critical volume fraction can be addressed from a point of view entirely different from that of the EMT; this independent body of science is percolation theory.[73,87] A self-contained discussion of percolation theory is beyond the scope of this report, but we wish to point out various of the concepts involved, especially the idea of the percolation probability. This quantity may be defined for our purposes with the aid of a regular cubic network of equi-valued resistors. Let a voltage be imposed across this network so that a current flows in the resistors along a cubic axis. Now begin removing resistors at random from the network leaving open circuits in place of each removed resistor. The percolation probability is defined as the probability that a given node is connected by resistors to infinitely many other nodes (in an infinite network). As more and more resistors are removed the percolation probability grows smaller, and when it finally vanishes, conduction ceases. Clearly this problem

is related to the problem considered by the EMT, and the critical volume fraction corresponds to the situation where the percolation probability changes from some finite value to zero. It has been shown[73] for resistor lattices that there is a finite density of remaining resistors at which the percolation probability indeed becomes zero. This critical density has been subjected to a number of analytical and numerical studies for various regular lattices in both two and three dimensions.[73,87] The results of these studies are not of direct relevance to us because they apply only to these regular lattices where individual resistors have been randomly removed.

However, Scher and Zallen, in a splendid paper,[88] pointed out that one could construct from the critical-resistor-density a critical-volume-density of conducting material that is independent of the particular lattice used, and which depends only on the dimensionality of the lattice. The critical volume fraction that they suggested should apply to any three dimensional heterogeneous continuum[89] is approximately (15 ± 2)%. This numerical result has been confirmed in two clean experiments, which we shall refer to in detail later,[86,90] and we accept it as correct. That is, there are compelling theoretical and experimental reasons for expecting the critical volume fraction for bulk conduction in a bi-phased heterogeneous material to be about 15%. This

should be contrasted to the value of 33% predicted by the EMT for spherical inclusions. Furthermore, we expect, in contradiction of the EMT, that this critical volume fraction is largely independent of the shape of the inclusions, so long as they are randomly arranged and there is rough topographical symmetry[89] between the two phases. (Exactly what is meant by "rough topographical symmetry" is given some delineation in a paper by Pike and Seager.[91])

The EMT fails to predict the percolation threshold because there is nothing in it to take account of large clusters of like inclusions--its only independent parameter is the shape of the inclusions, and changing their shape by drawing the material into wire reveals the shortcoming of this single parameter. To do the calcualtion correctly in the spirit of the EMT one would have to include terms that average the excess current through pairs of inclusions, and triplets and so on. Such a calculation[92] is very difficult and has not yet born fruit.[86] On the other hand we already have independent knowledge of the critical volume fraction from percolation theory, and by phenomenologically combining these two theories we can produce simple equations that describe diverse data.

C. Deriving the Phenomenological Theory

The phenomenological amalgamation of the EMT and of per-

colation theory is necessitated by our SQUID experiments on 5 and 10 atomic % Nb microcomposite wire made by Tsuei's process. Hereafter we shall refer to these samples in terms of their volume fractions of superconducting material, rather than their atomic fractions of Nb. Since Cu and Nb have about the same density, but Nb has about 1.5 times the atomic weight, the volume fraction for the 5 atomic % Nb material is about 7.5%. Similarly, the 10 atomic % material is about 15 volume %. The depolarizing factor for these wires may be calculated from equation (9-5) by using the relation between the eccentricity ε and the area reduction ratio R of the drawn wire: $1-\varepsilon^2 = 1/R^3$. For typical wire with a reduction ratio of 600, $X \simeq 10^{-7}$. Of course, this calculation involves a physical approximation since the filaments are not in the shape of perfect prolate spheroids.

The long tail in the SQUID amplifier data from the 7.5% sample (Fig. 31) on the higher current curves is roughly consistent with the resistance levels estimated in section 9.2. That estimate assumed that the filaments were typically isolated from each other by normal copper; hence this assumption would appear to be justified in this sample. The 15 % sample (Fig. 34) however, shows no such tail so that one would conclude that the filaments are not so isolated and either form genuine connections or else very good proximity effect junctions. These measurements, then, are consistent

with percolation theory but not with the EMT. (The EMT predicts a threshold at about 10^{-5} % by volume of superconductor since the demagnetizing factor for these well drawn out filaments is about 10^{-7}. Hence according to the EMT the 7.5% sample should certainly be superconducting.)

Thus we are faced with reconciling these facts: first, the percolation threshold should be about 15%; second, below this threshold the estimates of section 9.1 are approximately right; and third, the EMT fails completely at the percolation threshold, but should be approximately correct at very small superconducting volume fractions. A function that meets the test of these three conditions may be readily constructed in the spirit of Padé approximations.[93] That is, we shall try to construct a function as the ratio of two polynomials that satisfies the three basic facts known about the Tsuei wire system.

Since the first requirement is that the resistivity of the composite must be zero for concentrations above the percolation threshold, we choose the numerator of our Padé approximant to be the simplest function which has a zero at that point:

$$\text{numerator} = \rho_1(1 - C_2/C_2^*)$$

where $C_2^* \simeq 0.15$ and is the percolation threshold, but we

make the convenient approximation that $C_2^* = 1/6$. Having accounted for near neighbor connectivity in this brute force manner, we may now choose the denominator so that the elongated shape of the inclusions is accounted for:

$$\text{denominator} = (1 + C_2/X)$$

Hence we propose for the resistivity

$$\frac{\rho_m}{\rho_1} = \frac{(1 - 6C_2)}{(1 + C_2/X)} \quad , \qquad 0 \leq C_2 < 1/6$$

$$= 0 \quad , \qquad 1/6 < C_2 \leq 1 \qquad (9\text{-}12)$$

For $C_2 < X << 1$ this function is dominated by the denominator, and therefore agrees to first order with the EMT; but close to the threshold, clustering takes over and the numerator provides a manifest zero at the right place. Further, still in the limit of a small depolarizing factor, (9-12) has the form

$$\rho_m \simeq \rho_1 \frac{\ln(4R^3)}{2R^3 C_2} \quad , \qquad X < C_2 < 1/6 \qquad (9\text{-}12a)$$

which is very close to (9-3) and also suggestive of some results of Callaghan and Toth[69]. Equation (9-12) is therefore consistent with our measurements, although the details

of that equation are not confirmed by the two data points supplied by Figs. 31 and 34. However, there are already published experiments with more detailed results.[86,90] This simple theory works well for them too, even though the appropriate value of X is 1/3 and not 10^{-7}, so that there is no longer first order agreement with the EMT.

Before we can make a comparison between this theory and these experiments, we must point out more features of the theory. First, (9-12) applies only to an NS composite and we must now work out the analogous case for a metal-insulator composite, where the conductivity (rather than the resistivity) of one constituent goes to zero. For this case we refer to the simple EMT result (9-10). In contrast to the NS case, we expect (9-10) to be valid near $C_2 = 1$ rather than for $C_2 = 0$. Evidently, to make a first-order expansion we would be better off to write (9-10) in terms of C_1 which is small in the region of validity:

$$\frac{\sigma_m}{\sigma_2} = 1 - \frac{C_1}{1 - X} \quad , \qquad 0 \leq C_1 < 1 - X \qquad (9\text{-}13)$$

Notice that (9-13) has the same form as (9-11). We now generalize the EMT result with our Padé approach. The threshold should occur when the highly conducting material forms a connected network at a volume fraction of about 1/6 so that $C_2^* = 1/6$ or $C_1^* = 5/6$. Hence the analog to (9-12) is

$$\frac{\sigma_m}{\sigma_2} = \frac{1 - (6/5)C_1}{1 + C_1/(1 - X)} \quad . \tag{9-14a}$$

Rewriting (9-14a) in terms of C_2 for convenience in comparison, we have

$$\frac{\sigma_m}{\sigma_2} = \frac{1 - X}{5} \frac{6C_2 - 1}{2 - X - C_2} \quad , \quad 1/6 < C_2 \leq 1 \quad . \tag{9-14b}$$

Finally, we also rewrite (9-12) in terms of conductivity:

$$\frac{\sigma_m}{\sigma_1} = \frac{1 + C_2/X}{1 - 6C_2} \quad , \quad 0 \leq C_2 < 1/6 \quad . \tag{9-15}$$

These equations, (9-14b) and (9-15), are the fundamental results of our phenomenological theory, and they are in a sense complementary. That is, they are both derived from the assumption that the conductivity of material one is quite small compared to material two, but (9-14b) is valid for $C_2 \simeq 1$, while (9-15) is valid near $C_2 \simeq 0$. The two equations diverge in opposite directions at the percolation threshold, but as we shall see, they remain valid until very near that critical region provided $\sigma_1/\sigma_2 << 1$. We note that there is first-order agreement with the EMT in (9-14a) only if $X \simeq 1$, and in (9-15) only if $X \simeq 0$. It would be simple to add a linear term to the denominator of (9-14a) or the numerator of (9-15) that would guarantee first order agree-

ment with the EMT for all X in both equations, but the overall fit to the data in the following pages is best if (9-14) and (9-15) are used as written above. That is, we will see empirically that (9-14) and (9-15) work well for all values of X and for all values of C_2 except in the immediate vicinity of $C_2 = 1/6$. The EMT with $X = 1/3$ works well only for C_2 near one, and it is a mistake to demand first-order agreement with the EMT on both sides of the threshold.

D. Comparison to Experiment

A table-top experiment performed by Fitzpatrick, Malt, and Spaepen,[90] (FMS) is an example of the case where σ_1 may be taken to be effectively zero and $X = 1/3$. Random close-packed lattices of insulating and metallic spheres were put together in glass beakers with aluminum foil electrodes and the conductivity as a function of relative densities of the two kinds of spheres was studied. Since one conductivity may be taken as zero we expect (9-14) to apply. To compare the results we switch to the notation of FMS, and plot the conductivity as a function of the number fraction of insulating spheres. That is, if q is the insulating number fraction, then C_1, the insulating volume fraction is $C_1 = .65q + .35$ where the filling factor of the lattice is taken to be 0.65 (see reference 94). Hence we may use (9-14a) with C_1 in terms of q, and $X = 1/3$, and plot the results directly over

the data of FMS. This is presented in Fig. 36. The high conductivity data appear too high in comparison to our theory, but this is consistent with the experimental errors reported by FMS. The low conductivity data and the threshold fit quite well, and overall we feel that this experiment is consistent with our theory.

A more detailed set of mathematical and experimental data are compiled in a paper by Webman, Jortner, and Cohen[86] (WJC). They compare conductivity data[95] from a Li-NH_3 system to data derived from computer simulations. The simulations involved calculating the effective conductivity of a cubic resistor network in which each resistor may have one of only two values, and in which the resistor values are correlated over a length larger than the distance separating the nodes but are random on a scale larger than the correlation length. Hence their simulation is just the sort of inhomogeneous system considered in this report, with X = 1/3, and they demonstrate convincingly that the metal ammonia system is described very well by their model network. We shall therefore compare our phenomenological theory both to WJC's numerical simulations and to the Li-NH_3 data which they present in their paper. In Fig. 37, equations (9-14a) and (9-15) with X = 1/3 are compared to the metal-ammonia data and the EMT result. The phenomenological fit is remarkably good with no adjustable parameters except the conduc-

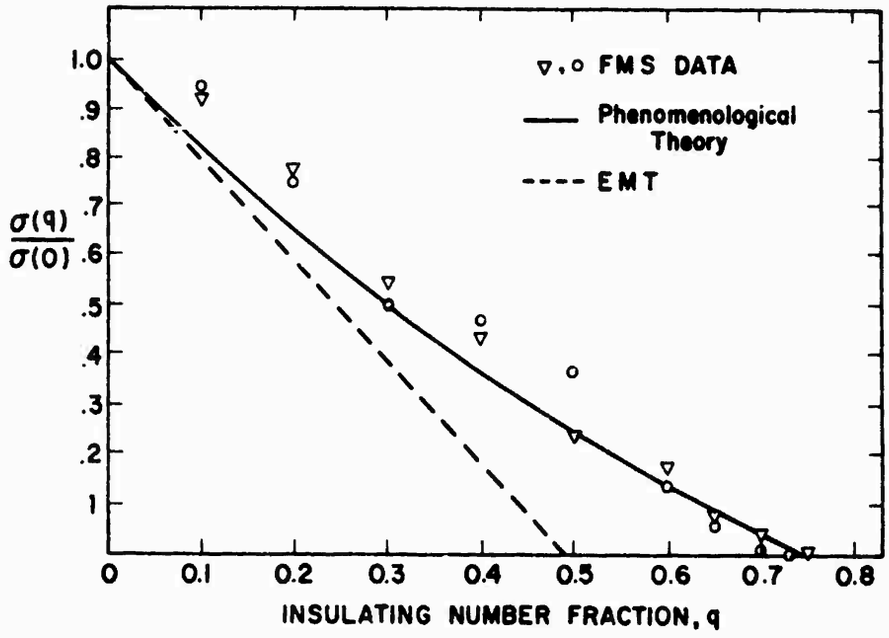

Fig. 36 Conductivity as a function of the fraction of insulating spheres in an experiment by FMS (ref. 90). To apply our theory we take the interstitial spaces as part of the insulating volume fraction. The results of the EMT are also plotted. Note that the data and both theories have been normalized not at zero volume fraction, which is unattainable in this system, but at zero number fraction.

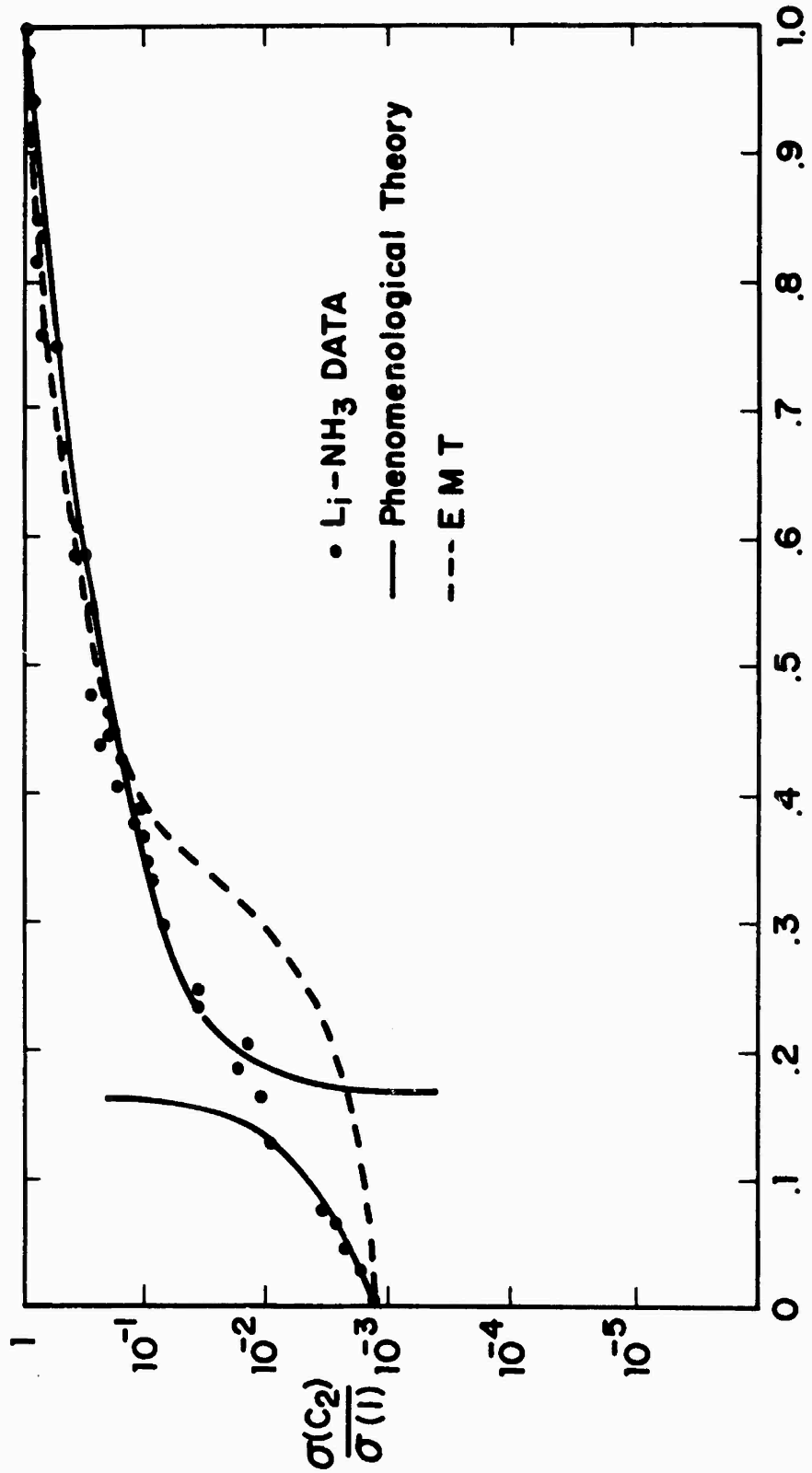

Fig. 37 Comparison of Li-NH_3 data (ref. 86 and 95) with the EMT and the penomenological theory.

tivity values at either extreme of the C_2 scale. Of course, at the percolation threshold the phenomenological theory diverges, but the fit to the data is good except within $\Delta C_2 = \pm 0.03$ around the threshold. Even within this divergent area it is easy to interpolate a straight line, tangent to both curves, that adequately describes the data. A feature that is emphasized by the log plot in Fig. 37 is that as the ratio σ_1/σ_2 is varied the shapes of the two curves generated by (9-14b) and (9-15) are unchanged, but their relative positions slide vertically. It is therfore apparent that for conductivity ratios near unity the phenomenological theory will be unsatisfactory, but that for more extreme differences the two curves will come closer to approximating a single smooth curve.

This feature is clearly visible in Fig. 38, which compares (9-14b) and (9-15) for the case of $\sigma_1/\sigma_2 = 10^{-5}$ to one of WJC's numerical simulations. The two phenomenological curves now come very close together and still give a nice fit to the numerical data, again with no adjustable parameters. We have also plotted in Fig. 38 two curves generated by the EMT. These curves are plots of (9-9) with appropriate values of conductivities. One curve uses a depolarizing factor of 1/3, as would seem appropriate for the isotropic nature of WJC's simulation, and the complete failure at the percolation threshold is apparent. On the other

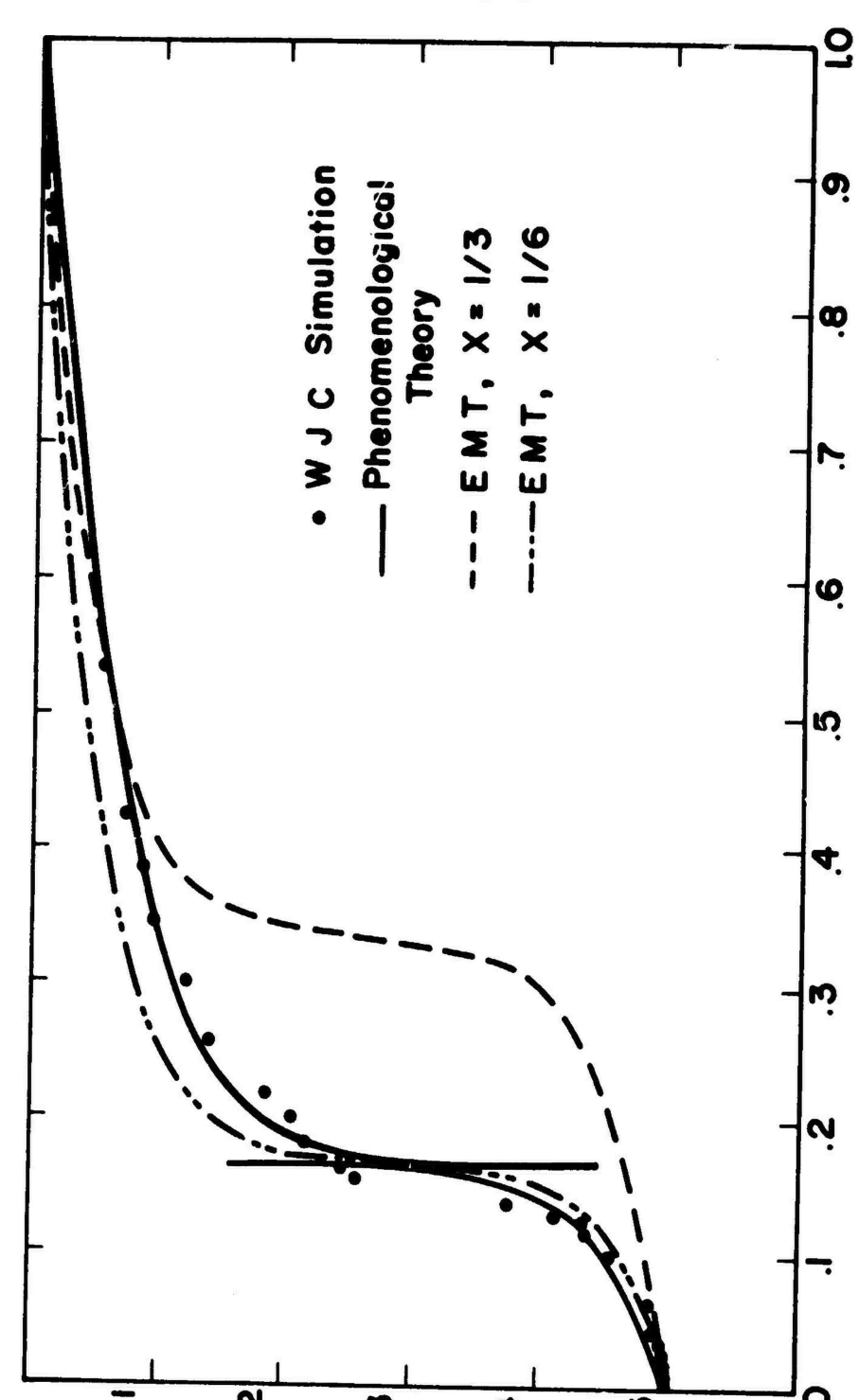

Fig. 38 Comparison of a WJC (ref. 86) simulation for $\sigma_1/\sigma_2 = 10^{-5}$ to the EMT with X = 1/3 and 1/6, and to our phenomenological theory.

hand, the curve has some appeal because it has the correct qualitative shape, and one might be tempted to improve upon its shape by artificially moving the threshold over to the correct value. The resulting curve, again (9-9) but with $X = 1/6$, is the remaining curve in Fig. 38. Indeed the behavior is better at the threshold and below, but worse above. Furthermore this approach has no hope of coping with the separation of the depolarizing factor and percolation threshold for drawn anisotropic wire. We are left then with the phenomenological approach.

E. The Phenomenological Theory and Tsuei's Wire

The phenomenological theory just presented fits the observed behavior of our samples of microcomposite wire. The presence and rough magnitude of the remnant resistance in the 7.5 volume % wire is accounted for in (9-12a). We note that the logarithm in that equation tends to reduce the error between theory and experiment in Table 2. For typical parameters (9-12a) is larger than (9-3) by an order of magnitude, and so would tend to bring the last two columns of Table 2 into better agreement. That no remnant resistance appears in our 15 volume% wire is also correctly predicted since this material is at the percolation threshold. A detailed comparison to our own experiments is impossible, however, because of the relatively few samples available

for tests and because of interdependent parameters. Ideally we would like to change the Nb concentration of the material without affecting the mean free path in the copper. But these two parameters are coupled in our materials, so that the effects of touching filaments in the 15 volume % wire are masked by an extended proximity effect.

The proximity effect can be incorporated into our phenomenological theory, however, if the superconducting copper is included in C_2, the total superconducting volume fraction. Such a combined theory could then explain the low temperature zero resistance state of the 7.5 volume % material. When superconductivity is induced in enough copper to raise C_2 from the intrinsic value of 7.5% to 15% a supercurrent can percolate, and the resistance drops to zero. The derivation of such a combined theory, however, is complicated by the statistical nature of the problem. One must view the composite media as an ensemble of SNS junctions with a suitably random spread of parameters. Each junction would be either superconducting or normal according to its particular values of T_c, J_c, and how much current (another random variable) is flowing through it. We have made a few simple attempts at such a theory, but so far none have completely accounted for the detailed behavior of the 7.5 volume % sample in Fig. 31.

Our phenominological theory, however, may be directly compared to some work by Callaghan and Toth.[69] They worked with a single ingot of 7.7 volume % Nb material, and measured the resistance as a function of current between successive stages of area reduction. Since they did not take data from several different ingots, but only one, they obtained a clear trend in resistivity results. Their resistivity data, plotted as a function of reduction ratio, is presented in Fig. 39. At a given reduction their measured resistivity depends dramatically on the current used to make the measurement. We interpret this result within the frame of our theory as due to a variation with current level of the volume of superconducting copper. As the current is raised, less and less copper is superconducting, and the resistivity should approach a limit set by the volume fraction of Nb. That limit, according to our theory, is the solid line at the top of the graph in Fig. 39. This line is equation (9-12) with $C_2 = 0.077$, and X calculated from (9-5) with $1 - \epsilon^2 = 1/R^3$. This theoretical curve is a reasonable limit because the trend of measured resistivity with current density is consistent with the magnitude of the prediction. Given the large gap between the 100 and 1000 amp/cm^2 curves, there is no experimental reason to believe that the 1000 amp/cm^2 curve represents a limit on remnant resistivity. In fact, judging from the general trend

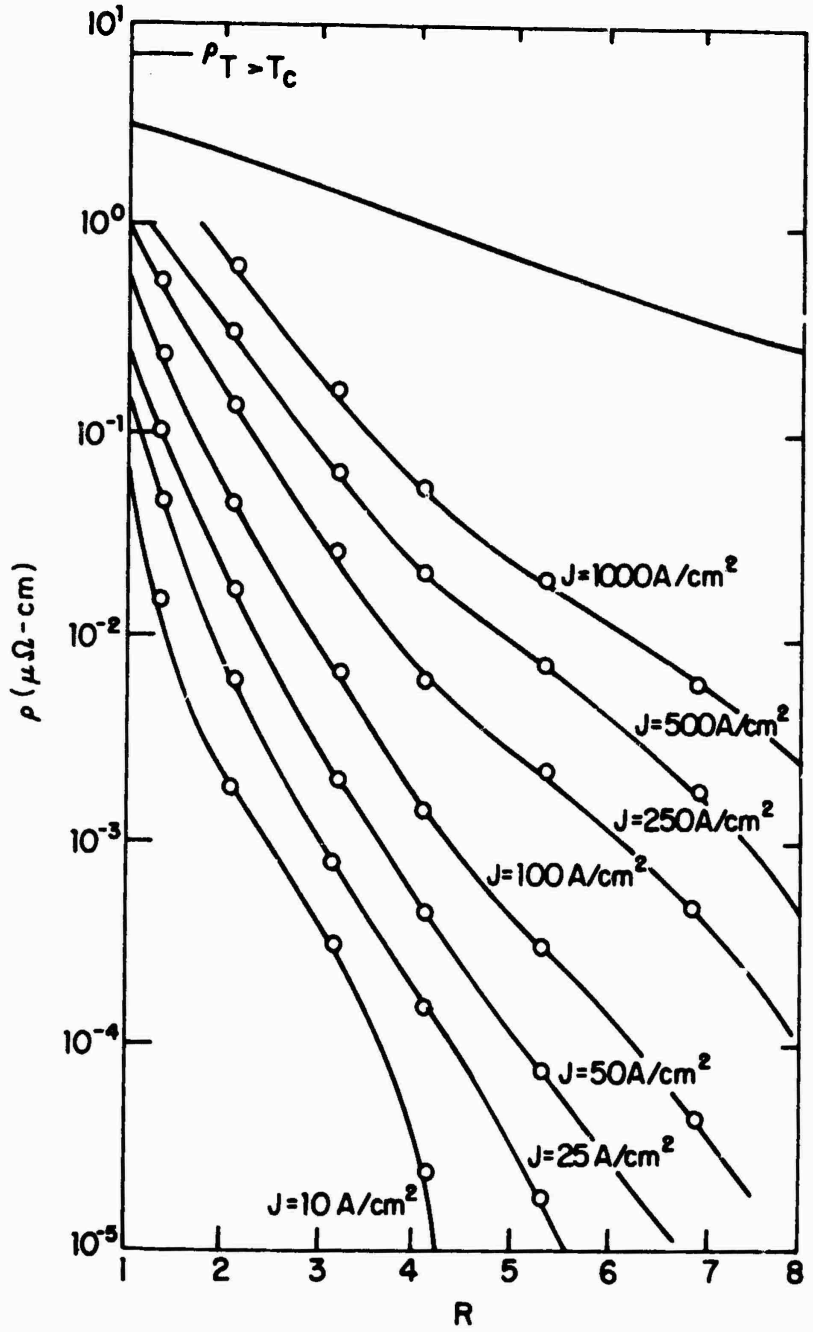

Fig. 39 Resistance measurements of Callaghan and Toth (ref. 69). The solid curve at the top is our theoretical limit on resistance as current density is increased.

another factor of 10 in current density might be sufficient for the resistivity to approach the theoretical limit over most of the range of reduction studied by Callaghan and Toth.

There is another important implication of (9-12) for proper interpretation of data. Samples with large reduction ratios (hence very small values of the depolarizing factor, X) will be very sensitive to small superconducting volume fractions. If $X = 10^{-7}$ then from (9-12) the resistivity will be down a factor of 10^4 from its zero fraction value for only 0.1 volume % of superconducting material. At low currents the wire may thus appear to be fully superconducting when only a small fraction of filaments are below their transition temperatures. Hence it would be of some importance to measure the spread of T_c's in these materials independently.

In conclusion, a combination of the proximity effect interfilamentary coupling model, and the percolation model based on a normal copper matrix, is consistent with our own resistivity data, and with those of Callaghan and Toth. A phenomenological theory based on the percoaltion model predicts the order of magnitude of remnant resistivity in the 7.5 volume % wires. It further predicts correctly that the 15 volume % sample has no remnant resistivity. Finally, the percolation model sets a reasonable upper limit on the cur-

rent dependent resistivity measured by Callaghan and Toth.

The proximity effect, however, is also important. It explains by itself all of the magnetization data presented in Chapter Seven. We also invoke superconductivity in the copper to qualitatively explain the details in the current dependent resistivities that both we and Callaghan and Toth have observed. Hence there is reason to believe that neither the proximity effect model alone, nor the percolation model alone is sufficient to explain the interfilamentary coupling in microcomposite superconductors made by Tsuei's process. The percolation model, however, suggests that the material's behavior can be divided into two regimes: with superconducting volume fraction less than 15% the filaments are more or less isolated and the proximity effect dominates the coupling, while for superconducting volume fractions larger than 15% the filaments tend to form a connected network of some sort, so that random contacts dominate.

CHAPTER TEN: CONCLUDING TOPICS

We have developed a phenomenological theory of conduction in microcomposite material made by Tsuei's process, but experimental verification of this theory is sparse. In this final chapter, therefore, we discuss additional experiments that should be done to complete the picture. We expect these additional experiments to verify the idea that there is a threshold in Nb concentration above which random contacts between filaments become important. However, we expect difficulty in establishing the contact mechanism. More experiments to determine the ultimate technological applicability of these microcomposites will be discussed. Finally, we shall summarize what has been done, and what remains.

10.1 Further Experiments

The two compositions of microcomposite material that we have studied are not enough to verify the existence or magnitude of the percolation threshold. We have studied wire containing 5 atomic % Nb and 10 atomic % Nb. The behavior of the 5 % wire is consistent with that expected below the percolation threshold in a percolation picture, but the 10 % wire is ambiguous. The 5 % wire showed a distinct resistance plateau in its resistive transition, indicating

the presence of little direct contact between filaments. The resistive transition of the 10 % wire, however, shows no resistive plateau at the level expected from a model based on normal copper and no contact between filaments. We are tempted to ascribe this behavior to touching filaments in the 10 % wire, but there is a complication. The copper in the 10 % wire has a significantly longer mean free path than in the 5 % wires, and therefore a longer range proximity effect. Hence proximity effect coupling in the 10 % specimens could also explain the absence of a resistance plateau. If the matrix in the 10 % material were made as dirty or dirtier than that in the 5 % material, then the two possible mechanisms could be distinguished. The proximity effect model for the 10 % wire would lead to a resistive plateau very much like that in the 5 % wire, but the touching filament model would eliminate a plateau in the resistive transition, so long as the percolation threshold was exceeded.

To settle this question the following experiments must be done. The mean free path of the copper must be varied independently of the Nb concentration. Then one could do two series of resistance measurements with the SQUID amplifier. The first series would be done exclusively with clean copper, but with the Nb concentration ranging perhaps from a fraction of 1 atomic % to the apparent limit for the manufacturing process, about 20 atomic %. The second series of

experiments would involve the same range of Nb concentrations but with quite dirty copper, to suppress the proximity effect. Such a series of experiments should settle the question of proximity coupling versus random contact between filaments, but it would probably have to be done on material that had not been subjected to the final Nb_3Sn forming anneal. That way the cleanliness of the Cu matrix would be controlled by varying the Sn concnetration. (Since the Sn would in that case be present only to shorten the mean free path in the Cu, some other metal, such as Al, might be substituted for it.) The resulting wire would then have Nb filaments without a layer of Nb_3Sn, and so could not be practical. But it should have the same structure as our present wire, and so it should confirm or disprove the structure-related concept of supercurrent percolation through random contacts.

10.2 Touching Filaments

Although controlling the purity of the Cu matrix should help in validating the concept of a threshold in Nb concentration, such experiments will probably not explicate the mechanism of contact. Here we distinguish two such mechanisms: welding, and the ubiquitous proximity effect. By "welding" we mean a superconducting metallurgical bond between filaments. Since these materials undergo a great

deal of cold working when they are drawn into wire, and are subsequently annealed for two days at a temperature of 600 ^{o}C, it is quite plausible that welds between filaments could exist. Callaghan and Toth[69] purposefully looked for evidence of welding in their materials, and found none. However, their materials contained only 7.7 volume % Nb. From percolation theory, one would not expect very much welding at that concentration. Further, if welding were present, it is not clear that simple microscopic examinations would reveal them. We suggest alternatively that the mechanical strength of the material may depend upon the presence of welds, and so could be used as a possible test for establishing their existence.

The concept of touching filaments, however, does not depend upon the existence of welded filaments. For strong coupling of supercurrent between neighboring filaments, all that is required is that the filaments be in close proximity to one another. Then there could be a locally very strong proximity effect bond between them, which could be almost as good for superconduction as a weld. In this case, one may view the proximity effect as softening the criterion for good contact between filaments. The minimum length scale to which the neighboring filament separation could be compared is the shorter of the electron mean free path in the copper, or the normal coherence length. Thus even in dirty copper,

filaments separated by as much as 100 Å would be still in good contact.

If the proximity effect is the primary contact mechanism, then the distinction between the proximity effect coupling model and the random contact model vanishes. The resulting unified view would then be that all superconduction between filaments is through copper made superconducting by the proximity effect, but with the chances of developing a superconducting path through the sample still determined by percolation theory. We suspect that the only distinction between this unified proximity-percolation view, and the touching filament view, is one of language. Observable predictions of the two viewpoints are likely to be the same.

10.3 Technical Applicability

If our idea is right that a critical concentration of Nb is required for connected behavior of the filaments in micro-composite wires, then there are important implications for the ultimate utility of this wire in technological applications. The primary obstacle to applications of microcomposites with Nb concentrations less than the critical value is the remnant resistance that they display. Clearly, if the wires are too resistive they will not compete with conventional composites. The value of resistivity below which successful competition appears feasible is about 10^{-14} ohm cm,

as discussed in some detail in reference 4. Our 5 atomic % samples fall three to four orders of magnitude above this benchmark, so they cannot be considered practical. Presumably, however, such wire with larger reduction ratios could fall below the benchmark due to the $1/R^3$ factor in (9-12a). Even so, the low Nb wire may not be competitive because of a concomitant low overall critical current density. To overcome this difficulty it would be necessary to use as large a Nb concentration as possible.

If microcomposite wire with a Nb concentration above the critical value is used, however, a different sort of problem emerges. The problem has to do with the stability of the zero resistance state in these high Nb composites in the presence of time-dependent magnetic fields. In conventional composites the problem is solved by twisting the wire to limit the size of eddy currents flowing in the material due to time-dependent applied fields, as discussed in Chapter Five. In microcomposites with low Nb concentrations, it has been suggested that the isolated filament length could play the role of the twist pitch in conventional composites. In high Nb wire, however, there is no well defined filament length to rely upon, and twisting will not affect the fundamentally connected nature of the material. Hence it appears that high Nb wire may lack ac stability.

In other words, the more the filaments behave as though interconnected in a continuous network, the more they will behave like a bulk superconducting wire with a diameter equal to the overall diameter of the whole composite. In that case, the appropriate parameter d in the adiabatic stability condition, (5-8), is this bulk diameter, and not an individual filament diameter. It is clear from (5-8) that this large diameter will result in poor stability. Since the ultimate utility of the wire will be determined by its stability, experiments should be done to determine the ac stability of microcomposites with Nb concentrations both above and below the critical concentrations. These proposed measurements would include magnetization measurements in large swept fields, and of course, solenoid tests. Solenoid tests, however, will have to await the production of large quantities of uniform quality wire.

10.4 Conclusions

The work presented in this report has not settled the question of the ultimate utility of microcomposite superconducting wire made by Tsuei's process, but progress has been made in that direction and in other more purely scientific directions. Since the mechanism by which current flows from one filament to the next is essential for predicting the behavior of the wire in practical situations, our experiments

have been aimed at probing the coupling mechanism. Our magnetization measurements in a small parallel field show conclusively that supercurrents can flow from one filament to the next. Further, the detailed magnetic behavior of our different samples is qualicatively consistent with a proximity effect model of superconduction through copper from filament to filament. Our conventional electrical measurements in large fields and currents have shown that the 5 atomic % Nb wire has a remnant resistance but that the 10 atomic % Nb wire appears strictly superconducting to very large currents in zero field. Our sensitive SQUID voltage measurements, which measured the resistive transition of the material as a function of temperature, confirmed the existence of the remnant resistivity in the low Nb samples, but failed to detect any such resistance in the high Nb specimens.

Finally, we developed a phenomenological theory based on percolation theory and the effective medium theory of conduction in heterogeneous media. Our new theory is not only consistent with all of our data on superconducting microcomposites, but also with data generated by widely different experiments on systems of normal conductors. The basic concept of the theory, as applied to Tsuei's material, is a critical volume concentration of superconducting inclusions. Below the critical concentration the inclusions are isolated,

and above they form a kind of connected network. The critical volume fraction predicted by the theory is just the volume fraction of Nb in our 10 atomic % samples. Although our experiments with the 10 % samples are consistent with our theory, they do not conclusively confirm it because of the relatively clean copper in the high Nb samples. Clean copper has a very long range proximity effect, which could make the sample superconducting even with a sparse array of isolated superconducting filaments, and certainly would be expected to change the effective superconducting volume fraction. We have suggested experiments with controlled purity copper to settle the question.

If our ideas are correct, however, and a connected network of filaments does form, then the ultimate limit to the utility of the material may not be its remnant resistance, but its limited stability against catastrophic flux jumps in time varying magnetic fields. That is, if the filaments form a connected network, screening currents will tend to flow through the bulk of the material rather than within individual filaments, so the stability of the multifilamentary composite will be lost. If further experiments confirm the existence of a critical concentration of Nb, the next step would be to measure the stability of the wire as a function of concentration.

APPENDIX A: CONVENTIONAL VOLTAGE MEASUREMENTS AT HIGH CURRENT

Heating at the current contacts was the principal problem we encountered in making conventional electrical measurements on samples carrying high currents. If there is a contact resistance of even 10^{-6} ohm, then with currents of 100 amperes, 10^{-2} watts will be dissipated at the current junction. If the characteristic dimension of the junction were one millimeter, then the junction would dissipate to the helium bath a heat flux of one watt/cm^2. Normal helium (temperatures above the lambda point) can not ordinarily handle such a flux of heat without developing a film of helium gas around the contact, and the temperature of the junction would rise. Its temperature could even exceed the critical temperature of the superconducting sample. Further, the thermal healing length (over which Joule heat is transferred to the bath) for typical samples could be the order of one centimeter, so that a sizable fraction of the length of the sample would become hot.

All of these problems make high current experiments on short samples unreliable. The solution is to make the current contacts with as low a resistance as possible, spread over as large an area as possible, and as far as possible from the region where the voltage probes are placed.

An arrangement of current and voltage contacts that we used for samples about 15 cm long is shown schematically in Fig. 40a. The arrangement was attached to the end of a cryostat designed to fit in the 2.5 cm bore of the insert dewar of a 7 tesla NbTi superconducting magnet. The sample is bent into a "U" shape and the sides are clamped into grooves on the copper bus bars and soldered. When the solder is set, the clamps are removed, the voltage probes attached, and a thin phenolic sheath is slid over the entire assembly for protection and insulation. We have successfully run about 200 amperes through this apparatus without evidence of excessive heating at the current contacts.

The high current supply that we built for these measurements contained three features worth noting: it was battery powered; the bias resistors for the power transistors were of a novel design and water cooled; and a unique feedback network was used. A battery supply was essential for smooth low noise operation over the entire current range. The simplest arrangement would have been to control the current from a storage battery with a rheostat. But rheostats for currents over 100 amperes are large, noisy, and impossible to operate smoothly. Therefore we developed a transistorized controller for the battery current. A schematic

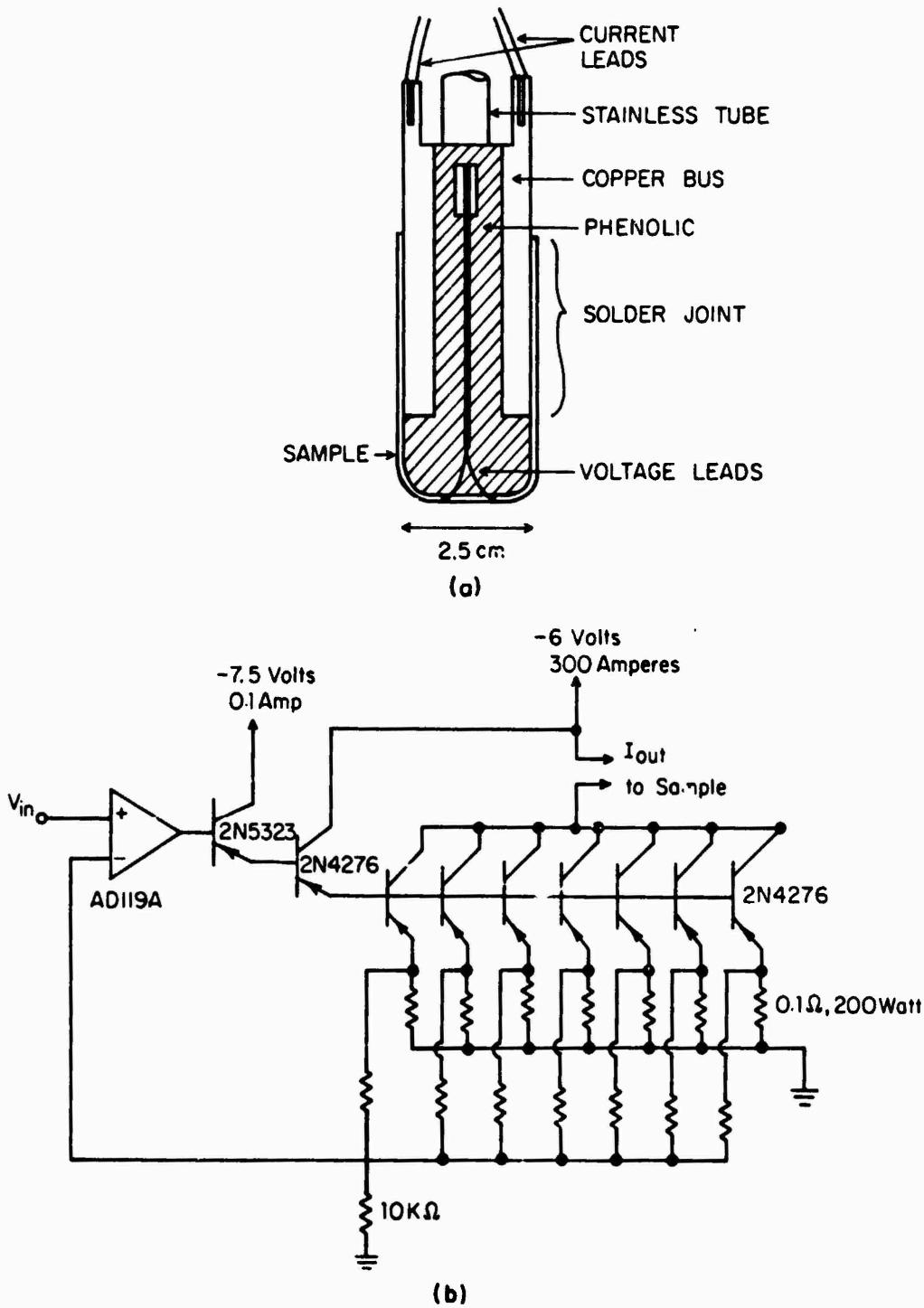

Fig. 40 a) Experimental arrangement for high current voltage measurements. b) Schematic of high current power supply.

circuit is shown in Fig. 40b. The battery consisted of two or three lead-acid six volt storage batteries connected in parallel. Each battery was rated at 300 ampere-hours. The current was controlled by seven power transistors, type 2N4276, connected in parallel. These transistors were used in a Darlington arrangement with two other transistors as a current boost output for an Analog Devices AD119A op-amp. The whole circuit was connected in a non-inverting feedback mode. Current through the sample was controlled by a voltage applied to the non-inverting input of the op-amp. The current voltage relationship was quite linear, and the supply has been used to produce steady currents of over 200 amperes.

The most difficult part of making the supply was designing the emitter bias resistors for the seven parallel power transistors. Commercial resistors that were both compact and able to handle currents in excess of 30 amperes were not available. The design we settled on was a strip of one mil (0.0025 cm) brass, approximately 0.3 cm wide and 10 cm long arranged in a sandwich structure of copper, thermally conductive grease, and mylar. The sandwich was made as follows. First the grease was applied sparingly to a water-cooled copper base that served as the common electrode for all the resistors. One mil mylar insulation was pressed onto the grease, and then greased itself. The brass resistor was pressed onto the new grease atop the mylar, but with one end

extended slightly beyond the mylar to make contact with a clean area of the copper base. A small bead of solder on the end of the brass strip helped to make contact to the copper but it was not feasible to solder the brass to the copper. More grease, mylar, grease, and the top copper plate completed the sandwich. Contact between the upper copper plate and the brass resistor was made in the same way as between the resistor and the copper base. An insulated brass clamp tightened the assembly to the copper base to insure good thermal contact between the copper and the brass strip.

Initially, feedback voltage to the op-amp was taken across a 2×10^{-4} ohm resistor connected between the common point of the emitter resistors and ground. This arrangement resulted in a greatly reduced loop gain, however, so the circuit in Fig. 40b was adopted to insure high loop gain and good linearity. Each emitter of the seven power transistors was connected through a 100 ohm resistor to a common point. It can be shown that the voltage at that point is the average of the voltages at the seven emitters. This voltage was then fed back to the op-amp. In essence, the feedback loop kept this feedback voltage equal to the input voltage. Hence an input of one volt biased each emitter at one volt on the average. Each transistor then put out about ten amperes, and since there were seven transistors, the ratio of output current to input voltage was about 70 amperes/volt.

APPENDIX B: SQUID VOLTAGE MEASUREMENTS

Our SQUID amplifier cryostat was designed to minimize the consequences of resistive electrical contact with the sample. Resistive contacts are one of many problems that must be dealt with when trying to use the extraordinary sensitivity of SQUID amplifiers in practical experiments. A thorough discussion of these problems is given in R.S. Newbower's Ph.D. thesis.[29] However, the relatively low temperatures involved in Newbower's experiment allowed him to avoid the particular problem of resistive contacts: his connections to the sample were all superconducting. Our samples, on the other hand, required measurements over the broad temperature range of 2 to 18 K. The conductors that connected the sample to the SQUID amplifier were therefore made of Nb_3Sn to insure that they would remain superconducting over the whole temperature range, but the connections to the sample itself were resistive.

B.1 Resistive Contacts

Resistive contacts limit the sensitivity of SQUID amplifier measurements through Johnson noise and the Seebeck effect. Johnson noise was not a serious problem for us. Contact resistances of less than a micro ohm were not difficult to achieve with ordinary solder connections, so from

the Nyquist formula $V_{rms} = \sqrt{4k_B RTB}$, the Johnson noise voltage was about 10^{-14} volts/$Hz^{1/2}$. Here k_B is Boltzmann's constant, R, the resistance, T the temperature, and B the bandwidth of the measurement. A sensitivity of 10^{-14} volts would have been adequate for our experiments. Unfortunately, the Seebeck effect can produce much larger voltages than Johnson noise for these low resistance contacts. A temperature difference of 10^{-3} K across the resistive contact could make as much as a nanovolt signal that would be added to the true voltage across the sample. Thermal emf's in our final cryostat design, shown in Fig. 41a, were limited to about 10^{-11} volts if the temperature was swept at a rate less than about 3 K per minute. By automating the temperature sweep with a motor-driven potentiometer the thermal voltages could be reproduced from sweep to sweep during a given run within about 10^{-12} volts. At lower temperatures the resolution was better, and below the transition temperature of the solder connections (about 7 K), all thermal voltages disappeared.

B.2 The Cryostat Design

We designed the cryostat to accomodate two principal constraints: the voltage leads had to be made of Nb_3Sn, and thermal gradients in the vicinity of the sample had to be minimized. We used solder coated Nb_3Sn tape that was one mil thick for the voltage leads. The tape was flexible, had

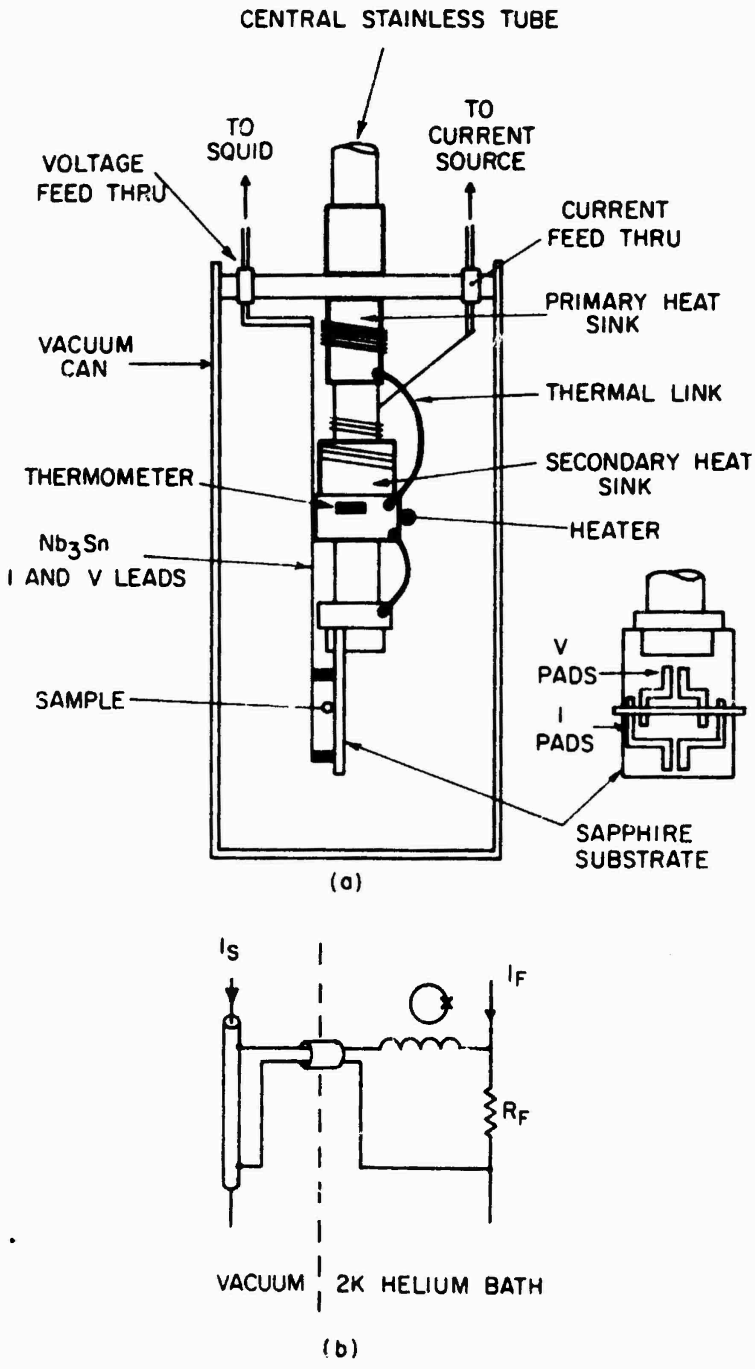

Fig. 41 a) Experimental arrangement for SQUID voltage measurements. b) Schematic of SQUID circuit.

no copper (and hence a low thermal conductance) and was easily con. ted to the sample with a low power soldering iron. (Excessive heat tended to remove the solder coating.) The tape also had an ideal geometry for heatsinking. Wherever possible in the construction of the cryostat, the Nb_3Sn tape voltage leads were stacked one atop the other separated by one mil mylar insulation and glued in place with GE7031 varnish. This proceedure minimized self and mutual inductances, and proved compact and convenient. The voltage leads were cut from the tape in one piece, and extended from the voltage feedthrough at the top of the vacuum can to the sample.

The sample was mounted as shown in Fig. 41a, on a single crystal sapphire substrate obtained from the Adolf Meller Company.[96] The pre-cut voltage leads were indium soldered to the substrate to form pads that the sample could be laid across for easy soldering. Current pads were also cut from Nb_3Sn tape and indium soldered to the substrate. Current was brought to these pads by a combination of copper wires and Nb_3Sn tape, with soldered connections. These components were arranged so that the sample was in intimate contact with the high thermal conductivity sapphire, but isolated from the rest of the cryostat by the low thermal conductance Nb_3Sn tape. The sapphire substrate was clamped to a copper fitting that was attached to the structure extending from the top of the vacuum can.

The arrangement of this supporting structure was crucial for minimizing thermal gradients near the sample. A hollow electrolytic-tough-pitch (ETP) copper cylinder extended about 2.5 cm on either side of the top brass flange of the vacuum can. The top half of this copper piece was therefore in direct contact with the helium bath, and was also soldered to a central stainless steel tube. This tube extended to the top of the cryostat, and served as the main structural support of the entire assembly, as well as the vacuum pumping line and the conduit for electrical leads to the heater and thermometer in the vacuum can. The lower half of the copper cylinder served as the primary heat sink for all the structures within the vacuum can. The electrical leads carried down from room temperature were therefore wrapped tightly around and glued to the bottom half of the copper cylinder. The sample current and voltage leads, however, were exposed to the bath and entered the vacuum can through specially designed feedthroughs, of the sort described in Newbower's thesis.[29] Direct heat sinking to the bath at the copper cylinder was therefore not necessary for them.

A second copper heat sink was supported a short distance from the primary heat sink by a thin-wall stainless steel tube. This tube extended all the way through the secondary heat sink and supported the sapphire substrate and clamp at the other end. The entire structure within the vacuum can

was a little over 7.5 cm long. All electrical leads as well as the heater and the thermometer were thermally attached to the secondary heat sink. Thermal links consisting of copper braid connected the secondary to the primary heat sink, and also connected the clamped sapphire to the secondary heat sink.

Approximately 0.1 watt supplied to the heater could raise the temperature of the secondary heat sink and the sample to about 20 K. If power were removed from the heater at 20 K, the sample would relax to within a few tenths of a degree of the bath temperature in about two minutes. The temperature was measured with a calibrated germanium resistance thermometer, biased with a constant current of 10 microamperes. The approximately exponential response of this thermometer at low temperatures was tamed somewhat by a logarithmic amplifier between the thermometer and the X-Y plotter. Without the logarithmic amplifier the temperature range from 2 to 18 K could not bave been plotted in a single continuous sweep.

Our initial design did not incorporate the secondary heat sink. Rather, the sapphire substrate was indium soldered to a copper slab, and the heater and thermometer and all electrical leads were attached to the same slab. The welter of heat sources and sinks resulted in large thermal gradients in the vicinity of the sample, and the best voltage resolu-

tion we obtained was about one nanovolt. The idea behind using a secondary heat sink was to move most of the temperature gradients from the vicinity of the sample. Then, by subtracting out the reproducible signals due to the remaining gradients, we could resolve 10^{-12} volts. To do better, one would probably have to work out some arrangement to spot weld the voltage leads to the sample to reduce further the magnitude of the temperature gradients across the contacts.

B.3 A typical Run

The way in which the resistive transitions of our samples were observed over nine to ten decades of resistance is as follows. First, the helium bath was pumped down to a temperature below the lambda point (about 2.2 K). Operation of the SQUID amplifier in superfluid helium was essential to eliminate thermal emf's across the feedback resistor, R_F. (R_F was chosen to be as large as possible without contributing excessively to the noise. We usually used 10^{-4} ohm.) The desired current was then applied to the sample. The sensitivity of the SQUID amplifier was set by choosing an appropriate value for R_o (see Fig. 7). Feedback for the SQUID amplifier was then applied and adjusted for zero feedback current. Finally, the temperature of the sample was swept through the transition by ramping the heater current with a motorized potentiometer. The temperature signal,

amplified by the logarithmic amplifier, and the SQUID amplifier output were recorded simultaneously on an X-Y plotter. When the transition was completed, the sample was allowed to cool, and a new SQUID sensitivity or sample current was chosen for the next sweep. All permutations of the chosen sample currents and sensitivities were plotted for each sample in this manner. Hence, each continuous curve in Fig. 31 and Fig. 34 represents four temperature sweeps, since each curve covers about four decades in voltage sensitivity. Thermal emf's could be subtracted by reversing the current and repeating each sweep before going on to the next permutation of current and sensitivity.

REFERENCES

1. Present address: Department of Applied Physics, Stanford University, Stanford, Claifornia 94305.

2. Present address: Bioengineering Unit, Harvard Medical School, Massachusetts General Hospital, Boston, Massachusetts 02114.

3. A. Davidson, R.S. Newbower, and M.R. Beasley, Rev. Sci. Instrum. 45, 838 (1974).

4. A. Davidson, M.R. Beasley, and M. Tinkham, IEEE Trans. Magn. MAG-11, 276 (1975).

5. A.B. Pippard and G.T. Pullan, Proc. Camb. Phil. Soc. 48, 188 (1952).

6. I.M. Templeton, J. Sci. Instrum. 32, 314 (1955).

7. D.A. Buck, Proc. IRE 44, 482 (1956).

8. V.L. Newhouse, and H.H.Edwards, Proc. IEEE 52, 1191 (1964).

9. B.D. Josephson, Phys. Lett. 1, 251 (1962).

10. P.W. Anderson and J.M. Rowell, Phys. Rev. Lett. 10, 230 (1963).

11. J. Clarke, Phil. Mag. 13, 115 (1966).

12. J.E. Zimmerman and A.H. Silver, Phys. Rev. 141, 367 (1966).

13. J.E. Zimmerman, P. Thiene, and J.T. Harding, J. Appl. Phys. 41, 1572 (1970).

14. A rough upper limit on the time scale is et by the energy gap Δ: $\tau = h/\Delta$, where h is Planck's constant. See M. Tinkham, Introduction to Superconductivity, Ch. 6, McGraw-Hill, New York (1975).

15. J. Matisoo, The Science and Technology of Superconductivity, Vol. 2, 607, Edited by W.D. Gregory, W.N. Mathews Jr., and E.A. Edelsack, Plenum Press, New York (1973)

16. V.L. Newhouse, Superconductivity, Vol. 2, 1283, Edited by R.D. Parks, Marcel Dekker, New York (1969).

17. V.L. Newhouse and J,W Bremer, J. Appl. Phys. 30, 1458 (1959).

18. A.E. Brenneman, J.J. McNichol, and D.P. Seraphim, Proc. IEEE 51, 1009 (1963).

19 Bascom S. Deaver Jr., The Science and Technology of Superconductivity, Vol. 2, 539, Edited by W.D. Gregory, W.N. Mathews, and E.A. Edelsack, Penum Press, New York (1973).

20. J. Clarke, Proc. Roy. Soc. A.308, 447 (1969).

21. R.A. Kamper and J.E. Zimmerman, J. Appl. Phys. 42, 132 (1971).

22. R.P Feynman, R.B. Leighton, and Matthew Sands, The Feynman Lectures on Physics, Vol. III, p.21-15, Addison-Wesley, Reading Massachusetts (1965).

23. H. Marshak and R.J. Soulen, Low Temperature Physics-LT13, Vol. 4, 498, Edited by K.D. Timmerhaus, W.J. O'Sullivan, and E.F. Hammel, Plenum Press, New York (1972).

24. M. Tinkham, Introduction to Superconductivity,Ch. 6, 192, McGraw-Hill, New York (1975).

25. For an excellent general review of superconducting quantum devices and their application in low-frequency instrumentation, see J. Clarke, Proc. IEEE, 61, 8 (1973).

26. J.E. Lukens, R.J. Warburton, and W.W. Webb, J. Appl. Phys. 42, 27 (1971).

27. R.P. Giffard, R.A. Webb, J.C. Wheatley, J. Low Temp. Phys. 6, 533 (1972).

28. J.W. McWane, J.E. Neighbor, and R.S. Newbower, Rev. Sci. Instrm. 37, 1602 (1966).

29. R.S. Newbower, Ph.D. Thesis, Harvard University (1970). Available as Technical Report #4, Division of Engineering and Applied Physics, Harvard University (1971).

30. J.Clarke, W.E. Tennant, and D. Woody, J. Appl. Phys. 42, 3859 (1971).

31. J. Kurkijarvi, Proc. 1972 Appl. Supercon. Conf., Annapolis, Maryland, IEEE publication number 72CH0682-5-TABSC.

32. J.H. Classen, J. Appl. Phys. 46, 5, 2286 (1975)

33. V. Radhakrishnan, V.L. Newhouse, J. Appl. Phys. 42, 129 (1971).

34. D.E. Prober, Rev. Sci. Instrum. 45, 848, (1974).

35. M. Tinkham, Introduction to Superconductivity, Ch. 6, 217, McGraw-Hill, New York (1975).

36. S. Letzter and N. Webster, IEEE Spectrum, pp 67-75, August, 1970.

37. R.A. Webb, R.P. Giffard, and J.C. Wheatley, J. Low Temp. Phys. 13, 384, (1973).

38. M. Tinkham, Introduction to Superconductivity, Ch. 6, 224, McGraw-Hill, New York (1975).

39. ibid.

40. H. Kamerlingh Onnes, Leiden comm. 120b, 122b, 124c (1911) and Leiden Comm. 140b, 140c, and 141b, (1914).

41. C.C. Tsuei, Science 180, 57 (1973).

42. C.C. Tsuei, J. Appl. Phys. 45, 1385 (1974).

43. C.C. Tsuei, M. Suenaga, and W,B, Sampson, Appl. Phys. Lett. 25, 318 (1974).

44. C.C. Tsuei and L.R. Newkirk, J. of Mat. Science 8, 1307 (1973).

45. C.C. Tsuei, IEEE Trans. on Magn. MAG-11, 272 (1975).

46. F.B. Silsbee, J. Was. Acad. Science 6, 597 (1916).

47. W. Meissner and R. Ochsenfeld, Naturwissenschaften 21, 787 (1933).

48. C.J. Gorter and H.B.G. Casimir, Physik. Z , 35, 963 (1934), and Z. Tech. Physik. 15, 539 (1934).

49. F. London and H. London, Proc. Roy. Soc. A 149, 71 (1935), and Physica 2, 341 (1935).

50. A.B. Pippard, Proc. Roy. Soc. A 216, 547 (1953).

51. V.L. Ginzburg, and L.D. Landau, Zh. Experim. i Teor. Fiz. 20, 1064 (1950).

52. A.A. Abrikosov, Zh. Eksperin. i Teor. Fiz. 32, 1442 (1957). [Soviet Phys.-JETP 5, 1174, (1957).]

53. L.V. Shubnikov, V.I. Khotkevich, Yu.D. Shepelev, Yu.N. Riabinum, Zh. Eksperim. i Teor. Fiz. 7, 221 (1937).

54. J. Bardeen, L.N. Cooper, and J.R. Schrieffer, Phys. Rev. 106, 162 (1957), Phys. Rev. 108, 1175 (1957).

55. L.P. Gor'kov, Zh. Eksperim. i Teor. Fiz. 36, 1918 (1959). [Soviet Phys. JETP 9, 1364 (1959).]

56. J.E. Kunzler, E. Behuler, F.S.L. Hsu, and J.E. Wernick, Phys. Rev. Lett. 6, 89 (1961).

57. B.B. Goodman, IBM J. Res. Develop., 6, 63 (1962), Phys. Rev. Lett. 6, 597 (1961).

58. M. Tinkham, Introduction to Superconductivity, Ch. 5, McGraw-Hill, New York (1975), and P.G. de Gennes, Superconductivity of Metals and Alloys, Ch. 3, W.A. Benjamin, New York (1966).

59. Y.B. Kim, C.F. Hempstead, and A.R. Strnad, Phys. Rev. Lett. 12, 145 (1964), Phys. Rev. 139, A1163 (1965).

60. M.R. Beasley, R. Labusch, and W.W. Webb, Phys. Rev. 181, 682 (1969).

61. Y.B. Kim and M.J. Stephen, Superconductivity, Ch. 19, Edited by R.D. Parks, Marcel Dekker, New York (1969).

62a. W.A. Fietz and C.H. Rosner, IEEE Trans. Magn. MAG-10, 239 (1974).

62b. Z.J.J. Stekly, The Science and Technology of Superconductivity, pp 497-538, Edited by W.L. Gregory, W.N. Mathews Jr., and E.A. Edelsack, Plenum Press, New York (1973).

63. A.R. Kantrowitz, and Z.J.J. Stekly, Appl. Phys. Lett. 6, 56 (1965).

64. C. Laverick, Proc. Intn'l Symp. on Magnet Tech., UC-28, p. 560, Stanford Univ. (1965).

65. P.F. Chester, Rep. Prog. Phys. XXX, Part II, pp. 561-614 (1967).

66. P.F. Chester, Proc. First Int'l Cryogenic Eng. Conf.,p. 147 Tokyo, Edited by K. Mendelssohn, Heywood Temple Publications,(1967).

M.N. Wilson, C.R. Walters, J.D. Lewin, and P.F. Smith, J. Phys. D; Appl. Phys. 3, (1970)

67. M. Tinkham, Introduction to Superconductivity, Ch. 5, 182, McGraw-Hill, New York (1975).

68. C.C. Tsuei, private communication.

69. Timothy J. Callaghan and Louis E. Toth, J. Appl. Phys. 46, 4013 (1975).

70. R. Roberge and R. D. McConnell, Scripta Metallurgica 8, 1267 (1974).

71. C.C. Tsuei, private communication.

72. G. Deutscher and P.G. de Gennes, Superconductivity, Ch. 17, p. 1005, Edited by R.D. Parks, Marcel Dekker, New York (1969).

73. V.K.S. Shante and Scott Kirkpatrick, Adv. in Phys. XX, 325 (1971).

74. J.P. Gollub, Technical Report #3, Division of Engineering and Applied Physics, Harvard University (1970).

75. D.E. Prober, Ph.D. Thesis, Harvard University (1975).

76. P.G. deGennes, Superconductivity of Metals and Alloys, Ch. 7, W.A. Benjamin, New York (1966).

77. R.G. Chambers, Proc. Roy. Soc. A215, 481 (1952).

78. J.-P. Hurault, Phys. Lett. 20, 587 (1966).

79. H.C. Montgomery, J. Appl. Phys. 42, 2971 (1971).

80. M. Tinkham, Univ. Michigan Report #005020, July, 1973. (Preliminary Reports, Memoranda, and Technical Notes of the Materials Research Council Summer Conference, La Jolla, California.)

81. R. Landauer, J. Appl. Phys. 23, 779 (1952).

82. Scott Kirkpatrick, Rev. Mod Phys. 45, 574 (1973).

83. J.C. Maxwell, A Treatise on Electricity and Magnetism, Vol. 1, Ch. XI, Clarendon Press (1892). This is an early treatment of the effective medium theory.

84. This expression was obtained by considering a prolate spheroid of arbitrary conductivity within the effective medium. A uniform axial electric field is applied, and Maxwell's equations are solved for the electric field in the effective medium at the surface of the spheroid. The current is then proportional to an appropriate surface integral of this field. See ref. 85.

85. A. Sommerfeld, Electrodynamics, Part II, sections 13 G and H, Academic Press (1964).

86. I. Webman, J. Jortner, and M. H. Cohen, Phys. Rev. B 11, 2885 (1975).

87. J.M. Hammersley and J.A. Welsh, Phys. Rev. 126, 949 (1962).

88. H. Scher and R. Zallen, J. Chem. Phys. 53, 3759 (1970).

89. R. Zallen and H. Scher, Phys. Rev. B 4, 4471 (1971).

90. J.P.Fitzpatrick, R.B. Malt, and F. Spaepen, Phys. Lett. 47A, 207 (1974).

91. G.E. Pike and C.H. Seager, Phys. Rev. B 10, 1421 (1974).

92. M. Hori and F. Yonezawa, J. Math. Phys. 16, 352 (1975).

93. G.A. Baker, Jr., Essentials of Padé Approximants, Academic Press (1975).

94. T.E. Faber, An Introduction to the Theory of Liquid Metals, Cambridge University Press (1972).

95. J.A. Shroeder and J.C. Thompson, Phys. Rev. 179, 194 (1971) and other references cited in ref. 86 above.

96. Adolph Meller Co., 120 A Corliss St. Providence, RI 02904, (401) 331-3717.

ACKNOWLEDGEMENTS

I am grateful to C.C. Tsuei, W.Y-K Chen, J. Bevk, and J. Harbison for providing samples of microcomposite wire for the experiments reported here. R. Rex was responsible for the construction of much of the apparatus, and I am grateful for his craftsmanship. C.J. Lobb made operational much of the equipment described in Appendix A, and helped tie some loose ends on the experiments.

I am also grateful to M. Tinkham, who provided the overall guidance of my graduate career, and who aroused my interest in Tsuei's materials. I thank W.J. Skocpol for lending a hand whenever it was needed, and for his constructive evaluations. I am especially grateful to M.R. Beasley for starting me off in low temperature physics, and for his constant interest in my work despite a separation of 3000 miles.

Finally, I am grateful to my wife, Janis S. Davidson, whose hard work and sacrifices kept us both going for five years of graduate study.

This research has been supported in part by the National Science Foundation, the Office of Naval Research, the Advanced Research Projects Agency, and the Joint Services Electronics Program.